STRUCTURAL AND FUNCTIONAL STUDIES OF THE RECEPTOR-BINDING AND GLYCOSAMINOGLYCAN-BINDING MECHANISMS OF A VIRAL CHEMOKINE ANALOG vMIP-II AND RATIONAL DESIGN OF CHEMOKINE-BASED HIGHLY POTENT HIV-1 ENTRY INHIBITORS

A Dissertation

by

BO ZHAO

Submitted to the Office of Graduate Studies of
Texas A&M University
in partial fulfillment of the requirements for the degree of

DOCTOR OF PHILOSOPHY

May 2011

Major Subject: Biochemistry

Structural and Functional Studies of the Receptor-binding and Glycosaminoglycan-binding Mechanisms of a Viral Chemokine Analog vMIP-II and Rational Design of Chemokine-based Highly Potent HIV-1 Entry Inhibitors

STRUCTURAL AND FUNCTIONAL STUDIES OF THE RECEPTOR-BINDING AND GLYCOSAMINOGLYCAN-BINDING MECHANISMS OF A VIRAL CHEMOKINE ANALOG vMIP-II AND RATIONAL DESIGN OF CHEMOKINE-BASED HIGHLY POTENT HIV-1 ENTRY INHIBITORS

A Dissertation

by

BO ZHAO

Submitted to the Office of Graduate Studies of
Texas A&M University
in partial fulfillment of the requirements for the degree of

DOCTOR OF PHILOSOPHY

Approved by:

Co-Chairs of Committee,	Patricia J. LiWang
	Vlad Panin
Committee Members,	Pingwei Li
	Julian Leibowitz
Head of Department,	Gregory D. Reinhart

May 2011

Major Subject: Biochemistry

ABSTRACT

Structural and Functional Studies of the Receptor-binding and Glycosaminoglycan-binding Mechanisms of a Viral Chemokine Analog vMIP-II and Rational Design of Chemokine-based Highly Potent HIV-1 Entry Inhibitors.

(May 2011)

Bo Zhao, B.S., Peking Univerisity, Beijing, China

Chair of Advisory Committee: Dr. Patricia J. LiWang

Chemokines are small immune system proteins mediating leukocyte migration and activation, and are important in many aspects of health and diseases. Some chemokines also have the ability to block HIV-1 infection by binding to the HIV-1 co-receptors CCR5 (CC chemokine receptor 5) and CXCR4 (CXC chemokine receptor 4). The first part of this work is to determine the mechanism of action of a human herpesvirus-8 encoded viral chemokine analog vMIP-II (viral macrophage inflammatory protein-II) by characterizing its interactions with endothelial surface glycosaminoglycans (GAGs) and cell surface receptors. Nuclear magnetic resonance (NMR), mutagenesis and molecular-docking were conducted and results show that vMIP-II tightly binds glycosaminoglycans using residues distributed along one face of the protein, such as R18, R46 and R48, and that there is a shift in the GAG binding site between the monomer and dimer form of vMIP-II where the N-terminus is involved in GAG binding for the dimer. This study, for the first time, provides a model that explains

the mechanism of how quaternary structure affects chemokine-GAG binding. Mutagenesis and competition binding assays were conducted to study the receptor-binding mechanism of vMIP-II. Preliminary results suggest that vMIP-II uses the same positively charged binding surface comprising R18, K45, R46 and R48 to interact with the negatively charged N-termini of CCR5 and CXCR4. NMR studies on how vMIP-II interacts with N-terminal peptides of CCR5 and CXCR4 is on-going.

The second part of this work was to rationally design HIV-1 entry inhibitors based on our knowledge of the mechanisms of chemokine-receptor binding and HIV-1 cell entry. We successfully designed two chimeric HIV entry inhibitors composed of CCR5-targeting RANTES variants (5P12-RANTES and 5P14-RANTES) linked to a gp41 targeting C-peptide, C37. In *in vitro* assays, chimeric inhibitors 5P12-linker-C37 and 5P14-linker-C37 showed the highest anti-viral potency yet published with IC_{50} values as low as 0.001 nM against certain virus strains. On human peripheral blood mononuclear cells, the chimeric inhibitors also exhibited very strong inhibition against R5-tropic and X4-tropic viruses, with IC_{50} values as low as 0.015 nM and 0.44 nM, respectively. A clear delivery mechanism was observed and characterized. These fully recombinant inhibitors can be easily produced at low cost and are excellent candidates for HIV microbicides.

DEDICATION

This work is dedicated to my dear parents, Songgen Zhao and Guihua Zhang. It is your love and support that made me who I am.

Special thanks to my Ph.D. advisor, Dr. Patricia J. LiWang. It is been a great pleasure working with you.

ACKNOWLEDGEMENTS

I would like to thank my committee co-chairs, Dr. Patricia LiWang and Dr. Vlad Panin, and my committee members, Dr. Julian Leibowitz and Dr. Pingwei Li, for their guidance and support throughout the course of this research.

I would also like to thank Dr. Andy LiWang, Dr. Xiangming Kong, Dr. David Gravano, Dr. Hongjun Jin, Dr. Ioannis Kagiampakis, Dr. Yongguang Gao, Dr. Yonggang Chang, and Dr. Nai-wei Kuo, for the training and technical assistance they provided during my doctoral research.

Thanks also go to all my friends and colleagues and the department faculty and staff at Texas A&M University and the University of California, Merced.

Funding for this work was provided by the American Heart Association, Texas Affiliate (Grant 0655070Y) and National Institutes of Health Grant R21AI079777.

NOMENCLATURE

5P12	5P12-RANTES
5P12-linker-C37	5P12-RANTES covalently linked with gp41 binding peptide C37 via a 10-amino-acid peptide GGGGSGGGGS
5P14	5P14-RANTES
5P14-linker-C37	5P14-RANTES covalently linked with gp41 binding peptide C37 via a 10-amino-acid peptide GGGGSGGGGS
AIDS	acquired immune deficiency syndrome
AIR	ambiguous interaction restraint
AUC	analytical ultracentrifugation
BBXB	a part of the 40's loop of chemokines, for "Basic-Basic-Any-Basic" amino acid
BME	β-mercaptoethanol
BSA	bovine serum albumin
CCR	CC chemokine receptor
CHO	Chinese hamster ovary
CPRG	chlorophenol red-β-D-galactopyranoside
CXCR	CXC chemokine receptor
DMEM	Dulbecco's modified eagle medium

DSS	4,4-dimethyl-4-silapentane 1-sulfonate
FACS	fluorescence activated cell sorting
FITC	fluorescein isothiocyanate
GAG	glycosaminoglycan
HADDOCK	high ambiguity driven biomolecular docking
HEK	human embryonic kidney
HIV	human immunodeficiency virus
HPLC	high performance chromatography
HSQC	heteronuclear single-quantum coherence
IC50	concentration of 50% inhibition
IPTG	isopropyl R-D-thiogalactopyranoside
Kd	dissociation constant
MW	molecular weight
NMR	nuclear magnetic resonance
PBMC	peripheral blood mononuclear cells
PBS	phosphate buffered saline
PCR	polymerase chain reaction
PEEA	Polyethyleneamine
PSI	pounds per square inch
RANTES	regulated on activation of normal T cell expressed and secreted (CCL5)
RMSD	root-mean-square deviation

RPMI	Roswell Park Memorial Institute medium
SDS-PAGE	sodium dodecyl sulfate polyacrylamide gel electrophoresis
SW	sweep width
TFA	trifluroacetic acid
vMIP	viral macrophage inflammatory protein
WT	wild type

TABLE OF CONTENTS

CHAPTER Page

LIST OF FIGURES

Page

LIST OF TABLES

Page

CHAPTER I

INTRODUCTION

Chemokines

Chemokines, also called chemotactic cytokines, are a family of small immune system proteins (8-17 KDa) that mediate leukocyte migration and activation (1-4). As such chemokines are directly involved in regulating immune responses and inflammation. In addition to the pivotal role chemokines play in developing and maintaining the host immune systems (5), they are also involved in embryogenesis (6), wound healing (7), angiogenesis/angiostasis (8-9) and in tumor development and metastasis (4). Recently, some chemokines were also found to be able to block HIV-1 cell entry (10-12).

Chemokines are classified into four sub-families based on the positions of the conserved cysteine residues in the N-terminal region of the protein (13). The biggest chemokine subfamilies are "CC" and "CXC". The CC subfamily (So-named because of the two adjacent Cys-Cys residues in the N-terminus) comprises 28 members, while the CXC subfamily (Cys-any-Cys) has 17 members. The two minor groups are CX3C (14) (3 variable residues between the two conserved Cys residuals) and XC (15) (only one conserved Cys), and they contain one member each. The CXC chemokines are further

---

This dissertation follows the style of *The Journal of Biological Chemistry*.

categorized into ELR+ chemokines and ELR- chemokines depending on the whether they have the conserved Glu-Leu-Arg motif at the N-terminus (13,16). In addition to human native chemokines, pathogens also encode certain chemokine analogs to facilitate their infection or escape from the host immune system (17). For example, human herpesvirus-8 (also called Kaposi's sarcoma-associated herpesvirus) encodes three viral chemokine analogs vMIP-I, vMIP-II, and vMIP-III, each with unique anti-inflammatory functions to help the survival of HHV-8 (18).

Chemokines bind to and activate specific cell surface chemokine receptors, which are G-protein coupled receptors (GPCRs). Corresponding to the four subfamilies of chemokines, the chemokine receptors are also divided in to four subfamilies, based on the chemokine ligands they bind to. There are ten CC chemokine receptors (CCRs) and seven CXC chemokine receptors (CXCRs), one CX3C chemokine receptor (CX3CR1) and one XC chemokine receptor (XCR1). Certain human cells also express decoy receptors, which bind to chemokines tightly, but do not trigger receptor-mediated signaling transduction. These decoy receptors also play important roles in the immune system, likely by regulating local concentration gradients of their cognate ligands and control leukocyte recruitment at inflammatory site (19). Certain viruses also developed strategies of mimicking chemokine receptors to counteract the pro-inflammatory chemokine triggered immune responses by encoding viral chemokine receptors (17,20) or viral chemokine binding proteins (21-22).

In addition to binding chemokine receptors, chemokines also bind to endothelial surface glycosaminoglycans (GAGs). GAG binding plays a vital role in chemokine

function. While GAG binding is not essential for receptor binding *in vitro* (23-26), several studies have demonstrated that the ability of a chemokine to bind GAGs is critical for *in vivo* function (27-29). GAGs control chemokine function in many ways: GAGs help immobilize chemokines on the endothelial cell surface (30-31), where natural chemokines presumably form a concentration gradient (31-36), and these chemokines recruit leukocytes to move along the gradient by activating chemokine receptors on the leukocyte surface (37). GAG binding also protects chemokines from proteolysis and induces chemokine oligomerization (38-39). Overall, GAG binding helps chemokines to increase their local concentrations and enhance receptor signaling (23,25,40-41).

As described above, chemokines carry out their functions by interacting with both the leukocyte surface chemokine receptors and the endothelial surface GAGs. Figure 1.1 shows a diagram illustrating the process of how chemokines recruit leukocytes by building up a concentration gradient on the endothelial surface GAGs.

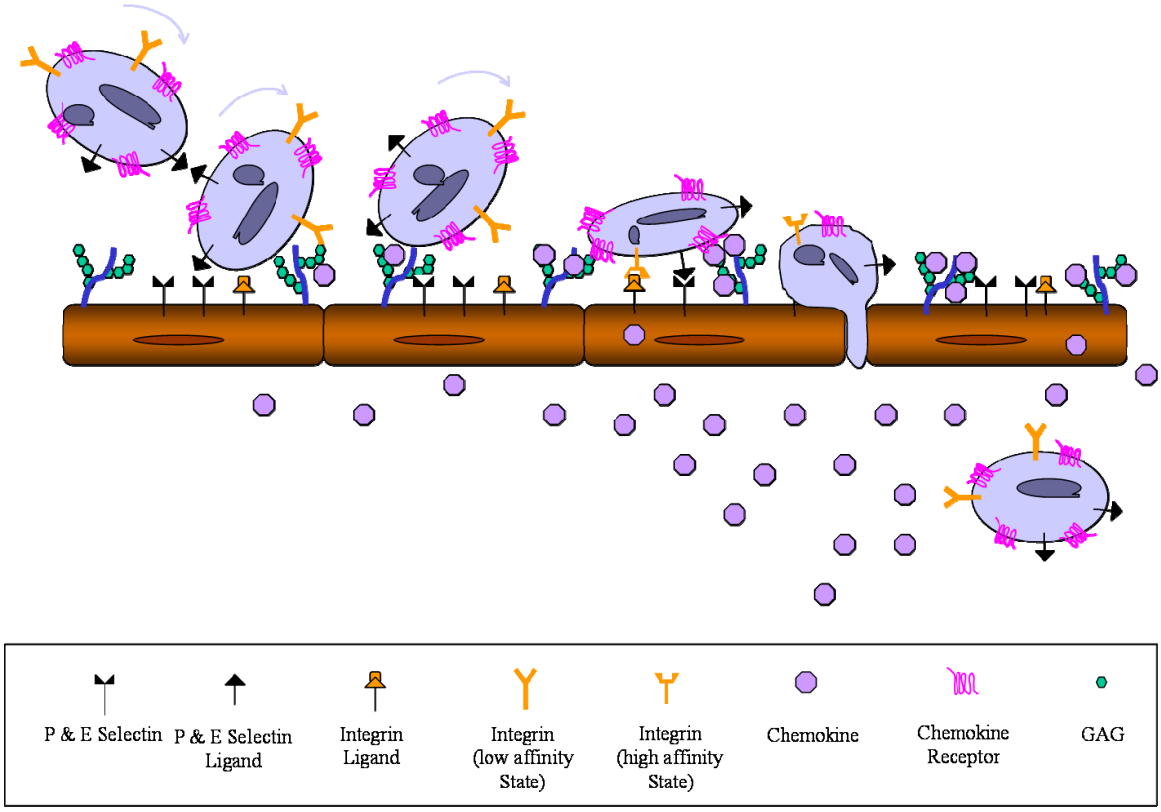

Figure 1.1 Leukocyte recruitment by chemokines. Chemokines (purple spheres) are secreted by tissues at the infection site. They bind to the endothelial cell surface glycosaminoglycans (GAGs, small green spheres) and presumably form a concentration gradient. Leukocytes in the blood vessel are captured and activated by chemokines through binding to the leukocyte surface chemokine receptors (pink). Activated leukocytes adhere to the endothelial surface through high affinity binding between integrins and integrin ligands, and they roll up along the chemokine concentration gradient. Receptor activation also triggers morphological changes of leukocytes which enable them to move across the endothelial layer to the center of the infection site.

Viral Chemokine Analog vMIP-II

vMIP-II (also called vCCL2) is a viral chemokine analog that is produced by human herpesvirus-8. This protein is unique because it binds to a wide range of chemokine receptors even across different subfamilies: it binds to CCR1, CCR2, CCR5, CCR10, CXCR4, CX3CR1, XCR1 as an antagonist, and binds to CCR3 and CCR8 as an agonist (42-47). The ability to selectively block or activate multiple receptors enables vMIP-II to preferentially inhibit acute Th1-associated inflammation, but up-regulate Th2 associated immune response to help the virus evade the host immune system (44-45). Due to its potent anti-inflammatory properties, vMIP-II has been successfully used to protect rat brain after ischemic brain injury and spinal cord injury (48-49), as well as increase tolerance of cardiac and corneal allograft transplant in mice (50-51). More recently, vMIP-II has been shown to be pro-angiogenic in both mature and progenitor endothelial cells, suggesting the possibility that this protein could be useful in organ transplantation (52). vMIP-II is also a valuable candidate as an HIV inhibitor, since it blocks HIV cell entry through both CCR5 and CXCR4 coreceptors and preferentially inhibits inflammation of monocytes and Th1 type T cells which are major targets for HIV-1 (43-45). vMIP-II therefore is biologically relevant in many diverse fields.

Because of these fundamental roles vMIP-II plays in diseases and its promising anti-inflammatory function as well as its ability to block both major HIV-1 co-receptors, it is very important that we study the structure and function of vMIP-II and understand its mechanism of action.

The structure of vMIP-II has been solved by both NMR (53-55) and X-ray crystallography (56-57). vMIP-II shares about 40% sequence identity with the human chemokine MIP-1β, 48% with MIP-1α and 37% identity with RANTES (Figure 1.2). vMIP-II also has a typical chemokine fold, comprised of three strands in a Greek key orientation, and followed by a C-terminal-helix. In terms of quaternary structure, vMIP-II is predominantly a monomer under most conditions (53-55,57), although under some crystallization conditions it has been observed as a dimer (56).

Just as its human chemokine analogs, vMIP-II also carries out its functions by interacting with chemokine receptors and endothelial surface GAGs. It is thus important for us to elucidate the GAG-binding and receptor-binding mechanisms of vMIP-II to understand the basis of its function.

vMIP-II binds GAGs very tightly, more tightly than most human chemokines. However, the biological significance of vMIP-II's tight GAG binding is not known, nor is the mechanism by which vMIP-II interacts with GAGs. As part of our study of vMIP-II, we mapped out the GAG binding site of vMIP-II, characterized its GAG-binding mechanism, and, for the first time, provided a model that explains the mechanism of how quaternary structural change affects chemokine-GAG binding. This part of research will be discussed in detail in Chapter II.

vMIP-II is very unique in binding chemokine receptors, because it binds to at least 9 different chemokine receptors, across all 4 different subfamilies (42-47). How vMIP-II binds to so many chemokine receptors remains one of the biggest questions about this protein. Great effort has been made toward understanding the intriguing mechanism

underlying vMIP-II's broad-spectrum receptor binding ability since it was first reported 13 years ago (43), however, it is still not precisely understood. Our study aims to understand the specific aspects of structure and amino acid placement that lead to vMIP-II's unique ability to bind multiple receptors, with a particular emphasis on characterzing the importance of vMIP-II's highly basic core domain surface in binding CCR5 and CXCR4. Details of this study will be further discussed in Chapter III.

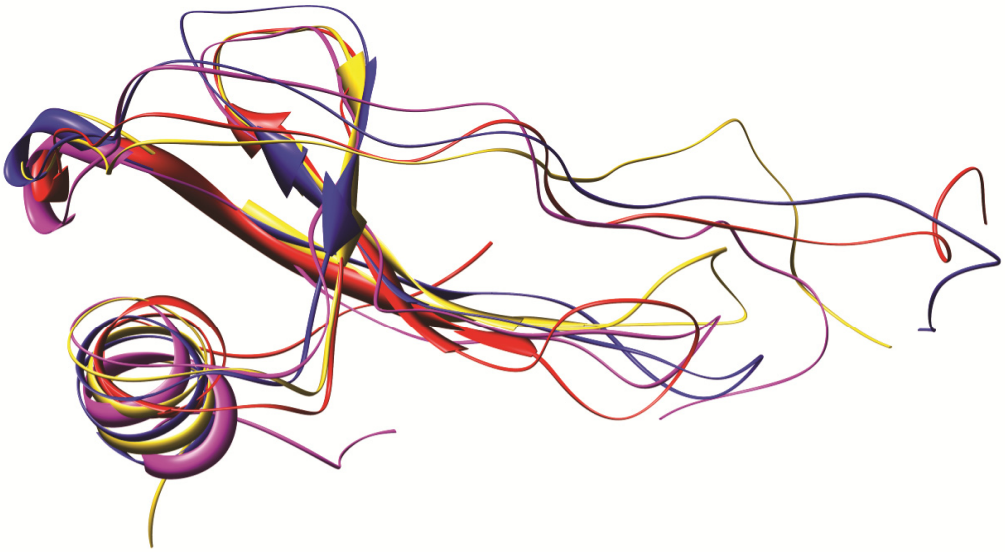

```
vMIP-II:    LGASWHRPDKCCLGYQKRPLPQVLLSSWYPTSQLCSKPGVIFLTKRGRQVCADKSKDWVKKLMQQLPVTAR
MIP-1β:     APMGSDPPTACCFSYTARKLPRNFVVDYYETSSLCSQPAVVFQTKRSKQVCADPSESWVQEYVYDLELN
MIP-1α:     -SLAADTPTACCFSYTSRQIPQNFIAAYFETSSQCSKPGVIFLTKRSRQVCADPSEEWVQKYVSDLELSA
RANTES:     SPYSSDT-TPCCFAYIARPLPRAHIKEYFYTSGKCSNPAVVFVTRKNRQVCANPEKKWVREYINSLEMS
```

Figure 1.2 Structure superimposition and sequence alignment of vMIP-II (red) with its three human analogs MIP-1β (blue), MIP-1α (yellow) and RANTES (pink).

Chemokines and HIV-1 Cell Entry Inhibition

A great deal of attention has been focused on the roles chemokines and their receptors play in HIV-1 infection.

AIDS is a global epidemic. According to the 2010 global report from the World Health Organization (WHO), approximately 33.3 million people were living with HIV, and there were 2.6 million people newly infected with HIV in the year of 2009. There is currently no vaccine, and treatments usually involve inhibiting viral activity post-infection, by inhibiting the HIV protease or reverse transcriptase. More recently, therapies that target other parts of the viral life cycle have been approved, including an HIV integrase inhibitor (58).

The relationship between chemokine/chemokine receptor and HIV infection was discovered about 15 years ago. In the year 1995, three CCR5 binding chemokines, MIP-1α, MIP-1β and RANTES, were first identified as the major components of the CD8+ T cell secreted HIV-suppressive factors (11). Around the same time, chemokine receptor CXCR4 was identified as a co-receptor for HIV-1 cell entry (12). These two independent discoveries first unveiled the key role chemokine receptors play as the co-receptor for HIV cell entry, and thus unveiled their chemokine ligands as natural anti-HIV agents. More and more discoveries were made in the following years, including the identification of CCR5 as another HIV-1 entry co-receptor (59-62), identification of SDF-1 as CXCR4 ligand and HIV-1 inhibitor (61), and the discovery of the HIV-1 resistant *CCR5-Δ32* mutation (63). Altogether, all these discoveries and the following

findings greatly enhanced our understanding of the HIV-1 cell entry mechanism, and opened a new gate for developing therapeutics for HIV entry inhibition.

Currently, a great deal is known about the HIV entry process. Figure 1.3 shows a diagram of HIV entry: The HIV surface protein gp120 first makes contact with the human cell surface protein CD4, which causes a conformational rearrangement in gp120, allowing the protein to then bind its co-receptor on the cell surface (either the chemokine receptor CCR5 or CXCR4). During this process, the HIV protein gp41 is exposed and its fusion peptide enters the cell surface. Toward the end of the infection process, the N-terminal helical trimer folds over to contact the C-terminal trimer of gp41, forming a 6-helix bundle that likely pulls the membranes of the two entities in closer proximity to assist fusion of the virus to the cell (64-65). Recently, it has been reported that some of these events may occur in the endosome (66). Because of the characterization of the important entry steps and the identification of the key players in this process, developing various inhibitors to block HIV cell entry has been made possible.

Development of entry inhibitors has become one of the most promising areas in the fight against HIV/AIDS. Entry inhibitors generally bind to either the viral surface or the human cell surface to stop HIV before it can enter a cell. There are three major steps in HIV cell entry that can be targeted: the gp120-CD4 interaction, the gp120-coreceptor (CCR5 or CXCR4) interaction, and the gp41 6-helix bundle formation. Inhibitors have been found or designed for each of these steps.

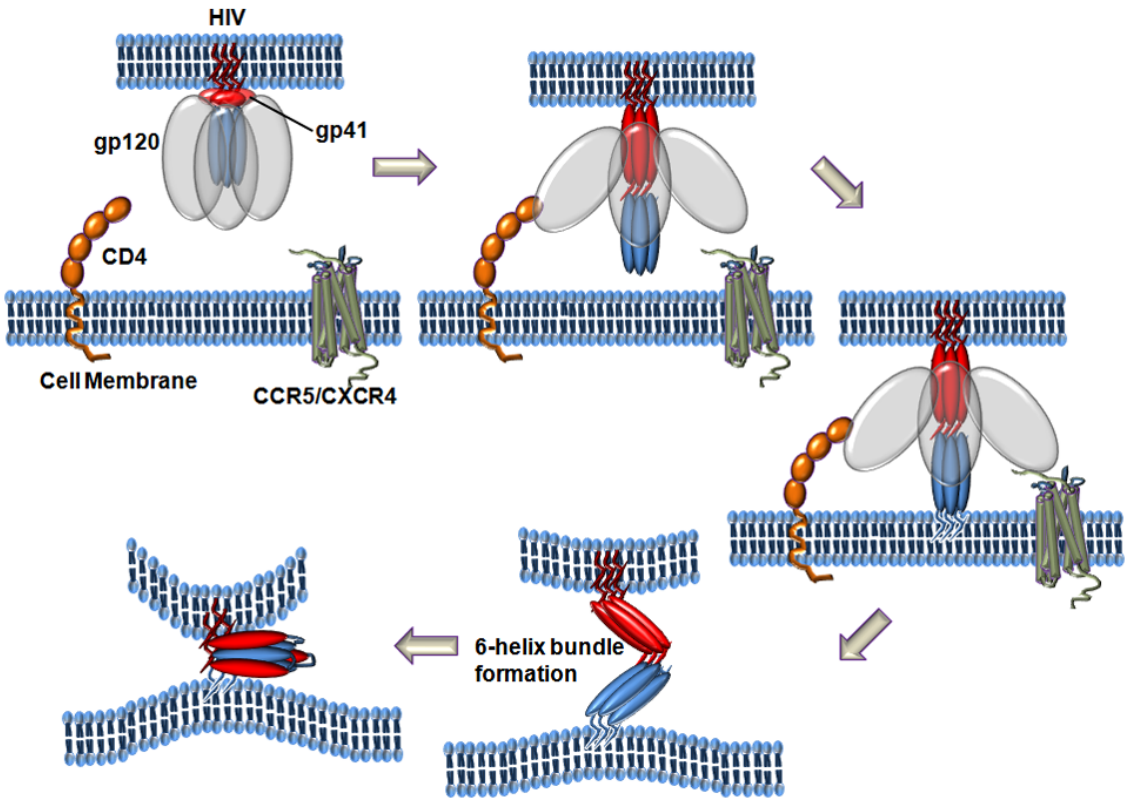

Figure 1.3 Diagram of the HIV cell entry mechanism. HIV gp120 (light gray ovals) makes contact with the human cell surface receptor CD4 (orange), which causes structural change in gp120, allowing its binding to the co-receptor (dark green) CCR5 or CXCR4 on the cell surface. During this process, the HIV protein gp41 is exposed and its fusion peptide enters the cell surface. At the end of the entry process, the N-terminal trimer of hairpins (blue) folds over to contact the C-terminal trimer (red) which leads to the formation of a 6-helix bundle that likely pulls the two membranes in closer proximity to assist fusion.

The most relevant to our current study is the development of coreceptor inhibitors which target the coreceptor binding step of HIV entry. The major advantage of targeting the coreceptor binding step is that the coreceptors are highly conserved and are not liable to HIV mutations. In addition, coreceptor binding is a requirement for HIV entry, since to date, no evidence of HIV infection without utilizing a coreceptor has been reported. Of the two HIV coreceptors, CCR5 is the primary target because of its vital role throughout the whole course of viral infection and disease progression. In the late phase of disease progression, dual or mixed tropic virus using both R5 and/or X4 tropic viruses emerge (67-68). The appearance of X4-tropic viruses are often associated with rapid CD4+ T cell depletion and AIDS (67,69-70). The corecepor usage switch is probably associated with mutation in the V3 loop of the HIV gp120 protein (71-72) under the selective pressure of the host immune system.

As natural ligands of HIV coreceptors, chemokines are able to inhibit HIV cell entry by pre-occupying the receptor and blocking the binding of HIV gp120 to the coreceptor. Natural chemokines MIP-1α, MIP-1β, RANTES and SDF-1 have been shown to possess anti-HIV activities (11,73). However, use of natural chemokines as anti-HIV therapeutics has been unsatisfactory because of the short life time and the inflammatory effects caused by chemokine receptor activation. It has been reported that in some *in vitro* systems, RANTES and other CC-chemokines actually enhanced HIV infection, probably due to enhanced cell activation (74-76). Another concern is that the use of CC-chemokines might accelerate the shift from the less pathogenic R5-tropic HIV to the X4-tropic HIV (77-78).

Therefore, tremendous efforts have been made to overcome these drawbacks. Various truncations, mutagenesis, chemical-modifications have been made to natural chemokines to increase their lifetime, reduce or eliminate their receptor activation activity and increase their inhibitory effect against HIV. Among all natural chemokines, the CCR5 receptor targeting CC-chemokine RANTES has likely been studied the most. N-terminal truncations caused RANTES to lose its agonist activity but retained the CCR5 binding activity: RANTES (3-68) and RANTES (9-68) were not able to activate receptors, but their HIV inhibitory potency was lower than that of the WT RANTES (79-80). A series of chemical modifications were made to the N-terminus of RANTES: methionylated RANTES (Met-RANTES) showed enhanced anti-HIV activity and no receptor signaling (81). Aminooxypentane (82)-RANTES (AOP-RANTES) showed reduced chemotaxis activity and even higher anti-viral potency than Met-RANTES (83). Later, PSC-RANTES was synthesized and it showed very potent activity against HIV with IC_{50} value of 0.04 nM in a cell-cell fusion assay (84). Chemical modification provides more versatility in inhibitor design, but a common problem of the chemically modified RANTES variants is that they cannot be easily produced in large amount and the cost is very high.

In the past decade, using large-scale screening methods, several recombinant RANTES variants have been found to be very potent HIV inhibitors. Hartley et al. selected two highly potent RANTES variants from a large pool of N-terminal randomly mutated RANTES variants (85). P1- and P2-RANTES showed strong inhibition effects which are comparable or better than that of AOP-RANTES. Recently, using the same

methods, several next generation N-terminal mutated RANTES variants were selected by the same group, 5P12-RANTES, 5P14-RANTES, and 6P4-RANTES have exhibited extremely strong anti-viral potency with IC_{50} values of around 0.03 nM in cell-cell fusion assays (86). 5P12 and 5P14 also showed no receptor signaling activity which made them excellent HIV entry inhibitors. Recombinant RANTES variants can be easily produced at very low cost, and are promising candidates for HIV microbicides.

Despite the effectiveness of the modified chemokine inhibitors, many of them have serious drawbacks. While the recent RANTES variants are extremely potent, they work by binding CCR5, so are only effective against R5 tropic virus, not against X4 tropic virus. The worry of accelerating the evolution of HIV to the more-pathogenic X4-tropic mutants also makes the use of CCR5 targeting chemokine inhibitors questionable. Our work with these variants attempts to overcome this obstacle.

In addition to the coreceptor inhibitors, inhibitors targeting other steps of HIV entry have also been found or designed. Proteins, particularly lectins that bind to gp120, have been shown to be effective inhibitors (87-89), as are peptides that bind to gp41 to stop 6-helix bundle formation (64). In particular, so-called C-peptides that are derived from the C-terminus of gp41 effectively bind to the N-terminus of gp41 to inhibit infection. One of these peptides, T-20, has been approved for clinical use (90-92). Figure 1.4 shows the mechanism of action of C-peptides, and a list of several gp41 derived C-peptides. While the C-peptides are effective against most strains of HIV, their potency is limited to nanomolar levels, and the virus can evolve so that the peptides bind less well (64,90-93).

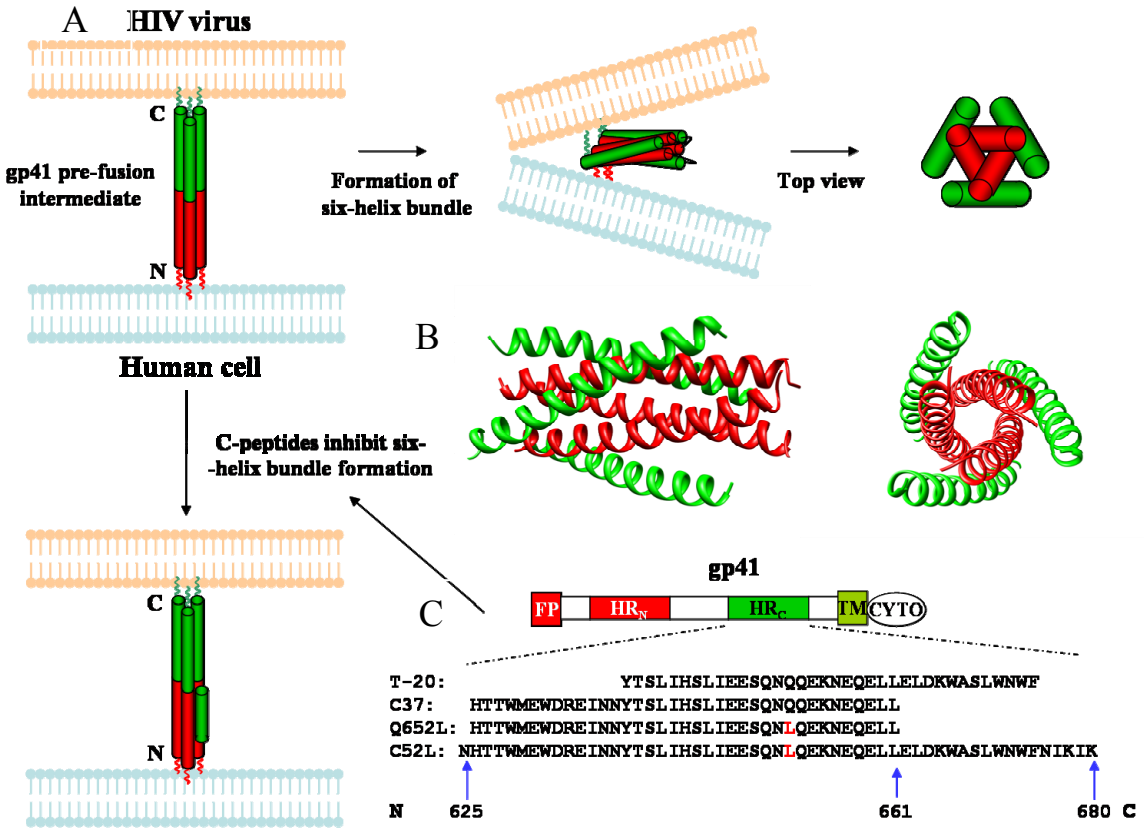

Figure 1.4 Mechanism of action of C-peptides. **A.** Simplified diagram of gp41 6-helix bundle formation and inhibition by fusion inhibition peptides; **B.** Crystal structure of 6-helix bundle formed by N- and C-peptides; **C.** Several fusion inhibiton peptides derived from HRC of gp41.

In the past three years, several studies have focused on a new direction of developing effective inhibitors through combining or linking HIV inhibitors targeting different steps of HIV cell entry. Simultaneously inhibiting multiple entry steps could lead to stronger and more comprehensive inhibition, and potentially overcome the disadvantages of each individual inhibitor or component. In 2008, Kopetzki et al. designed a bifunctional fusion inhibitor (BFFI) comprising a CCR5mAb covalently linked to two T-2635 fusion peptides (94). This BFFI exhibited stronger inhibition against R5-tropic viral strains than the parent CCR5mAb, and because of the linked T-2635 peptide, the BFFI also showed inhibition activity against X4-tropic virus in certain *in vitro* test systems, although it was ineffective against X4 virus under most conditions. In 2009, a second generation CD4-BFFI was reported (95). This new BFFI was created by covalently linking two T-2635 fusion peptides to one CD4 anchoring mAb. This new BFFI targets the CD4 receptor instead of CCR5, which makes the molecule active against both R5-tropic and X4-tropic viruses. In addition to this benefit, by simultaneously targeting both the cell surface CD4 receptor and the virus gp41, the BFFI showed extremely high anti-HIV potency with IC_{50} value as low as 0.014 nM against certain virus strains, and the BFFI showed less susceptibility to cell surface receptor density change or virus mutation. Despite the strong inhibition activities, the major problem with these antibody-derived BFFIs is that they have to be produced in mammalian cells, which greatly increases the cost and difficulty of production and limits their practical value as anti-HIV therapeutics.

The newest "multi-purpose" inhibitor in this class was published by our lab. Griff37 comprises one gp120 targeting protein griffithsin covalently linked to one C-peptide, C37 (96). Griff37 showed higher anti-viral potency than either griffithsin or C37 when they were acting alone. It also inherited the ability of griffithsin and C37 to inhibit both R5- and X4-tropic viruses. Griff37 is fully recombinant, and is easy to produce in large amounts in *E. Coli*.

During my Ph.D. study, we independently developed a similar strategy, and designed two new chimeric HIV inhibitors. These chimeric inhibitors showed extremely strong antiviral activities against both R5 and X4 strains with IC_{50} value as low as 0.004 nM, which is probably the strongest reported so far by anyone. They also work extremely well on human peripheral blood mononuclear cells, which are natural targets of HIV. The mechanism of action of the chimeric inhibitors was also characterized using biochemical methods. Results of this study also suggest a potent approach for optimizing existing HIV entry inhibitors or designing new inhibitors. Details of this study will be further discussed in Chapter IV.

CHAPTER II

CHARACTERIZATION OF THE GLYCOSAMINOGLYCAN-BINDING MECHANISM OF vMIP-II*

Introduction

GAG binding plays an important role in chemokine function. While GAG binding is not essential for receptor binding *in vitro* (23-26), several studies have demonstrated that the ability of a chemokine to bind GAGs is critical for *in vivo* function (27-29). GAGs control chemokine function in many ways: GAGs help immobilize chemokines on the endothelial cell surface (30-31), where natural chemokines presumably form a concentration gradient (31-36), and these chemokines recruit leukocytes to move along the gradient by activating chemokine receptors on the leukocyte surface (37). GAG binding also protects chemokines from proteolysis and induce chemokine oligomerization (38-39). Overall, GAG binding helps chemokines to increase their local concentrations and enhance receptor signaling (23,25,40-41).

Very little has been reported about vMIP-II's ability to bind glycosaminoglycans (GAGs) on the luminal surface of the endothelial cells. The major role of vMIP-II is regulating immune responses, and as with human chemokines, GAG binding may be

---

* Part of the data reported in this chapter is reprinted with permission from "Characterization of the Interactions of vMIP-II, and a Dimeric Variant of vMIP-II, with Glycosaminoglycans" by Bo Zhao and Patricia LiWang, 2010, Biochemistry, 49, 7012-7022, Copyright 2011 by American Chemical Society.

essential for for vMIP-II to perform its natural function *in vivo*. vMIP-II may build up its own concentration gradient at the infection site and disrupt leukocyte recruitment, possibly by competing with human chemokines for binding to many chemokine receptors on the leukocyte surface, and/or by displacing chemokines from cell surface GAGs to disrupt the normal human chemokine gradient. Therefore, it is important to understand the GAG binding mechanism of vMIP-II.

Several structural studies suggested that chemokines' GAG binding is mediated by basic residues on the chemokine surface, since cell surface GAGs are negatively charged polysaccharides. Previous studies on MIP-1β and RANTES confirmed that positively charged residues like R18, and the 40's loop BBXB domain residues (named for Basic-Basic-Any-Basic amino acids) are critical for GAG binding (24,97-98). For MCP-1, basic residue R18, K19, R24, and K49 forms the primary GAG binding site (99). Quaternary structure of the chemokine also plays an important role in GAG binding. The currently accepted hypothesis is that the dimer form is more capable of binding GAGs, while the monomeric form of the chemokine is responsible for binding the receptors (100). It is likely that chemokines bind GAGs in the dimer or oligomeric form and then dissociate into monomers to bind to the receptors (24,100-101).

The structure of vMIP-II has been solved by both NMR (53-55) and X-ray crystallography (56-57). vMIP-II is a highly basic protein with 8 Lys and 5 Arg out of 71 total residues, and is predominantly a monomer under most conditions (53-55,57), although under some crystallization conditions it has been observed as a dimer (56). In the present report, a high affinity vMIP-II dimeric variant has been designed. We

present full backbone assignments of the dimeric vMIP-II variant by NMR, and demonstrate that vMIP-II provides an excellent opportunity to study the structural and functional differences between the two quaternary structural forms of chemokines at the atomic level. Mutagenesis, NMR, chromatography, and molecular docking are described to characterize the GAG binding mechanism of both quaternary structural forms of vMIP-II. Results show that vMIP-II uses a very similar mechanism as human chemokines to bind GAGs despite having many more basic residues than its close homolog, human MIP-1β, and also show an interesting role for chemokine dimerization in GAG binding.

Experimental Procedures

Protein preparation. The gene for vMIP-II was synthesized using overlapping oligonucleotides. vMIP-II mutations were made using the QuikChange Site-Directed Mutagenesis method (Stratagene, La Jolla, CA). vMIP-II wild type and variants were expressed in the pET-32a(+) expression vector along with a thioredoxin fusion tag (Novagen, Madison, WI). The vectors were transformed into BL21(DE3), and grown in 1 liter ^{15}N minimal medium using $^{15}NH_4Cl$ as the only nitrogen source. For NMR chemical shift assignment experiments, ^{13}C-labeled glucose was used as the only carbon source to produce the ^{13}C-^{15}N-labeled L13F variant, while for other mutants unlabeled glucose was used. Protein production was induced with 1 mM IPTG. The cells were harvested by centrifugation 4 hours after induction. The cell pellet was resuspended in

refolding buffer (5 M Guanidinium/HCl, 3 mM EDTA, 50 mM Tris, 50 mM NaCl, pH 8.0) with 10 mM benzamidine, and French pressed twice at 16,000 psi. The solution was incubated at room temperature for 2 hours with stirring followed by a centrifugation at 20,000 ×g for 30 minutes. The supernatant containing the denatured protein was passed through a Ni chelating column and eluted with imidazole in 5 M guanidinium chloride, 50 mM Tris (pH 8.0), 500 mM NaCl. The purified proteins were slowly stirred overnight with the addition of 10 mM β-mercaptoethanol, and refolding was carried out by dialysis against 50 mM NaCl, 2 mM $CaCl_2$, 20 mM Tris-HCl (pH 8.0). To remove the fusion tag, recombinant enterokinase (Novagen, Madison, WI) was added and the solution was incubated 3-7 days at room temperature. Precipitated matter was removed by centrifugation at 20,000 ×g for 30 minutes and the enterokinase digested protein was purified on a C4 reversed phase chromatography column (Vydac, Hesperia, CA) using an Akta purification system (GE Healthcare), and lyophilized by the Labconco freeze dry system (Labconco Corporation, Kansas City, MO).

NMR spectroscopy. All NMR data were acquired at 25 °C on Varian Inova 500 or 600 MHz, or Bruker 600 MHz spectrometers. NMR samples were prepared by adding lyophilized proteins into 20 mM sodium phosphate (pH = 2.5, 5.4, or 7.4, depending on the specific requirement for each experiment). The effect of pH variation on chemokine quaternary structure was also evaluated by NMR. While many CC-chemokines require low pH to avoid aggregation, vMIP-II was soluble throughout the range of pHs examined. The chemical shift was referenced relative to internal DSS (2,2-dimethyl-2-silapentane-5-sulfonic acid) (102). The data were processed using NmrPipe (103) and

analyzed using PIPP (104). For 2D HSQC spectra, SW=6982.631 Hz (^{1}H) and 1700.030 Hz (^{15}N), with 512* points in ^{1}H and 128* points in ^{15}N. The 3D HNCACB experiments were acquired with SW=7804.117 Hz (^{1}H), 9599.232 Hz (^{13}C) and 1619.991 (^{15}N), number of points are 512* in ^{1}H, 64* in ^{13}C, and 32* in ^{15}N.

NMR titration. Titrations of wild type vMIP-II and vMIP-II dimeric variant Leu13Phe with disaccharide I-S (V-labs, Covington, LA) were performed in 20mM Sodium Phosphate buffer at pH 7.4. Aliquots from stock solutions of disaccharide (I-S also dissolved in 20mM Sodium Phosphate buffer at pH 7.4) were added to samples of 0.1–0.3 mM ^{15}N-labeled protein. At the concentrations used, wild type vMIP-II was observed to be entirely monomeric except upon the addition of 1500 μM disaccharide, and for the L13F variant, only a single set of peaks (dimer) were observed. Maximum concentration of I-S titrated was 1500 μM in wild type vMIP-II, and 900 μM in vMIP-II L13F. One ^{1}H-^{15}N HSQC spectrum was acquired after each titration. The change in pH of the protein sample upon addition of disaccharides was negligible. For every I-S titration experiment, the change in HSQC cross-peaks of the backbone amide groups of the vMIP-II proteins were calculated as in Equation 1 (105), the observed total chemical shift perturbation (Δδobs) for each residue can be calculated as the weighted average chemical shift changes of the ^{1}H (ΔδH) and ^{15}N (ΔδN).

$$\Delta\delta obs = \{[(\Delta\delta H)^2 + (\Delta\delta N/5)^2]/2\}^{1/2} \quad \text{(Eq. 1)}$$

In the presence of different concentrations of disaccharides, the chemical shifts for vMIP-II is the population-weighted average of the chemical shifts of free and disaccharide-bound protein. As defined in Equation 2, the observed chemical shift

perturbation Δδobs is related to the ratio of disaccharide-bound vMIP-II to total vMIP-II (Vb/Vt),

$$\Delta\delta obs = (Vb/Vt) * \Delta\delta max \quad \text{(Eq. 2)}$$

where Δδmax is the difference of the chemical shifts between the fully bound and free form of vMIP-II, Vb is the concentration of bound vMIP-II, and Vt is the total concentration of vMIP-II. Assuming that one disaccharide binds only one vMIP-II monomer (or one subunit of the dimeric vMIP-II L13F variant), the ratio Vb/Vt can be calculated by Equation 3 (106),

$$Vb/Vt = 0.5\{(1 + KdVt + Dt/Vt) - [(1 + Kd/Vt + Dt/Vt)^2 - 4*Dt/Vt]^{1/2}\} \quad \text{(Eq. 3)}$$

where Dt is the total concentration of disaccharide I-S and Kd is the apparent dissociation constant of the vMIP-II I-S complex. For each titration, the ratio Dt/Vt and the Δδobs for those residues that undergo disaccharide-induced chemical shift changes are fit to Equations 2 and 3 using KaleidaGraph 3.5 (Synergy Software, Reading, PA) to give an apparent dissociation constant Kd for each residue.

Heparin chromatography. Lyophilized proteins were dissolved in 0.5 mL 50 mM Tris buffer (pH 7.4) and injected into a 1 mL Hi-Trap heparin column (GE Healthcare). The column was rinsed with 5 mL Tris buffer and followed by a NaCl concentration gradient from 0 M to 1 M in the same buffer (50 mM Tris, pH 7.4) with the flow rate of 0.5 mL/min. The absorbance at 280 nm was monitored. Each experiment was done in duplicate to ensure the repeatability of the results. The same experiments were repeated on 1 mL Hi-Trap SP columns (GE Pharmacia) as a control. Essentially no differences in

results were observed when 50 mM sodium phosphate buffer was used instead of Tris buffer.

Analytical ultracentrifugation (AUC). Sedimentation equilibrium analyses were performed at 25 °C on a Beckman Optima XLA analytical ultracentrifuge, using an AN 60 Ti rotor with multiple speeds and variable protein concentrations to obtain the molecular weight and dimer dissociation constant of the proteins. Wild type vMIP-II and L13F samples of different concentrations were dissolved in 20 mM sodium phosphate buffer containing 150 mM NaCl at pH 2.5, 5.4 and 7.4. Samples were centrifuged at 3,000, 15,000, 35,000, and 42,000 rpm. During each equilibrium experiment, samples were monitored by measuring the absorbance at 280 nm. The data were processed with the software "Origin" (107), and each set of experimental data was fit to single ideal model or monomer–dimer equilibrium model using a nonlinear least squares fit. Wild type vMIP-II at pH 2.5 and 5.4 only fit a to single ideal monomer model, and were not able to be fit to a monomer-dimer equilibrium. Wild type vMIP-II at pH7.4 and vMIP-II L13F at all pH values fit best to monomer-dimer equilibrium models. Vbar for each protein was estimated using software Sednterp (www.rasmb.org), and the dimer dissociation constant (108) was calculated using the standard method described previously (109-110) using the fit Ka from Origin (107).

NMR constraint-driven molecular docking. Molecular docking of disaccharide Heparin I-S on monomeric and dimeric vMIP-II (protein data bank code: 1VMP, 1CM9 respectively) was performed using the software HADDOCK2.1 (Alexandre Bonvin, Utrecht University). Experimental data such as the chemical shift perturbation data from

the NMR titration and mutagenesis data on the heparin column are introduced as Ambiguous Interaction Restraints (AIRs) to drive the HADDOCK docking process.

Residues with a chemical shift perturbation higher than the average chemical shift perturbation plus one standard deviation were selected as “active” residues as defined in HADDOCK instructions. The protein structures were further analyzed using the VADAR server, and residues with less than 50% surface accessibility were excluded. “Passive” residues are defined as the residues that are within or near the “active” residues, but only residues with more than 50% surface accessibility were selected. “Active” and “passive” residues were used to generate the Ambiguous Interaction Restraints (AIRs) (111) to drive the docking.

Optimized parameters for liquid simulation (OPLS) were used, as described in the HADDOCK instruction manual. The geometric coordinate and parameter files for the proteins were parallhdg5.3.pro and topallhdg5.3.pro. For the ligand (H1S from the RANTES disaccharide complex 1U4L), the parameters were calculated and optimized using the PRODRG server (112).

For both monomeric and dimeric vMIP-II, the docking was performed in 1:1 ratio of disaccharide: protein (the dimeric vMIP-II was defined to use only one of the two identical subunits for docking). For each docking experiment, a total of 1000 complex structures were calculated during the rigid body docking, and the best 200 structures in terms of intermolecular energies were further analyzed with semiflexible annealing and water refinement. The root-mean-square deviations (rmsd) of the final set of docked structures were calculated, and the final structures were clustered using the algorithm

described in Daura et al. (113). The clusters were scored using a weighted sum of a combination of energy terms.

Results

Design of a vMIP-II dimer in solution. Chemokines can exist in a variety of quaternary states, which are influenced by solution conditions (97,101,114). However, the viral chemokine analog vMIP-II is observed to be predominantly monomeric in solution under most conditions, even at millimolar concentrations (Figure 2.1B) (53-55). To investigate how different quaternary states of vMIP-II interact with disaccharide in solution, we designed a vMIP-II variant which is a high affinity dissociable dimer in solution. Most human CC chemokines have a Phe or Tyr in the 13th position. In MIP-1β, the human analog of vMIP-II, Phe13 is the single most important residue for both of its quaternary structure and function. The mutant Phe13Leu disrupts dimer formation in MIP-1β, greatly reduces its GAG binding affinity (24), and also caused more than a 100 fold drop in CCR5 receptor binding affinity (115). vMIP-II, unlike its human analogs, has a Leu in its 13th position. To further investigate the role of the 13th position in vMIP-II, we mutated Leu13 to Phe and analyzed the structural and functional changes. Analytical ultracentrifugation (AUC) experiments on this vMIP-II variant revealed that vMIP-II L13F is a dimer in solution, with a Kd of 41 μM at pH 5.4, while wild type vMIP-II is a monomer under these conditions (Figure 2.1A). Moreover, the dimerization of vMIP-II L13F was found to be dependent on pH, with a Kd ranging from 129 μM at

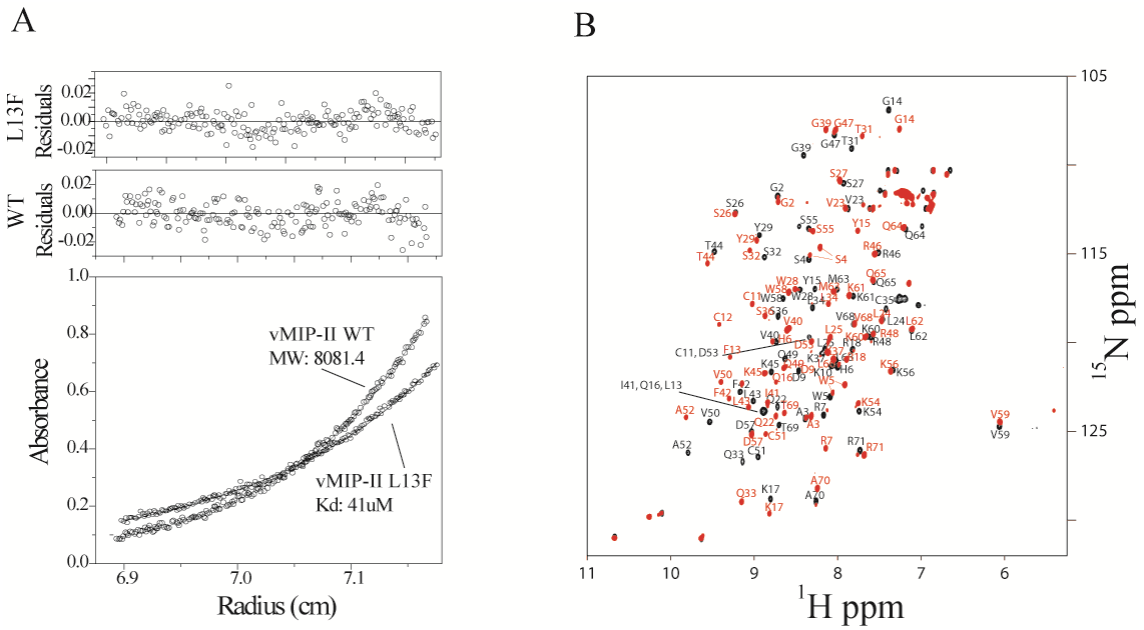

Figure 2.1 vMIP-II L13F is a dimer in solution. **A.** Analytical Ultracentrifugation data at pH 5.4. Wild type vMIP-II fits only to a single ideal monomer model, giving a fitted molecular weight that is the same as that calculated from the protein sequence. The vMIP-II L13F mutant fits to a monomer-dimer equilibrium model, with a dissociation constant of 41 μM. **B**. Overlay of the chemical shift assigned ^{15}N HSQC spectra of wild type vMIP-II (black) and vMIP-II L13F (red), both at pH 5.4 and 1 mM concentration. Peak shifts upon mutation were observed at many residues, not only at the mutation site.

pH 2.5; a Kd of 41 μM at pH 5.4; to a Kd 0.74 μM at pH 7.4 (data not shown). This is in contrast to wild type vMIP-II, which is almost universally observed as a monomer, although AUC experiments show that it has a very weak tendency to dimerize at pH 7.4.

As shown in Figure 2.1B, the L13F mutation causes dramatic change in the ^{15}N HSQC spectrum compared to the wild type protein, not only at the 13th position, but also at many other residues. Given the results of the analytical ultracentrifugation, it is likely that the change in spectrum in the mutant is due to dimerization, a possibility that is supported by the known structures of chemokine dimers. Chemokines form two different kinds of dimer, the CC type dimer (which uses the N-terminus and 30's loop as dimer interface) (116), and the CXC type dimer (which uses β-strand 1 and the C-terminal helix to dimerize) (117-119). Since a crystal structure of wild type vMIP-II shows a CC-type dimer (PDB code 1CM9) (56), it is likely that the dimer form of vMIP-II L13F is also a CC type dimer. To enable further analysis of the dimerization of L13F, an HNCACB experiment was performed. Full backbone chemical shift assignments (^{1}H, ^{15}N, $^{13}C\alpha$, $^{13}C\beta$) of vMIP-II L13F were determined using standard methods, and the assignment is shown in Figure 2.1B. This sequence assignment enabled a residue-by-residue comparison with the wild type protein, resulting in an estimation of the relative extent of structural changes for each residue. The results (Figure 2.2) showed that the greatest chemical shift perturbations occurred in the N-terminus, N-loop, 30's loop, and residues 50-52 which are the same areas expected to be involved in a CC chemokine dimer, and correspond well to the vMIP-II dimer crystal structure, indicating that vMIP-II L13F indeed very likely forms a CC type dimer.

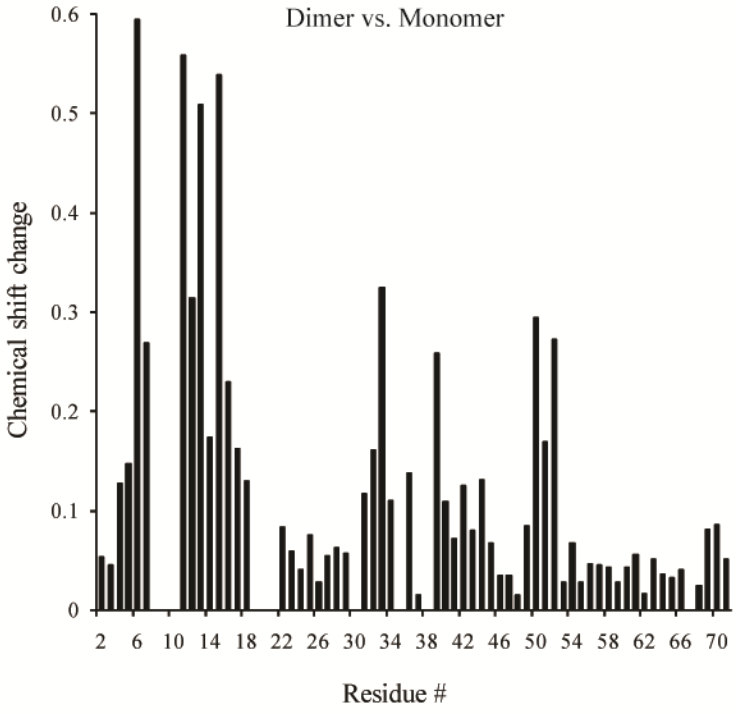

Figure 2.2 Chemical perturbation chart. The chemical shift difference of each residue between the monomer (wild type) form and the dimer form (vMIP-II L13F) is mapped out.

Wild type vMIP-II and vMIP-II L13F therefore show two distinct forms of quaternary structure in solution, which provide a good model to study the relationship between chemokine quaternary structure and chemokine - GAG binding function.

NMR studies of disaccharide binding by wild type vMIP-II. NMR studies were carried out to map the important residues in the vMIP-II - GAG interaction. Polysaccharides would be ideal for studying this interaction, but the presence of either heparin or low molecular weight heparin (which is a mixture of heparins with an average length of about 10 saccharide units) in solution caused dramatic aggregation of the protein. So the disaccharide I-S, which has been used in several chemokine binding studies, was used instead (97-98,101,120). Using the known sequential assignments of the wild type vMIP-II, ^{1}H-^{15}N HSQC experiments were carried out to monitor the chemical shift changes of each residue upon titration of the protein with heparin disaccharide I-S. An overlay of the HSQC spectra of wild type vMIP-II containing different concentrations of disaccharide clearly shows changes, indicating binding or conformational change in several areas (Figure 2.3). Another notable difference observed after titrating in 1500 μM I-S was the appearance of new peaks. These indicate the formation of a vMIP-II dimer, consistent with previous results that adding high concentration disaccharide does promote dimerization of chemokines (24,40,101,121), even for this "monomeric" chemokine.

The chemical shift perturbation of each residue upon titration with heparin I-S disaccharide is shown in Figure 2.4A, where red stars indicate the regions that undergo the most change in chemical shift during the titration. Residue R18, L25, K45, R48,

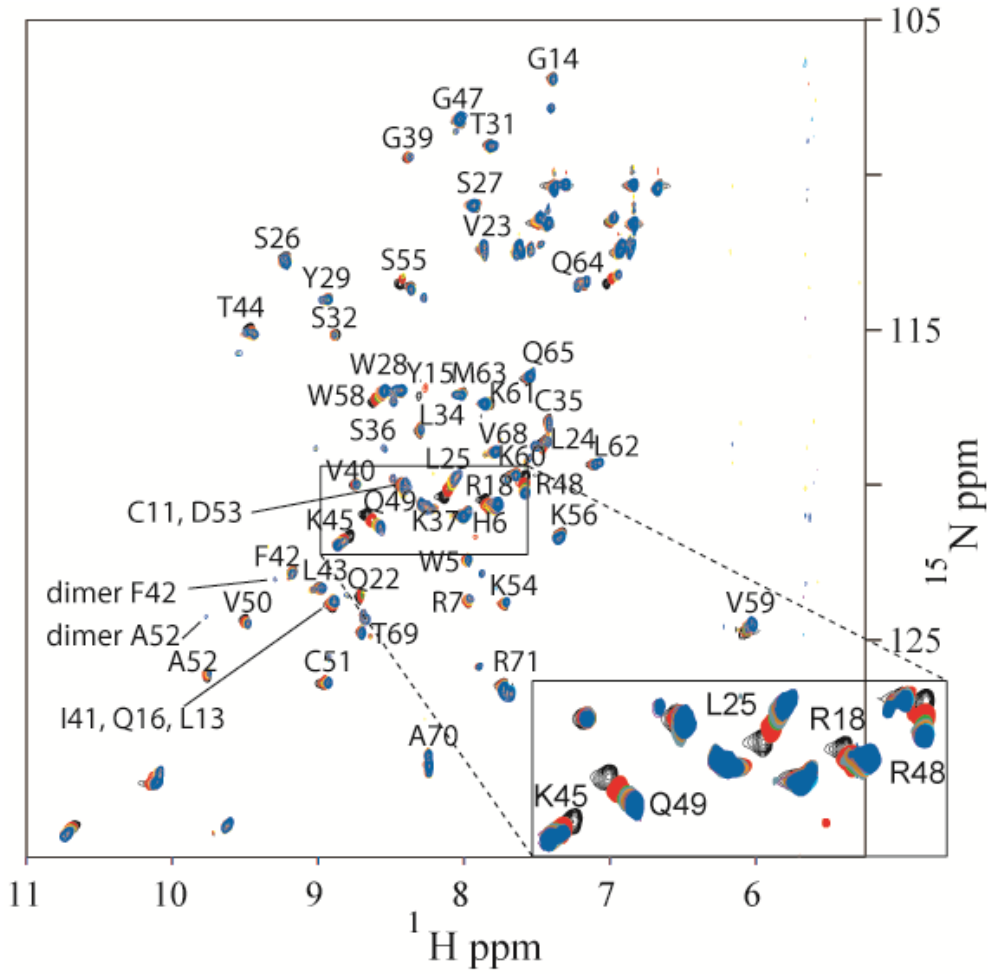

Figure 2.3 ^{15}N HSQC spectral overlay of wild type vMIP-II (150 μM, pH 7.4) titrated with heparin I-S disaccharide with peak assignment. Selected peaks are labeled. A separate color is shown for the spectrum at each titration amount: Black, 0 μM I-S; Red, 200 μM I-S; Green, 400 μM I-S; yellow, 600 μM I-S; Purple, 800 μM I-S; Brown, 900 μM I-S; Turquoise, 1100 μM I-S; Salmon, 1300 μM I-S; Blue, 1500 μM I-S.

Q49 and W58 undergo the most significant chemical shift change, and the apparent affinity of I-S binding to these residues is calculated by plotting the chemical shift perturbations at different I-S concentrations and fitting to a saturation curve (Figure 2.4B). The maximum concentration of disaccharide titrated was 1500 μM, since higher concentration caused severe precipitation, so the fully saturated concentration may not have been achieved. This residue-specific data allows an estimation of the binding affinity of the heparin I-S to vMIP-II. The data of the 3 adjacent 40's loop residues K45, R48 and Q49 all can be fit with a similar Kd around 113 μM, and another positively charged residue R18 also has a similar apparent Kd of 160 μM. These residues possibly form a binding groove for the disaccharide, which is in agreement with findings on its human chemokine analogs that R18 and the 40's loop BBXB domain are critical GAG binding sites. The other basic residue, R46 in vMIP-II's BBXB domain, was not visible on these HSQC spectra at pH 7.4, so we were unable to assess the importance of this residue on disaccharide binding with this NMR experiment. Interestingly, a comparison of the structure of vMIP-II with the chemical shift perturbation shows that the residues undergoing the most significant chemical shift changes are all located on one face of the protein. In contrast, residues from the other surface of the protein do not show significant changes, even the positively charged residues K37, K54, K56, K60 and K61 (Figure 2.5).

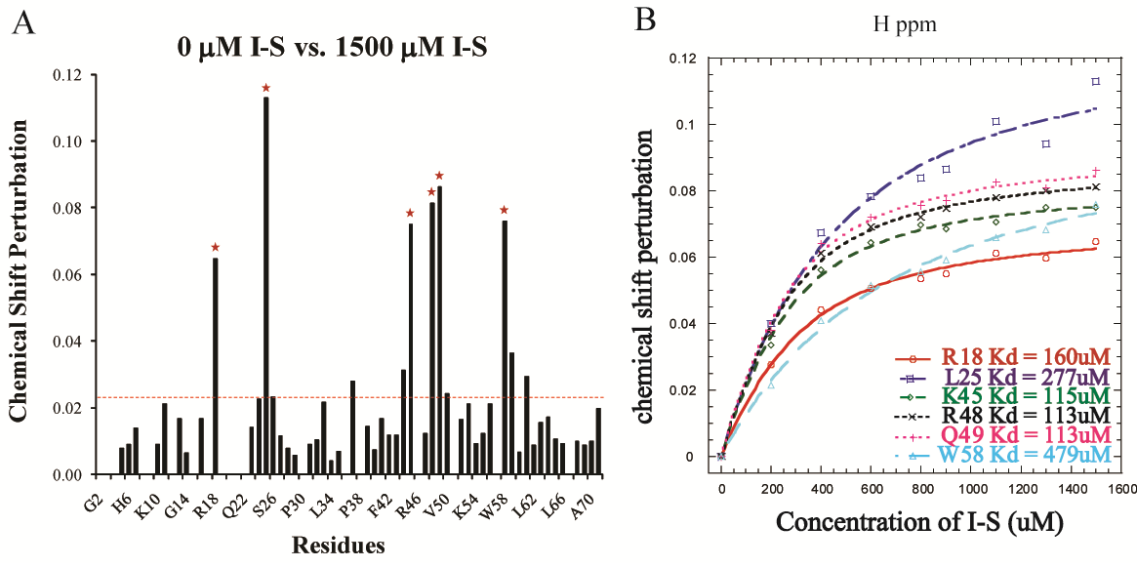

Figure 2.4 Chemical shift perturbation of vMIP-II WT upon I-S titration and I-S binding affinity calculation. **A**. Chemical shift perturbation of wild type vMIP-II after titration with 1500 mM disaccharide I-S. The red dashed line indicates the average value of the chemical shift perturbation; the red stars indicate the residues that undergo the significant chemical shift change and do not overlap with other residues in the spectra. **B**. Heparin I-S binding affinity calculation for the 6 residues labeled by red stars in A.

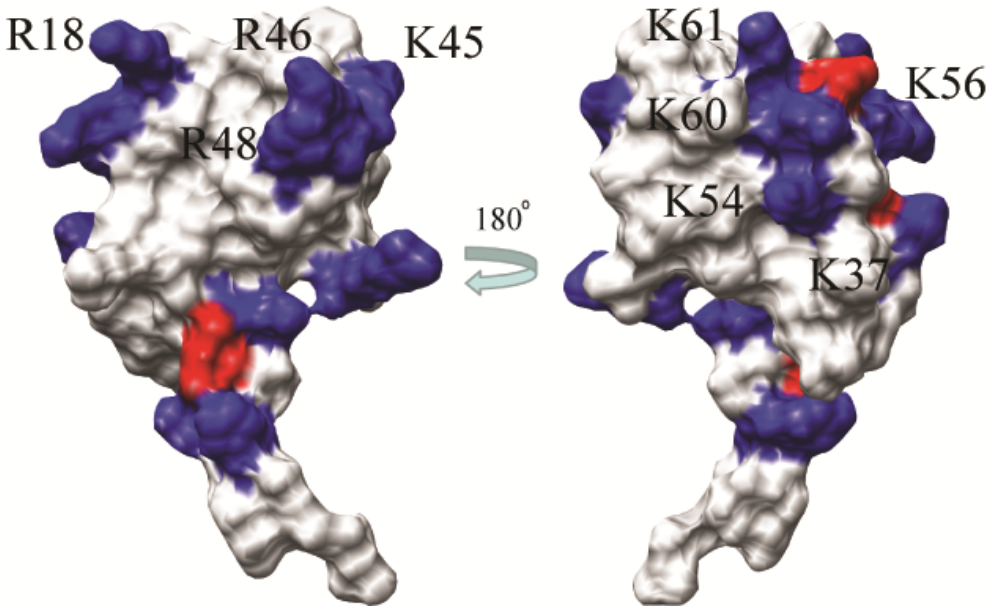

Figure 2.5 Surface charge figure of vMIP-II. Residues with positive charge and negative charge are colored blue and red, respectively. Left panel, the "front" surface, containing R18, R46, and R48; Right panel, the "back" surface of vMIP-II.

Heparin chromatography of vMIP-II variants. The small size of heparin I-S (MW = 665) makes it in several ways unlike a physiological GAG, which has many more saccharide units that likely confer higher affinity binding due to avidity and possibly structural arrangement. As mentioned above, NMR experiments in the presence of the longer "low molecular weight heparin" resulted in precipitation and no usable results could be obtained (data not shown). Therefore, to confirm our findings from the NMR experiments, and to provide data on the interaction of vMIP-II with longer chain GAGs, heparin chromatography was carried out on vMIP-II and its variants to determine whether the residues mapped by NMR in the presence of disaccharide are also important in binding polysaccharides.

Several variants of vMIP-II were constructed and purified (Table 2.1). The HSQC NMR spectrum of each variant was measured, and all mutants showed similar spectral attributes as the wild type vMIP-II (data not shown), indicating the mutations did not affect the overall structure of the protein. Commercially prepared immobilized heparin is a highly sulfated polysaccharide with 20-25 repeated units of disaccharides. Proteins are loaded onto the heparin column, and then eluted using NaCl buffer. The elution concentration of NaCl indicates the strength of the interaction between the protein and heparin. As a control, the same experiments are repeated on an SP cation exchange column, which contains only the negatively charged sulfate but not the polysaccharides, to estimate the extent of specific binding to heparin versus the electrostatic binding to the sulfate groups of the SP column.

Table 2.1 Heparin binding affinities for vMIP-II variants as measured by NaCl elution concentrations.

vMIP-II Mutant	Heparin NaCl (mM)	SP NaCl (mM)	$\Delta NaCl^{Hep}$ (mM)	$\Delta NaCl^{SP}$ (mM)
WT	630±1.5	623±1	/	/
R18A	473±1/585±1.5	487±0.5	157/45	136
K45A	593±0.5	545±0.5	37	78
R46A	535±0.5	503±1.5	95	120
R48A	514±2	512±0.5	116	111
R46AR48A	449±0.5	419±1	181	204
K45AR46AR48A	438±1	390±1	192	233
K54A	611±1.5	617±1	19	6
L13F	753±1	653±2	-123	-30
P8AL13F	561±1	626±1	69	-3
L13A	564±2	626±0.5	66	-3

Every experiment was done in duplicate.

ΔNaCl indicates change in NaCl elution concentration from the wild type value.

All elution profiles are similar in peak shape and height, and no unbound flow-through peaks were observed.

For R18A, 2 peaks of about equal size were observed.

As shown in Table 2.1, wild type vMIP-II binds tightly to the heparin column, requiring 630 mM NaCl for elution. As a comparison, human chemokine MIP-1β has been shown to elute earlier, at 500 mM NaCl (24,100); and the chemokine RANTES, a more basic protein than MIP-1β and also a dimer, has been shown to elute at 800 mM (122). Single point mutations in vMIP-II at R18 and each of the basic residues of the BBXB motif to Ala significantly decreases the binding affinity of vMIP-II to heparin (Table 2.1). Among the 40's loop point mutants, R46 and R48 show a significant effect, and K45A shows the least effect. Double mutant R46A/R48A and triple mutant K45A/R46A/R48A on the 40's loop BBXB domain were also made, and these variants showed the greatest loss of heparin binding affinity among all mutants (Table 2.1). As a control, each mutant was also bound to a sulfate-containing cation-exchange SP column (Table 2.1). As expected, all the mutants with a loss of a positively charge residue exhibited reduced affinity for the negatively charged SP column.

Unlike the basic residues in the putative binding site formed by R18, K45, R46 and R48, positively charged residues on the other face of vMIP-II are not very important for GAG binding. For instance, residue K54 is located in the middle of the "back" surface. Heparin and SP chromatography results showed that the K54A mutation did not affect binding to GAGs (Table 2.1).

For these variants with mutations on the positive charged residues, the heparin and SP chromatography profiles showed that the vMIP-II - GAG interaction is site-specific, and the nature of this interaction is almost purely electrostatic between the positively charged residues of the binding site and the negatively charged sulfate groups on GAGs.

Dimeric vMIP-II variant binds GAGs more tightly than the wild type protein. The vMIP-II L13F dimeric variant requires 753 mM NaCl for elution from the heparin column, which is much more than for the wild type protein (Table 2.1). As a control for the presence of Phe at the 13th position (as opposed to dimer formation), a mutation at a different site was made to vMIP-II L13F to abrogate the dimer. The mutation from proline to alanine at the 8th position has been shown for several chemokines to disrupt the wild type dimer (115,123). We made a P8A mutation in addition to the L13F mutation on vMIP-II, and this double mutant was indeed a folded monomer in solution as judged by NMR (data not shown). The P8AL13F vMIP-II did bind to heparin column with much lower affinity than L13F vMIP-II (Table 2.1), indicating that quaternary state is indeed a key mediator of GAG binding. In a comparison with wild type vMIP-II, the P8AL13F variant showed slightly reduced binding affinity to the heparin column. To further test the importance of the 13th position in vMIP-II, we made an L13A mutation which would reduce the size of the wild type side chain. As judged by HSQC spectrum, L13A was also observed to be a monomer in solution as expected (data not shown). L13A not only showed a large decrease in the elution concentration of NaCl from the dimeric L13F, but also a moderate decrease compared to the wild type protein (Table 2.1).

Chromatography experiments on an SP sepharose column were carried out as a control for electrostatic interactions versus specific binding to GAGs (Table 2.1). Since no change in charge was involved in these mutations, little difference between L13 mutants and wild type protein was observed for SP column elution, as expected, unlike

the large difference observed for the heparin column. Similarly, the P8AL13F and L13A mutations, which gave a moderate decrease in affinity for heparin column, had almost no effect on binding the cation-exchange SP column. This indicates that the overall structure (i.e. dimer) of the L13F mutant is responsible for the tighter binding to heparin, rather than simply an increase in local positive charges.

NMR studies of disaccharide binding by the dimeric vMIP-II L13F. Since different quaternary states of vMIP-II clearly have different GAG binding ability, a NMR titration experiment was carried out to study the disaccharide binding properties of the vMIP-II L13F dimer. Heparin I-S was titrated to the vMIP-L13F protein solution, up to 900 μM (higher concentrations of I-S caused aggregation). The resulting chemical shift perturbation upon titration of heparin I-S with dimeric L13F is shown in Figure 2.6. The backbone sequence assignment allows a residue-by-residue comparison between the wild type and dimeric variant upon GAG binding. Similar to the wild type protein, the important residues for heparin I-S binding on the L13F variant are also apparently located at R18 and the 40's loop. The residues L25, V59, basic residues of the N-loop K17, R18, basic residues of the 40's loop K45, R46, and R48 undergo the most spectral change upon heparin I-S binding. Large differences in chemical shift are also apparent at the N-terminus of the L13F mutant upon titration with disaccharide (Figure 2.6A), unlike the wild type protein, where the N-terminal peaks are either not significantly perturbed or not visible in the spectrum.

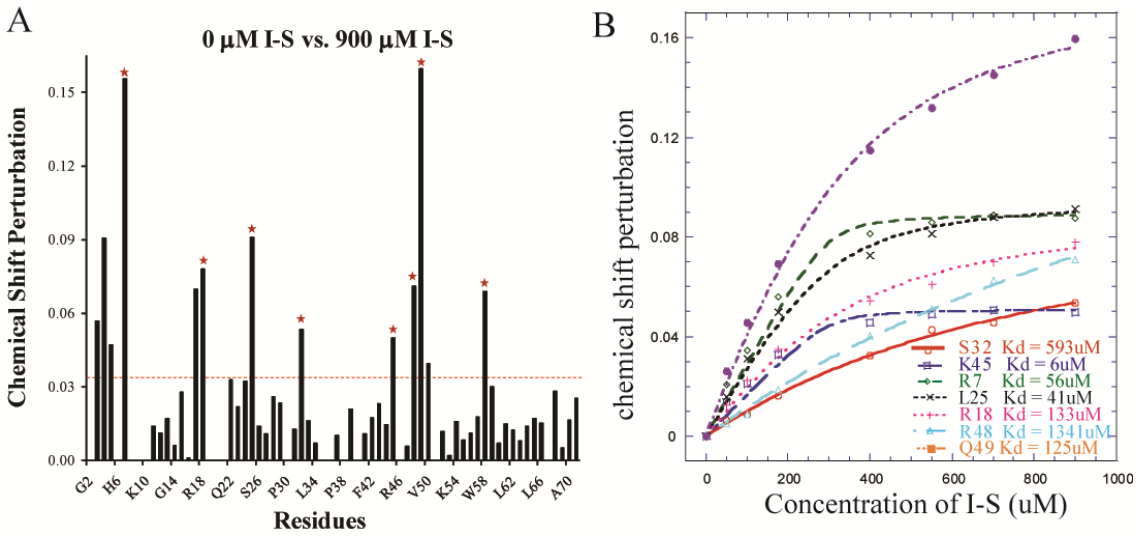

Figure 2.6 Chemical shift perturbation of vMIP-II L13F upon I-S titration and I-S binding affinity calculation. **A**. Chemical shift perturbation chart of vMIP-II L13F titrated with heparin disaccharide I-S. The red dashed line indicates the average value of the chemical shift perturbation; the red stars indicate the residues that undergo the most significant chemical shift change and that do not overlap with other residues on the spectra. **B**. Heparin I-S binding affinity calculation for the residues labeled by red stars in A.

Modeling of disaccharide interaction with monomeric and dimeric vMIP-II. To further characterize and compare the GAG binding mechanisms of monomeric and dimeric vMIP-II, we used molecular docking calculations, using HADDOCK2.1 (124), a well-established method which uses experimental data as well as energetic and shape complementarity factors to drive molecular docking (125). Chemical-shift data were used to generate the ambiguous interaction restraints (AIRs) for the docking. HADDOCK calculations produced clusters of complex structures, and revealed interesting insights into the likely GAG binding mechanism of vMIP-II.

A representative structure of I-S binding to wild type monomeric vMIP-II (the best structure of the best ranking cluster, in terms of intermolecular binding energy, Table 2.2) is shown in Figure 2.7A and 2.7B, where the disaccharide fits in the binding pocket formed mainly by R46, R48 and R18. An overlay of 8 structures from the same cluster showed a similar binding site with slight variations on the orientation of I-S (Figure 2.8A). The binding site correlates very well with the NMR titration data (Figure 2.8C). Figure 2.7B shows the residues of vMIP-II that possibly contribute to I-S binding. As expected, electrostatic interactions between the negatively charged sulfate groups and the positively charged Arg residues play an important role. While NMR showed a large chemical shift change for L25, which is located in the middle between R46, R48 and R18, this residue is not exposed on the surface, so the significant chemical shift change is probably due to structural perturbations, not direct saccharide binding.

Figure 2.7 HADDOCK model of the vMIP-II/disaccharide I-S interaction. Positively charged and negatively charged surface regions of vMIP-II are shown in blue and red, respectively. For both vMIP-II and disaccharide, yellow, red, and blue colors represent sulfur atoms, oxygen atoms, and nitrogen atoms, respectively. **A**. A model of the interaction of monomeric vMIP-II (PDB code 1VMP) in complex with disaccharide I-S (from PDB 1U4L). A representative complex structure from Cluster 1 is shown. **B**. A close-up view of the binding site of A, with side chains of the important residues shown. **C**. An energetically less favorable model calculated by HADDOCK which represents a possible alternative mode for monomeric vMIP-II – disaccharide interaction. **D**. A close-up view of the binding site of C, with side chains of the important residues shown. **E**. HADDOCK model of interaction of dimeric vMIP-II (PDB code 1CM9) in complex with disaccharide I-S (from PDB 1U4L). **F**. A close-up view of the binding site of E, with side chains of the important residues shown.

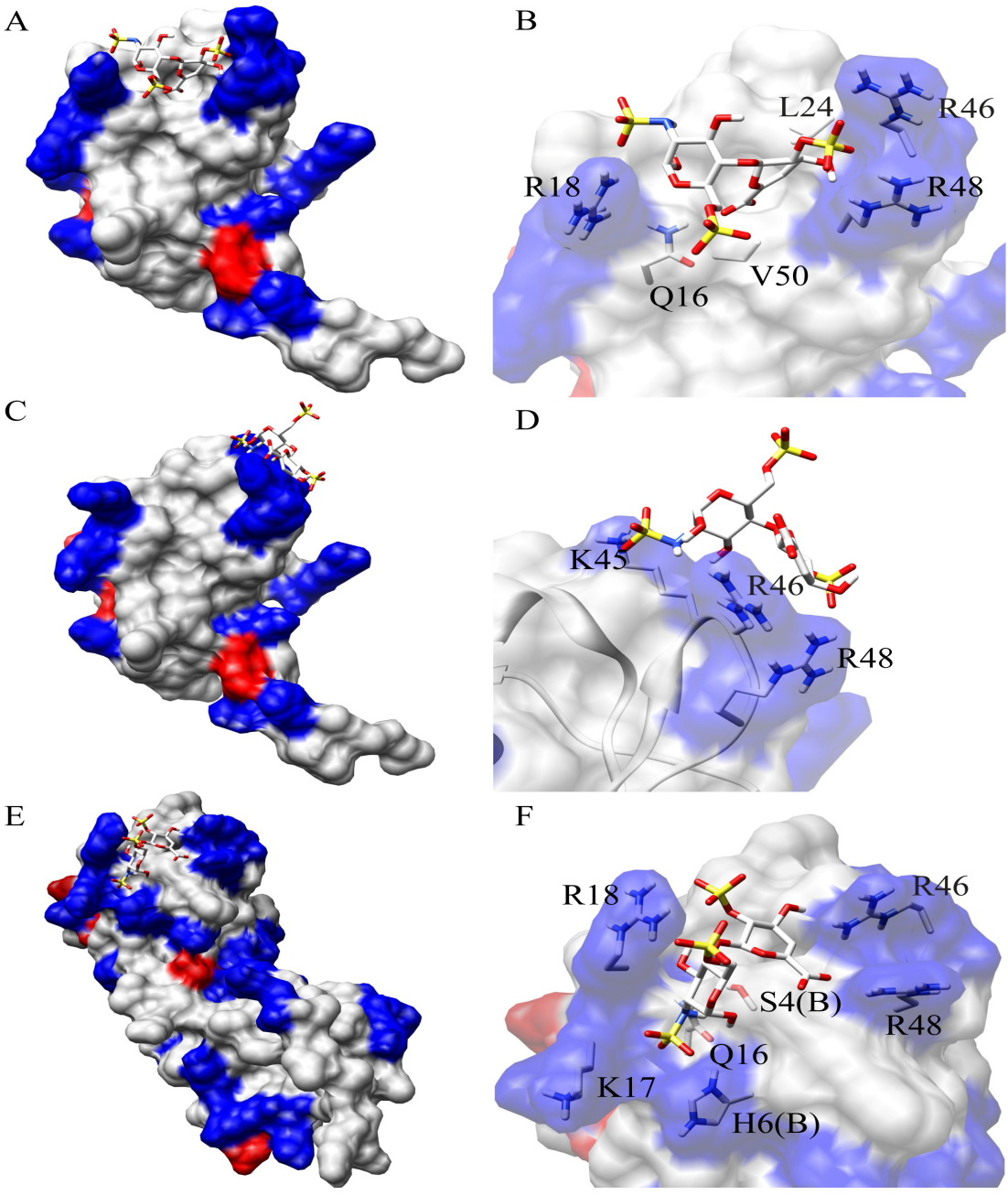
A
B
L24
R46
R18
R48
V50
Q16
C
D
K45
R46
R48
E
F
R18
R46
S4(B)
R48
Q16
K17
H6(B)

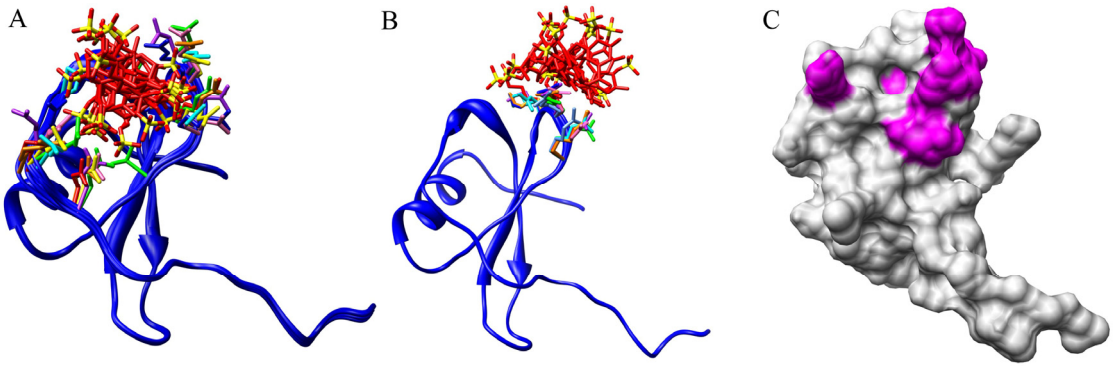

Figure 2.8 HADDOCK clusters of structures of wild type vMIP-II in complex with disaccharide I-S. vMIP-II is shown in blue, with differently colored side chains representing interacting residues from different complex structures. Disaccharide I-S is shown in red, and the sulfur atoms are colored yellow. **A.** Superimposition of the best 8 complex structures from Cluster 1 as calculated by HADDOCK. **B.** Superimposition of the best 8 complex structures from Cluster 2 as calculated by HADDOCK. **C.** Surface map of the vMIP-II monomer structure (1VMP), with magenta regions representing the residues that undergo significant chemical shift perturbations (>1 average + 1 standard deviation) upon disaccharide titration.

Table 2.2 Statistics of the HADDOCK structures of wild type vMIP-II I-S complex[a].

Cluster number	#struc	HADDOCK score[c]	RMSD from best score[d] [Å]	Evdw[e] [kcal Mol^{-1}]	Eelec[e] [kcal Mol^{-1}]
Cluster1	15	-22.7 ± 4.3	0.7 ± 0.1	-11.4 ± 4.1	-14.5 ± 2.7
Cluster2	11	-16.0 ± 6.6	1.2 ± 0.2	-9.3 ± 2.9	-8.8 ± 4.9
Cluster3	5	-9.7 ± 5.3	1.4 ± 0.1	-6.1 ± 1.7	-7.2 ± 3.4

Table 2.3 Statistics of the HADDOCK structures of vMIP-II L13F I-S complex[b].

Cluster number	#struc	HADDOCK score[c]	RMSD from best score[d] [Å]	Evdw[e] [kcal Mol^{-1}]	Eelec[e] [kcal Mol^{-1}]
Cluster1	31	-37.3 ± 5.6	1.8 ± 0.6	-18.0 ± 3.1	-15.3 ± 3.0
Cluster2	8	-37.9 ± 2.8	1.6 ± 0.4	-17.5 ± 1.5	-14.5 ± 1.4
Cluster3	4	-31.0 ± 5.5	2.2 ± 0.7	-21.5 ± 1.2	-19.2 ± 1.4

a) The structures for the wild type vMIP-II I-S complex were clustered with a 2.8 Å cut off according to RMSDs requiring a miminum of four structures per cluster. The clusters are ranked according to the average HADDOCK score.

b) The structures for the vMIP-II L13F I-S complex were clustered with a 1 Å cut off according to RMSDs requiring a miminum of four structures per cluster. The clusters are ranked according to the average HADDOCK score.

c) The HADDOCK score is defined as a weighted sum of energies that are involved in the protein ligand interaction. The default calculation equation provided by the software was used. A lower score indicates lower intermolecular binding energy.

d) Average RMSD of the cluster compared to the lowest energy structure of all calculated structures.

e) Vdw, the van der Waals energy; Elec, the electrostatic energy.

The docking calculation also generated an energetically less favorable cluster, Cluster 2. A representative structure (Figure 2.7C, D) and the structure overlay (Figure 2.8B) shows that in this case I-S binds on a different, nearby site of the protein, making major contact with K45, R46 and R48 (Figure 2.7D). The presence of this Cluster 2 may suggest a possible secondary binding site that may be used when multiple disaccharides or a long chain polysaccharide binds to vMIP-II.

When calculating disaccharide binding of the dimeric form of vMIP-II (Table 2.3), the structures were closely clustered and generated only one binding model. Dimer clusters 1, 2, and 3 all showed very similar structures within 1 Å rmsd to each other, and in all structures the I-S binds in the middle of the pocket formed by R46, R48 and R18 of one subunit and the N-terminus of the other subunit (Figure 2.7E, F and 2.9A). The results also correlated well with the NMR data (Figure 2.9B). Figure 4F shows that in the bound dimer of vMIP-II, the N-terminus of the other subunit inserts into the binding cleft, and is clearly involved in I-S binding. The much lower energy terms compared to the monomer binding calculations also indicates that disaccharide binding to the dimer is more stable and tight, which is consistent with our experimental results such as heparin chromatography.

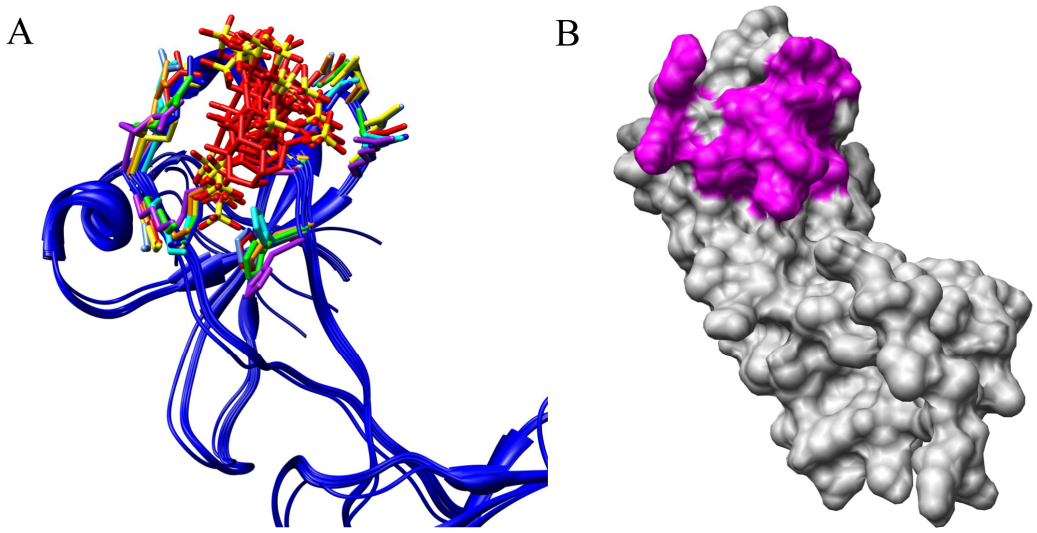

Figure 2.9 HADDOCK clusters of structures of vMIP-II L13F in complex with disaccharide I-S. vMIP-II is shown in blue, with differently colored side chains representing interacting residues from different complex structures. Disaccharide I-S is shown in red, and the sulfur atoms are colored yellow. **A.** Superimposition of the best 8 complex structures from Cluster 1 as calculated by HADDOCK. **B.** Surface map of vMIP-II dimer structure (1CM9), with magenta regions representing the residues that undergo significant chemical shift perturbations (>1 average + 1 standard deviation) upon disaccharide titration.

Discussion

The importance of chemokine quaternary structure in GAG binding has been shown in many chemokine studies (24,97,100-101). The quaternary state of chemokines is determined by many factors. For instance, it has been shown that concentration, pH, and the presence of certain ions such as phosphate can affect the monomer-dimer equilibrium for chemokines (114,126). It has also been shown that GAG binding promotes dimer formation of chemokines (24,40,101,114,121).

The viral chemokine homolog vMIP-II is observed as a monomer in solution under most conditions, including millimolar concentration, in the presence of phosphate, and at a variety of pH values, although under certain crystallization conditions, it has been observed as a CC-type dimer (53-57). In the present experiments, wild type vMIP-II is predominantly observed as a monomer in solution. But the dimeric form of vMIP-II may also play a role in its function as evidenced by its weak tendency to dimerize in analytical ultracentrifugation experiments at physiological pH, and also by the appearance of a small proportion of dimer peaks in the HSQC spectrum in the presence of 1500 μM of Heparin I-S disaccharide. To assist in understanding the GAG binding mechanism of vMIP-II, the ability to manipulate its quaternary state is important.

The point mutant L13F apparently transforms vMIP-II from a largely monomeric protein to a CC chemokine-type dimer. The NMR chemical shift changes upon L13F mutation are wholly consistent with expected changes based on the dimeric crystal structure of vMIP-II (56). In particular, residues undergoing the most significant

chemical shift change include the N-terminus and N-loop, which are a critical part of the CC chemokine dimer interface, making contact with residues 50-52 and the 30's loop of the other subunit (respectively), all of which also exhibit chemical shift changes.

Many studies have been performed to drastically increase the dissociation of dimeric chemokines to form largely monomeric variants (97,115,123,127-129), but vMIP-II L13F is the first dimer made from a predominantly monomeric chemokine by a single point mutation. With wild type vMIP-II being predominantly monomeric and vMIP-II L13F being predominantly dimeric throughout the NMR titration, we have an excellent model to study the role of dimerization in chemokine disaccharide interaction.

The NMR titration results provide an indication of which region is used by wild type vMIP-II to interact with GAGs (Figure 2.4). Basic residues, in particular the N-loop residue R18 and the 40's loop residues, play an important role in the interaction with the negatively charged sugar. Two hydrophobic residues, L25 and W58, also have resonances that shift significantly upon binding I-S, but it is likely that the chemical shift change is due to overall structural change propagation rather than being involved in GAG binding directly, since L25 is an internal residue located in the middle of the groove formed by R46, R48 and R18, and W58 is located outside of this groove with the bulky hydrophobic side chain pointing near the backbone of R18.

To investigate how vMIP-II interacts with longer polysaccharides, heparin chromatography was used. Variants R18A, R46A, and R48A showed the most significant decrease in heparin binding affinity which is consistent with NMR titration results indicating these residues form a heparin binding site, similar to human

chemokines MIP-1β and RANTES (24,98,122). Perhaps surprisingly, the vMIP-II variant K45A did not show a great change in heparin binding affinity, although the residue is part of the so-called BBXB GAG binding domain, and significant change was observed for the nearby single mutants R46A and R48A. Further, the double mutant R46A/R48A showed almost the same loss of affinity for the heparin column as the triple mutant K45A/R46A/R48A, again indicating that K45 is not particularly important in GAG binding. This was not expected since the NMR titration in the presence of the disaccharide heparin I-S, showed large movement of this residue. In similar studies with MIP-1β, it was found that K45A, and R46A mutations caused significant decrease in NaCl elution concentration in heparin column binding, while in that case K48A mutation had no effect (24). While this may suggest a different binding mode between vMIP-II and MIP-1β, examination of both of their structures clarifies the issue. Both proteins have basic residues at positions 18, 45, 46, and 48 (the latter three being the BBXB motif). However, the surface charge figure of vMIP-II (Figure 2.5) shows that R18, R46 and R48 form a clear binding surface while the residue K45 is located away from the surface. In contrast, the dimeric MIP-1β has a clear binding surface comprised of R18, K45 and R46 (97,130). These findings indicate that GAG binding on chemokines is site-specific, and vMIP-II likely binds GAGs using its positively charged surface formed by R18, R46, and R48, which is shifted from the binding site of MIP-1β which primarily uses R18, K45 and R46.

Interestingly, as opposed to the patch of basic residues encompassed by R18, R46 and R48, the other face of vMIP-II, which also has many basic residues (Figure 2.5),

does not appear to be involved in high affinity GAG binding. Basic residues K37, K54, K56, K60 and K61 do not show significant chemical shift change upon titration with I-S, suggesting that these basic residues may not be directly involved in disaccharide binding. Further, when mutation was made to K54, this variant showed similar GAG binding affinity as wild type vMIP-II in heparin chromatography (Table 2.1). This indicates that vMIP-II binds GAGs fairly specifically at one site, encompassed by residues R18, R46, and R48, despite being overall a highly basic protein with many other positive charges throughout its surface. Basic residues on the "back" side of vMIP-II do not appear to contribute to high affinity GAG binding as much as the residues from the binding site do, but overall they may help maintain a basal level of electrostatic attraction to the GAG target. Mutating the whole BBXB domain in vMIP-II with the triple mutant K45A/R46A/R48A causes a significant drop in heparin binding affinity, but does not totally abolish GAG binding as the analogous mutant does in MIP-1β (24). This may be similar to the very basic chemokine RANTES, where mutating the BBXB domain significantly disrupts binding to heparin column but does not abolish binding completely (122).

Molecular docking based on our experimental data gave us a more comprehensive understanding of the disaccharide binding mechanism of vMIP-II. As is shown in Figure 2.7A and B, the docking model predicts that the groove encompassed by positively charged R46, R48 and R18 is the energetically favored binding site for disaccharide. Another set of less favorable complex structures (Cluster 2, Figure 2.7C and D) suggested a possible secondary binding site for disaccharide when multiple

disaccharides or a long chain polysaccharide binds to vMIP-II. This is supported by the heparin chromatography data of R18A variant which showed 2 elution peaks. When R18 is mutated to alanine, the original binding pocket may become less favorable, and a saccharide could then bind to multiple sites. No calculated structure shows binding to the positively charged residues on the "back" side of vMIP-II, indicating that this is not a favorable disaccharide binding site, which is also consistent with our NMR and mutagenesis data. Possibly, the "back" side is unfavorable because of the interference of the negatively charged D57 residue located in the middle of the patch, or perhaps the shape of the pocket is not energetically favorable.

With the NMR sequence assignment of both the monomeric and dimeric forms of vMIP-II, NMR titration allows a residue-specific comparison between their mechanisms of GAG binding. The chemical shift perturbation charts show that while many features of the overall binding site appear to be the same for the monomer and dimer forms of vMIP-II, differences are observed, particularly at the N-terminal region. In the dimeric L13F variant, the N-terminal residues undergo much larger chemical shift changes, indicating that the N-terminal residues are involved in disaccharide binding in the dimeric form of the protein. In the CC-type chemokine dimer structure, the N-terminus of one subunit is in close proximity to the conserved basic residues on other subunit, likely forming part of the saccharide binding site. A calculated docking model (Figure 2.7E and F) confirmed this hypothesis, predicting that disaccharide binds to dimeric vMIP-II (PDB 1CM9) at the new binding pocket encompassed by basic residues R46, R48， R18, and several N-terminal residues from the other subunit. The biggest

difference compared to the monomer model is the involvement of the N-terminus from the other subunit which is consistent with our NMR data. Compared to the monomer disaccharide binding model which has two major binding conformation and higher energy terms, the dimer vMIP-II – disaccharide interaction is more specific and energetically more favorable. This is consistent with the heparin chromatography data showing that vMIP-II L13F binds to the heparin column more tightly than wild type vMIP-II.

Previous GAG binding studies on vMIP-II's human analogs MIP-1β and RANTES have shown similar binding mechanisms to what we have shown for vMIP-II. For MIP-1β, basic residues of the BBXB domain and R18 form the principal binding pocket, and N-terminal residues are also shown to be involved in GAG binding for this dimeric chemokine (97). For RANTES, positively charged residues of the BBXB domain, but not the ones on the other side of the protein, are responsible for GAG binding (122). An X-ray crystal structure of RANTES in complex with disaccharide confirmed the role of the BBXB motif in GAG binding, but also showed unexpected disaccharide binding in the N-loop and 30s loop which was not easily explainable from previous studies (98). Generally, we can conclude that the viral chemokine vMIP-II binds GAGs using a similar mechanism as its human CC chemokines analogs. This could provide an explanation for its natural function: This viral chemokine that antagonizes many chemokine receptors could build up its own concentration gradient upon viral infection (as the human chemokines do), by binding to endothelial surface GAGs. vMIP-II could be protected from proteolysis and could interact with human cell

surface receptors more efficiently, and carry out its anti-inflammatory function. Since vMIP-II tends to bind to GAGs more tightly than many human chemokines, it might also disrupt the concentration gradient of human chemokines by displacing them from GAGs on the endothelial surface.

The present study also raises certain questions: assuming the viral chemokine vMIP-II evolved from a human chemokine ancestor, why did it adopt a Leu at the 13th position which resulted in weaker dimerization and GAG binding, instead of Phe, as its human analogs do? A functional comparison between vMIP-II and human CC-chemokine analog MIP-1β suggests a possible explanation. Unlike MIP-1β, which requires a Phe in the 13th position for both receptor binding and GAG binding (24,115), our preliminary results (manuscript in preparation) show that although the L13F mutation does significantly enhance the heparin binding ability, it does not change the affinity of vMIP-II for cell surface receptors CCR5 or CXCR4. So for receptor binding, L13 and F13 are equivalent for vMIP-II, and it has apparently achieved promiscuous receptor binding without Phe13. Regarding GAG binding, although the lack of Phe residue at the 13th position leads to a predominantly monomeric form, vMIP-II is still able to tightly bind GAGs, more tightly than the dimeric human chemokine MIP-1β. Considering vMIP-II's natural function, which is apparently to subvert the human immune system and antagonize multiple chemokine receptors, it is possible that binding GAGs more tightly (as does the Phe13-containing dimer form) would hinder its anti-inflammatory function, perhaps by decreasing its mobility.

In conclusion, NMR, mutagenesis and molecular docking were carried out to elucidate the structural features of GAG binding for the anti-inflammatory viral chemokine homolog vMIP-II. These experiments show that vMIP-II tightly binds glycosaminoglycans using residues distributed along only one face of the protein, such as R18, R46 and R48, even though the protein is highly basic throughout its surface. This study also provides a valuable model to study the role of chemokine quaternary state in GAG binding. With the wild type vMIP-II being predominantly monomeric, and the point mutant vMIP-II L13F being predominantly dimeric throughout the NMR titration experiments, we were able to analyze the difference in GAG binding mechanisms between the two quaternary states at the atomic level. NMR studies reveal a shift in the GAG binding site between monomer and dimer, where the N-terminus is involved in GAG binding for the dimeric form. Docking models confirmed this finding and suggested that GAG binding to the dimer form of vMIP-II is energetically more favorable. The tighter GAG binding of the vMIP-II L13F dimer also reinforces past results suggesting that the major physiologic role of the chemokine dimer may be to bind to GAGs. The results presented here clarify several aspects of the biochemistry of vMIP-II, suggest possibilities for how this viral chemokine analog may function, and shed light into understanding the mechanism of how quaternary structure affects GAG binding.

CHAPTER III

CHARACTERIZING THE IMPORTANCE OF vMIP-II'S HIGHLY BASIC CORE DOMAIN IN ITS BINDING TO CCR5 AND CXCR4

Mini Review of Chemokine/Receptor Interaction

Chemokines are small immune system proteins mediating leukocyte migration and activation, and thus play vital roles in health and various diseases. Chemokines are classified into four subfamilies: CC, CXC, CX_3C, and XC, based on the sequence of their N-terminal conserved cysteine motifs (13). Chemokine receptors belong to a sub-group of G-protein coupled receptors (GPCRs) and are classified into 4 subfamilies: CCR, CXCR, CX3CR, and XCR, corresponding to the subfamily of chemokine ligands they bind to. The CXC chemokines are further divided into ELR+ and ELR- chemokines depending on whether they have the N-terminal conserved Glu-Leu-Arg motif (13).

Up to date, there are about 50 chemokines and 20 chemokine receptors reported. There are many chemokines that can bind to multiple receptors and there are many chemokine receptors that can bind to multiple chemokine ligands. However, in most cases, chemokines of one subfamily only bind to receptors of the corresponding subfamily, and there is strict receptor-ligand binding selectivity. Because of the significant role chemokines and their receptors play in health, development and diseases,

it is extremely important that we understand the profound mechanisms underlying chemokine/receptor binding and chemokine induced receptor activation.

Great effort has been made to characterize the chemokine/receptor interplay structurally and functionally. In the past two decades, a wealth of information has been obtained on the chemokine part. NMR and X-ray crystallography studies have resolved the structures of many chemokines (118,130-133). Structural comparison of many chemokines even across subfamilies revealed that chemokines share an exceptionally conserved tertiary structure, called the "chemokine fold". A typical chemokine fold comprises a flexible N-terminus with the conserved cysteine motif, an N-loop, three β-strands placed in a Greek key orientation, and followed by a C-terminal-helix (16). Although structures of the chemokine ligands have been unveiled, the progress toward understanding the mechanism of chemokine/receptor interaction is still severely hindered by the lack of structural information of the other binding partner, the chemokine receptor. Chemokine receptors are seven-transmembrane cell surface GPCRs. Until late in the year 2010 (134), there was no direct structural information available on chemokine receptors. Previously solved structures of the similar seven-transmembrane GPCRs Rhodopsin (135), β1 and β2 adrenergic receptors (136-138) and the adenosine receptor A2A (139) shed light on the prediction of the structures of chemokine receptor through analogous comparison. Very recently, the crystal structure of a chemokine receptor CXCR4 has been reported (134), which opened up a new era of research. This newly published CXCR4 structure also confirmed the previous predicted structural features of chemokine receptors: the chemokine receptor has seven

transmembrane helices, and the extracellular domains consist of a sulfated N-terminus, three extracellular loops, ECL1, ECL2, and ECL3, while the cytosolic domains include three cytosolic loops and the C-terminus.

Although the first chemokine receptor was only reported 4 months ago (134) (Oct 2010), and no structure of complete chemokine/receptor complex has been reported, extensive structural and functional studies have been carried out to elucidate the chemokine/receptor binding mechanisms using mutagenesis and truncation methods and by studying chimeric chemokines and chemokine receptors.

Studies mainly focused on CXC chemokine/receptors, especially how IL-8 (interleukin-8, CXCL8) interacts with its receptors CXCR1 and CXCR2. As early as 1991, Clark-Lewis et al. found that residues of the N-terminus, especially residues Glu4, Leu5, and Arg6 (later identified as the ELR motif) are essential for IL-8's receptor binding and activation of neutrophils, while the C-terminus is not required, since a truncation analog missing the C-terminal 22 residues is still functional (140). Moser et al later reported that mutation or truncation of the ELR motif abolished IL-8's function to activate receptors (141). Introduction of the ELR motif to the CXCR3 binding chemokine PF4 gave it comparable ability to activate neutrophils, however, chemokines IP-10 and MCP-1 with ELR mutations didn't acquire the same ability (142). These results indicate that there are other receptor binding determinants than the ELR motif. This group later proved that in addition to the ELR motif and the conserved cysteines of the N-terminus, the 30's loop region is also important for receptor binding (143). Through analogous comparison between rabbit IL-8 and human IL-8 and mutagenesis

study, N-loop residue Tyr13 and Lys15 were found to account for the 200-fold difference in binding affinity between the two IL-8 chemokines (144). In 1996, two groups using two distinct methods reported similar results, that in addition to the ELR N-terminal motif, IL-8 has a second receptor binding site: Hammond et al. reported through single amino acid mutation and domain substitution studies that the hydrophobic surface-accessible pocket composed of Tyr13, Ser14, Phe21, and Lys49 is the second binding site required for receptor binding (145); while Williams et al. used NMR methods and identified the hydrophobic residues on the surface of IL-8 (Phe17, Phe21, Ile22, and Leu43) that form the second binding site (146). An NMR study carried out by Skelton et al. have shown direct structural information on how IL-8 interacts with the N-terminus of CXCR1 (147). Results indicated that IL-8 uses the hydrophobic cleft formed by the N-loop region and the 3rd β-strand to interact with the hydrophobic Pro21-Pro29 region of the CXCR1 peptide.

Studies on the IL-8 receptors supported a similar conclusion that there are two distinct sites of interaction for IL-8/receptor binding and activation. Two groups studying the IL-8 receptors independently showed that the ligand binding selectivity and activity largely depend on the N-terminus of the receptor (107,148). Wu et al. proved the vital role of CXCR1 and CXCR2 N-termini in ligand selectivity, and pointed out that the receptors undergo conformational changes after ligand binding and this change is required for further receptor activation (149). Hebert et al. reported that the conserved Glu-275 and Arg-280 on the extracellular loop 3 of CXCR1 are responsible for interacting with the ELR motif of IL-8 (150). Katancik et al. identified critical residues

for IL-8, NAP-2 and GROα, and argued that residues required for cell activation and ligand binding are not necessarily the same (151).

Extensive studies on IL-8 and IL-8 receptors led us to a clear conclusion that the IL-8/receptor interaction occurs at two distinct sites. IL-8 uses its surface cleft formed by residues from the N-loop region and the 3rd β-strand to interact with the N-terminus of the receptor; this part of interaction determines the receptor-ligand binding affinity and specificity. The N-terminus of IL-8, especially the ELR residues, interacts with the extracellular loop region and the transmembrane domains of the receptor and is responsible for receptor activation.

This 2-site binding model has been proved to be true for other chemokines and chemokine receptors. The binding determinants of the chemokine IP-10 for CXCR3 binding have been identified. At binding site 1, IP-10 uses the binding pocket formed by charged residues of the N-loop region (residues 20-24) and the 40's loop residues 46 and 47 to presumably interact with the N-terminus of CXCR3, this interaction does not account for receptor activation. While at the second binding site, IP-10 probably uses its N-terminus, especially residue Arg8 to bind the extracellular loops of CXCR3 and activates it (152-153). Another well studied pair is the CXC chemokine SDF-1 (stromal cell-derived factor-1) and its receptor CXCR4. Crump et al. reported the solution structure of SDF-1 and showed that SDF-1 N-loop region RFFESH motif (residues 12-17) is probably responsible for the initial docking of the chemokine to the receptor, while the N-terminus, especially Lys1 and Pro2 are critical for receptor activation (154). N-terminal analog peptides of SDF-1 (1-9, 1-17) could bind and activate CXCR4,

although less potent than native SDF-1, indicating the role of SDF-1 N-terminus in receptor activation and site-2 binding (155). Mutagenesis studies on CXCR4 revealed 2 distinct binding sites: N-terminal residues on CXCR4 are important for binding but not activation which presumably form the one binding site, while residues on the extracellular loop 2 & 3, transmembrane domain II and VII form the binding site, since they are critical for both binding and activation (156-157). Recently, the Volkman group reported a structure of SDF-1 in complex with tyrosine sulfated CXCR4 N-terminus, and provided more details in how SDF-1 uses its core domain surface binding cleft to interact with tyrosine sulfated CXCR4 N-terminus (158). In 2009, Kofuku et al. used a novel transferred cross-saturation NMR method and identified the molecular interface in SDF-1 and CXCR4 binding. They showed that binding of SDF-1 N-terminus to the transmembrane domain of CXCR4 (responsible for receptor signaling and ligand-binding) and binding of the SDF-1 core domain surface to the CXCR4 N-terminus (only for ligand binding) are separate (159), which further proved the 2-site binding model.

Studies on CC chemokines MCP-1, MCP-3, Eotaxin, RANTES, MIP-1α, MIP-1β, and their receptors, especially CCR2 and CCR5, revealed similar mechanisms of ligand binding and receptor activation (24,115,123,160-172). RANTES/CCR5 interaction has been characterized using similar methods as previously introduced. RANTES N-terminus, especially residue Pro2, has been shown to be extremely important in CCR5 binding and activation (160,165). Pakianathan et al. showed that N-loop residues F12 and I15 are critical for CCR5 binding (168). An NMR study mapped out the determinants of RANTES for binding tyrosine sulfated CCR5 N-terminal peptide (171).

At the core domain of RANTES, residues from the N-loop, β-strands and the 30's and 40's loop constitutes a strongly positively charged binding surface for the Y10 Y14 sulfated negatively charged peptide. Blanpain et al. carried out a series of studies on the CCR5 receptor and proved that the CCR5 N-terminal negatively charged residues Asp2, Tyr3, Tyr10, Asp11, and Glu18 are important in RANTES binding while the transmembrane helices are important for RANTES induced signaling (160-162). Taken together, RANTES uses its highly basic core domain binding surface to interact with the N-terminus of CCR5, while the N-terminal residues, especially Pro2, bind and activate CCR5 at the other site.

Studies on another CCR5 binding chemokine MIP-1β were mainly carried out in our lab. Through mutagenesis and NMR studies, Laurence et al. have proved that residues at the N-terminal of MIP-1β are critical for both receptor binding and activation, and that Phe13 is the single most important residue, since mutation of the aromatic Phe13 to Ala resulted in more than 1000 fold decrease in MIP-1β's receptor binding and signaling activity (115). A structural comparison of wild type MIP-1β and the F13A mutant confirmed that the 1000 fold drop of binding affinity and signaling activity was due to local binding site change rather than a global structural change (128). It was later found that, in addition to the residues in the N-terminus, positively charged residues R18, K45, R46 and K48 on the N-loop and 40's loop region are also critical mediators for binding CCR5 (24). Bondue et al. in collaboration with other labs did a more extensive mutation scan on residues of the N-loop region of MIP-1β and found out that Pro21 and three positively charged residues Arg18, Lys19, and Arg22 also contribute to CCR5

binding (163). It was thus clear that MIP-1β uses it positively charged binding surface comprising basic residues from the N-loop and the 40's loop to interact with the sulfated, negatively charged N-terminus of CCR5 and then uses its N-terminus to bind and activate CCR5.

Although each chemokine uses distinct residues and contact slightly different domains of the receptor, a clear 2-site binding model can be concluded: 1. generally, chemokines use their core domain binding surface comprising certain residues from the N-loop region, β-strands and/or the 40's loop to interact with the N-terminal domain and/or certain extracellular loop region of the receptors, this interaction (site 1 binding) determines receptor/ligand selectivity and binding affinity, but not receptor activation; 2. Chemokines use their flexible N-termini, sometimes with the help of the 30's loop residues (146,168,173-174), to interact with the extracellular loop or transmembrane region of the receptors, this interaction (site 2 binding) accounts for receptor activation (175). It's also shown that binding at the two sites are not independent, and that they could be coupled to each other (176). Binding at one site might positively or negatively regulate binding at the other site.

vMIP-II and Receptors

As previously mentioned, some chemokines can bind to multiple receptors, and some receptors can bind to multiple chemokines. This redundancy is probably essential for functional regulation of the chemokine network. However, in most cases,

chemokines of one subfamily can only bind to receptors of the corresponding subfamily. A viral chemokine analog vMIP-II, being able to bind at least 9 receptors across all four subfamilies, is a remarkably unique exception.

vMIP-II (vCCL2) is encoded by human herpesvirus-8. This protein is very unique because it binds to a wide range of chemokine receptors across all four different subfamilies: it binds to CCR1, CCR2, CCR5, CCR10, CXCR4, CX3CR1, XCR1 as an antagonist, and binds to CCR3 and CCR8 as an agonist (42-47). This unusual ability to selectively block or activate such a huge number of chemokine receptors probably enables vMIP-II to preferentially inhibit acute Th1-associated inflammation, but up-regulate Th2 associated immune response to help the virus evade the host immune system (44-45). Due to its potent anti-inflammatory properties, vMIP-II has been successfully used to protect rat brain after ischemic brain injury and spinal cord injury (48-49), as well as increase tolerance of cardiac and corneal allograft transplant in mice (50-51). More recently, vMIP-II has been shown to be pro-angiogenic in both mature and progenitor endothelial cells, suggesting the possibility that this protein could be useful in organ transplantation (52). vMIP-II is also a valuable candidate as an HIV inhibitor, since it blocks HIV cell entry through both CCR5 and CXCR4 coreceptors and preferentially inhibits inflammation of monocytes and Th1 type T cells which are major targets for HIV-1 (43-45). vMIP-II therefore is biologically relevant in many diverse fields.

Although it has been 13 years since vMIP-II was first reported (43), the intriguing mechanism underlying vMIP-II's broad-spectrum receptor binding ability is still not

precisely understood. Our study aims to understand the specific aspects of structure and amino acid placement that lead to vMIP-II's unique ability to bind multiple receptors, with a particular emphasis on characterizing the importance of vMIP-II's highly basic core domain surface in binding CCR5 and CXCR4. We choose to study vMIP-II's binding to CCR5 and CXCR4, because they are well studied receptors from two different subfamilies and they are also major coreceptors for HIV infection.

Sequence and structure of vMIP-II. Sequence-wise, vMIP-II is very similar to human CC chemokines: vMIP-II shares about 40% sequence identity with the human chemokine MIP-1β, 48% with MIP-1α and 37% identity with RANTES. NMR (53-55) and X-ray (56-57) structural studies have revealed that vMIP-II also has a very similar tertiary structure as human chemokines, featuring a typical chemokine fold comprised of a flexible N-terminus, an N-loop, three strands in a Greek key orientation, and followed by a C-terminal-helix (Figure 1.2). In terms of quaternary structure, vMIP-II is predominantly a monomer under most conditions (53-55,57), although under some crystallization conditions it has been observed as a CC-type dimer (56).

In the past two decades, structural studies have resolved the three-dimensional structures of a great number of human chemokines, and functional studies have provided us with a wealth of information on how they bind and activate chemokine receptors. A good way to characterize vMIP-II's structural basis for its broad-spectrum receptor binding ability is through analogous structural and functional comparison to other chemokines.

Structural comparison of vMIP-II with other CCR3 binding chemokines Eotaxin-1, RANTES, and MCP-3 revealed several unique structural features of vMIP-II, indicating that vMIP-II might use a different mechanism to bind and activate CCR3 (56). Structures of the three human chemokines have been resolved (126,129,177), and their CCR3 binding surfaces share a common structural pattern, however, different to that of vMIP-II: 1. their N-loop region is hydrophobic, and they all have a conserved aromatic residue, Phe or Tyr, directly after the CC-motif whose aromatic side chain constitutes a hydrophobic protrusion that is critical for CCR3 binding and activation, whereas vMIP-II has a Leu at this position, and the same region appears to be a positively charged groove (charge comes from the nearby Lys37) (Figure 3.1A); 2. All three human chemokines feature a positively charged protrusion at the 30's loop which is important in receptor binding (178) (Lys in Eotaxin and RANTES, His in MCP-3), whereas vMIP-II has a Leu34 at this position (Figure 3.1B). 3. In all three human chemokines, Pro2 is of particular importance in signaling and binding (168,179), and the other N-terminal residues are small non-polar residues. In contrast, vMIP-II does not have a Pro, and contains more bulky or charged residues in its N-terminus (Figure 3.1C). These major differences indicated that vMIP-II might use a different way to bind and activate CCR3.

Shao et al. compared the structure of vMIP-II with structures of CC chemokine MIP-1α (180), MIP-1β (130), RANTES (132), HCC-2 (181), MCP-1 (131) and eotaxin-1 (126). They confirmed the previous finding that the most significant differences in the structure of vMIP-II are observed at the N-terminus and the 30's loop. They also reasoned that in addition to the N-terminus, there are other epitopes on the chemokine

surface that determine receptor binding and further investigated the possible interactions with receptor CCR2. They predicted from sequence alignment that vMIP-II probably bind to CCR2 differently than MCP-1, MCP-2, MCP-3, and MCP-4 since it lacks the common receptor binding residues of human CCR2 binding chemokines (55).

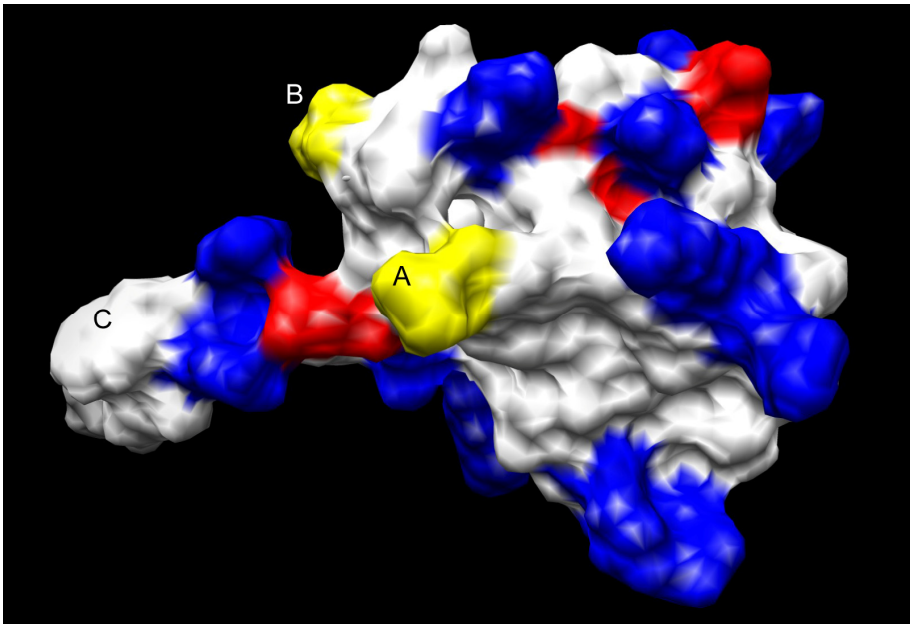

Figure 3.1 Major structural differences between vMIP-II and CCR3 binding human CC chemokines. **A.** Compared to the three CCR3 binding human chemokines eotaxin-1, RANTES, and MCP-3, vMIP-II has a Leu13 instead of an aromatic residue (Phe or Tyr) at the N-loop; **B.** vMIP-II has a Leu34 instead of a positively charged residue at the 30's loop; **C.** vMIP-II's N-terminus is bulkier and more charged. Positively charged residues are labeled in blue, negatively charged residues are labeled in red, and the Leu residues shown in positions A&B are labeled in yellow.

Through sequence and structural comparison, we gained a deeper understanding of the receptor binding features of vMIP-II. It binds to at least 9 chemokine receptors but probably not all in the same way as their native ligands do, which is reasonable since vMIP-II only has 71 amino acids and could not mimic the receptor binding features of all the chemokine ligands. vMIP-II therefore must have its own unique way to interact with these receptors. Our goal is to help understand this mechanism by studying the CCR5 and CXCR4 binding surfaces on its core domain.

CXCR4 binding of vMIP-II. Several studies have been done to investigate how vMIP-II binds CXCR4. A synthetic peptide (V1) derived from the first 21 amino acids of vMIP-II has been shown to bind CXCR4 but not CCR5 (182). Mutations on the V1 peptide revealed that the N-terminal residues (before the conserved Cys motif) are critical in CXCR4 binding, since L1A, W5A, R7A, and K9A all caused dramatic decrease in binding (183). These results along with others (184) further confirmed that vMIP-II N-terminus is critical in binding CXCR4, however, not in activating it (185). Peptides from other parts of vMIP-II (22-44, 36-57, 51-71, 30-40 cyclic, and 41-51 cyclic) showed no binding to CXCR4 (183), so since there is more than 10-fold reduced binding affinity of V1 peptide compared to the native form of vMIP-II, it's likely that there is another binding site on vMIP-II but it requires the natively folded confirmation.

Site directed mutagenesis studies on CXCR4 revealed that the binding interfaces on CXCR4 for vMIP-II and SDF-1 are similar or partially overlap, since no major differences in vMIP-II and SDF-1 were observed for binding various mutants of CXCR4 (mutations were on the N-terminus, ECL2 and ECL3) (157). They also showed that

residues D20 and Y21 of N-terminus and residue E268 of the extracellular loop 3 are essential for SDF-1 and vMIP-II binding (157). This result is consistent with the previous 2-site binding model, and indicated that, in addition to the N-terminus, vMIP-II might have another CXCR4 binding site as SDF-1 does.

CCR5 binding of vMIP-II. CCR5 is another major chemokine receptor that vMIP-II is able to bind. Although very few studies have been done to characterize the CCR5 binding mechanism of vMIP-II, indirect evidence provided us valuable information on how vMIP-II may interact with CCR5. As previously stated, the N-terminal peptide of vMIP-II does not have the ability to bind CCR5 (182). Modified vMIP-II with the first 10 residues replace with D-amino-acids showed no significant changes in CCR5 binding, although the crystal structure of this D-amino-acid vMIP-II showed significantly different conformation at the N-terminus and the disulfide linked 30's loop region which are generally considered critical domains for receptor binding and activation in chemokines (186). These results indicate that the N-terminus and the 30's loop region are not involved in vMIP-II's CCR5 binding. This finding is also consistent with the conclusions of the previous structural comparison studies (55-56) that the most significant differences between vMIP-II and other CC chemokines are observed at the N-terminus and the 30's loop. A mutagenesis study on CCR5 have shown that vMIP-II binds CCR5 differently than RANTES and MIP-1α (187): 1. Competition experiments showed that vMIP-II may bind to a different site of CCR5 than RANTES and MIP-1α. 2. Alanine substitutions of the N-terminal negatively charged residues on CCR5 N-terminus abolished binding for all three chemokines, but mutations on the extracellular

loop 2 region which has been shown to be critical in receptor activation abolished binding for RANTES and MIP-1α, but not for vMIP-II. 3. Engagement of vMIP-II to CCR5, but not RANTES and MIP-1α could block the subsequent binding of certain CCR5 antibodies. This evidence suggests that vMIP-II probably only binds to the N-terminus of CCR5. Considering the fact that the N-terminus of vMIP-II is not involved in CCR5 binding, vMIP-II/CCR5 interaction probably is a rare exception of the 2-site binding model. vMIP-II probably uses its own unique binding surface on its core domain (since its N-terminus and 30's loop region are not involved) to interact with the negatively charged N-terminal domain of CCR5. Further considering the fact that vMIP-II probably binds CCR3 and CCR2 differently than the native chemokine ligands because of the differences in the sequence and the significant structural variations at its N-terminus and 30's loop (55-56), vMIP-II might use the same mechanism to interact with other CC chemokine receptors and this unique mechanism might help explain its broad-spectrum receptor binding ability.

Hypothesis. Based on previous findings, we conclude that: 1. vMIP-II has a binding surface at its core domain that is solely responsible for binding CCR5. 2. In addition to its N-terminus, vMIP-II has another CXCR4 binding surface at its core domain. The question is: are the core domain surfaces used by vMIP-II for binding CXCR4 and CCR5 binding overlapping/the same or are they different? What are the important features of the core domain binding surfaces.

As previously stated, because of the similarities in the sequences and in the quaternary structures, vMIP-II is more closely related to human CC chemokines than to

CXC chemokines. However, two noticeable differences were observed when comparing the sequences and structures of vMIP-II with those of MIP-1α, MIP-1β, and RANTES. 1. vMIP-II does not have the highly conserved Phe or Tyr residue which all human CC chemokines have after the CC-motif. Instead, it has a Leu at that position. This aromatic residue has also been shown to be critical in receptor binding and activation for MIP-1β (115), RANTES (168) and MCP-1 (123). This major difference has been pointed out before when comparing to CCR2, CCR3 and CCR5 binding chemokines (55-56); 2. vMIP-II is a much more basic protein than most human chemokines: out of 71 total residues, vMIP-II has 8 Lys and 5 Arg distributed on its surface. Considering the fact that site 1 binding usually involves the N-terminal domain of the receptor and the core domain of the chemokine, and that most receptor N-termini are heavily sulfated and negatively charged, it is quite possible that the high number of positively charged residues contribute to vMIP-II's broad-spectrum receptor binding.

Figure 3.2 shows the CCR5 binding surface of MIP-1β, and the analogous surface of vMIP-II. This same surface has been shown to be used by MIP-1β and vMIP-II to interact with the negatively charged endothelial surface GAGs (24,188). Except for the fact that vMIP-II does not have the Phe residue at its N-terminus, and that its surface is more basic, vMIP-II has positive charged residues distributed on this surface in the same pattern as the CCR5 binding residues on MIP-1β. It is possible that this analogous surface is used by vMIP-II to interact with the CCR5 N-terminus.

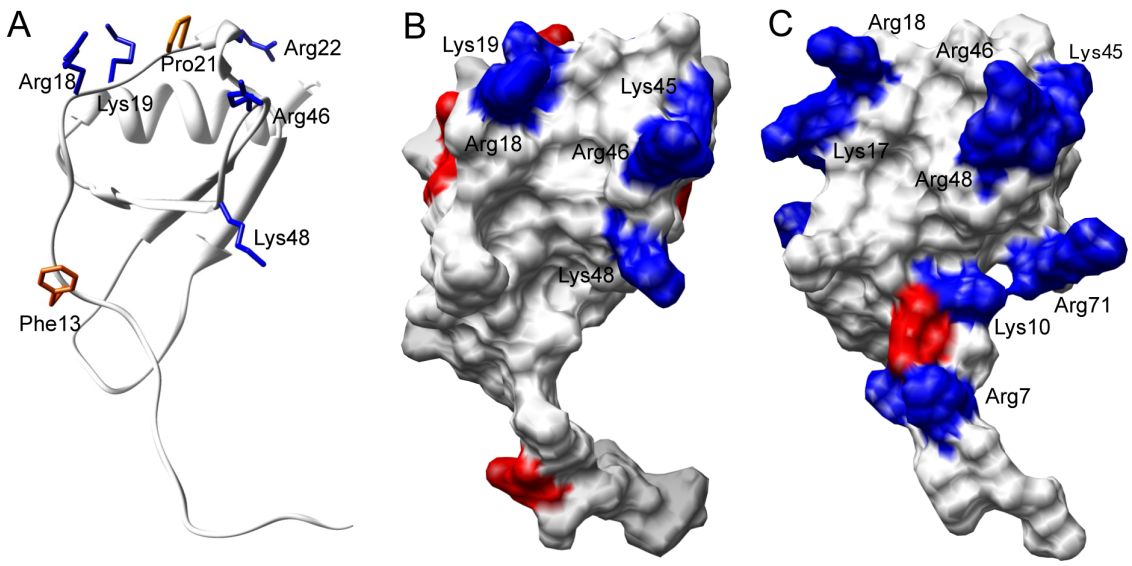

Figure 3.2 CCR5 binding surface of MIP-1β and the analogous surface of vMIP-II. **A.** Important CCR5 binding residues on MIP-1β as shown by mutagenesis and NMR studies (163). Positively charged residues are labeled in blue, while hydrophobic residues are labeled in orange. **B.** Surface graph of MIP-1β showing the same CCR5 binding surface as in A. Positively charged residues are labeled in blue, while negatively charged residues are labeled in red. **C.** Surface graph of the analogous surface on vMIP-II. Positively charged residues are labeled in blue, while negatively charged residues are labeled in red.

We hypothesize that this highly basic binding surface at the core domain of vMIP-II is important for its binding to CCR5 and CXCR4, and probably explains vMIP-II's broad-spectrum binding ability to other receptors.

Perhaps surprisingly, no mutagenesis study has been done on full length vMIP-II to evaluate the importance of certain domains and map out its binding determinants. In this study, we introduced mutations to vMIP-II's N-terminal non-conserved Leu13 residue and to the positively charged residues on surface of vMIP-II's core domain to evaluate their role in CCR5 and CXCR4 binding. Mutagenesis studies on the core domain of chemokines have been proved to be difficult. Since many surface residues of the core domain may contribute to binding, and the effect is cumulative, mutation of one such residue may not yield detectable influence. Studies on MIP-1β have shown the importance of the positively charged BBXB (basic-basic-any-basic) domain of the 40's loop in CCR5 binding that if all 3 basic residue were mutated, no binding to CCR5 can be observed. However, no obvious change in binding was observed when mutating any single one of these residues (24). An X-ray structural study on a human growth hormone/receptor complex identified the important binding sites for their interaction (189). However, a previous mutagenesis study could not identify these important residues using single mutations (190), probably because of the cumulative contribution of a large number of residues involved in binding. In this respect, we carried out multiple mutations in addition to single mutations to full length vMIP-II and evaluated the effects in binding CCR5 and CXCR4. To gain a more comprehensive understanding of vMIP-II's receptor binding sites, we are also trying to carry out NMR experiments to

study the interaction of vMIP-II with tyrosine-sulfated N-terminal peptides of CCR5 and CXCR4.

Experimental Procedures

Protein preparation. The gene for vMIP-II was synthesized using overlapping oligonucleotides (Thanks to Michael Pirics and Dr. Amanda Jacks). vMIP-II mutations were made using the QuikChange Site-Directed Mutagenesis method (Stratagene, La Jolla, CA). vMIP-II wild type and variants were expressed in the pET-32a(+) expression vector along with a thioredoxin fusion tag (Novagen, Madison, WI). The vectors were transformed into BL21(DE3), and grown in 1 liter ^{15}N minimal medium using $^{15}NH_4Cl$ as the only nitrogen source. For NMR chemical shift assignment experiments, ^{13}C-labeled glucose was used as the only carbon source to produce the ^{13}C-^{15}N-labeled L13F variant, while for other mutants unlabeled glucose was used. Protein production was induced with 1 mM IPTG. The cells were harvested by centrifugation 4 hours after induction. The cell pellet was resuspended in refolding buffer (5 M Guanidinium/HCl, 3 mM EDTA, 50 mM Tris, 50 mM NaCl, pH 8.0) with 10 mM benzamidine, and French pressed twice at 16,000 psi. The solution was incubated at room temperature for 2 hours with stirring followed by a centrifugation at 20,000 ×g for 30 minutes. The supernatant containing the denatured protein was passed through a Ni chelating column and eluted with imidazole in 5 M guanidinium chloride, 50 mM Tris (pH 8.0), 500 mM NaCl. The purified proteins were slowly stirred overnight with the addition of 10 mM β-

mercaptoethanol, and refolding was carried out by dialysis against 50 mM NaCl, 2 mM $CaCl_2$, 20 mM Tris-HCl (pH 8.0). To remove the fusion tag, recombinant enterokinase (Novagen, Madison, WI) was added and the solution was incubated 3-7 days at room temperature. Precipitated matter was removed by centrifugation at 20,000 ×g for 30 minutes and the enterokinase digested protein was purified on a C4 reversed phase chromatography column (Vydac, Hesperia, CA) on an Akta purification system (GE Healthcare), and lyophilized by the Labconco freeze dry system (Labconco Corporation, Kansas City, MO).

Cell lines. CCR5 expressing CHO cells were previously prepared in our lab (163). CXCR4 expressing HEK293 cells were stably transfected as described below. CHO-CCR5 cells were cultured in HAM's F12 medium supplemented with 10% fetal bovine serum (Thermo Scientific), 100 units/mL penicillin, and 100 μg/mL streptomycin (Thermo Scientific) and 50 μg/ml G418 (Invitrogen, Carlsbad, CA). HEK293-CXCR4 cells were cultured in DMEM medium supplemented with 10% fetal bovine serum (Thermo Scientific), 100 units/mL penicillin, and 100 μg/mL streptomycin (Thermo Scientific) and 50 μg/ml G418 (Invitrogen, Carlsbad, CA).

Stable transfection of 293 cells. Wild-type CXCR4 was transfected into 293 cells using Lipofectamine 2000 transfection reagent (Invitrogen, Carlsbad, CA) according to the product manual provided by the manufacturer. Selective medium containing 700 μg/ml geneticin (G418, Invitrogen, Carlsbad, CA) was used to isolate stable clones. Cells were then sorted using flow cytometry. Cells with high level of CXCR4 expression were selected, and each single cell was grown into a colony and the colonies

were further sorted. After two rounds of sorting, a colony grown from a single cell was used in binding assays.

Flow cytometry. Transfected 293 cells (1 × 106 cells/well) were washed with FACS buffer (1 × HBSS, 4.2 mM sodium bicarbonate, 0.1% sodium azide and 1% bovine serum albumin, Fraction V, pH 7.2.) twice and incubated with 10 μg/ml FITC conjugated anti-CXCR4 mAb 2B11 (BD Biosciences) for 30 min at 4°C. Flow cytometric analysis and sorting was performed using a FACSAria cytometer (BD Biosciences). Flow cytometric data was analyzed using FlowJo software (TreeStar).

NMR spectroscopy. All NMR data were acquired at 25 °C on Varian Inova 500 or 600 MHz, or Bruker 600 MHz spectrometers. NMR samples were prepared by adding lyophilized proteins into 20 mM sodium phosphate (pH = 2.5, 5.4, or 7.4, depending on the specific requirement for each experiment). The effect of pH variation on chemokine quaternary structure was also evaluated by NMR. While many CC-chemokines require low pH to avoid aggregation, vMIP-II was soluble throughout the range. The chemical shift was referenced relative to internal DSS (2,2-dimethyl-2-silapentane-5-sulfonic acid) (102). The data were processed using NmrPipe (103) and analyzed using PIPP (104). For 2D HSQC spectra, SW=6982.631 Hz (^{1}H) and 1700.030 Hz (^{15}N), with 512* points in ^{1}H and 128* points in ^{15}N. The 3D HNCACB experiments were acquired with SW=7804.117 Hz (^{1}H), 9599.232 Hz (^{13}C) and 1619.991 (^{15}N), number of points are 512* in ^{1}H, 64* in ^{13}C, and 32* in ^{15}N.

Radioactive competition binding assay. Cells expressing wild-type CCR5 (CHO-CCR5) or CXCR4 (HEK293-CXCR4) were resuspended from cell culture flasks, gently

pelleted for 2 min at 1000 ×g, and resuspended in binding buffer (50 mM Hepes, pH 7.4, 1 mM CaCl2, 5 mM MgCl2, and 0.5% BSA). Resuspended cells were then seeded in a 96 well plate with a density of 4×10^5 cells per well. 0.08 nM ^{125}I-labeled chemokine ligand (MIP-1β for CCR5 binding, SDF-1 for CXCR4 binding) (PerkinElmer, Covina, CA) was added to each well as a radioactive tracer. Variable concentrations of vMIP-II or its variants were added to compete with the binding of the radioactive ligand. The final volume of each well was adjusted to 0.1 mL. The level of total binding was measured in the absence of competitor, and the level of nonspecific binding was measured with a 100-fold excess of unlabeled ligand. Samples were incubated for 90 min at room temperature with gentle shaking, and then the bound tracer was separated by filtration through APFB 25 mm glass fiber filters presoaked in 0.5% polyethyleneimine solution. The filters were washed with 3 × 4 ml washing buffer (50 mM Hepes, pH 7.4, 1 mM $CaCl_2$, 5 mM $MgCl_2$, 0.5% BSA, and 500 mM NaCl) and then counted for radioactivity using a 1470 Wizard gamma counter (PerkinElmer, Covina, CA). Binding IC_{50} values were determined using KaleidaGraph (Synergy Software, Reading, PA) using nonlinear regression applied to a one-site competition model.

Preliminary Results and Discussion

The 13th position in vMIP-II is not involved in receptor binding. As previously stated, vMIP-II lacks the highly conserved aromatic residue at its 13th position which

has been shown to be critical in both receptor binding and activation for CC chemokines (115,123,168). Because of this and other differences, several studies predicted that vMIP-II may bind to CC chemokine receptors differently than native chemokine ligands (55-56).

To confirm this prediction, we introduced a series of mutations into this position. First, we mutated Leu13 to the conserved aromatic residue Phe. NMR studies confirmed that vMIP-II L13F is nicely folded (Figure 3.3). Competition binding assays were carried out to test the effect of L13F mutation on vMIP-II's binding to CCR5. As shown in Table 3.1, vMIP-II L13F exhibited no difference in binding CCR5 compared to the WT vMIP-II, indicating that the 13th position in vMIP-II is not important for receptor binding. As previously described in my studies, while the wild type vMIP-II is predominantly a monomer in solution vMIP-II, L13F is a dimer in solution (188) (Figure 3.3). It has been shown that chemokines interact with their receptors in the monomer form, and the quaternary state of a chemokine in solution does not affect its receptor binding (24,100). But, to rule out the possibility that the change of the quaternary structure affects binding of vMIP-II L13F, we made a P8AL13F double mutant which keeps the Phe in the 13th position and does not dimerize in solution (NMR spectra not shown). This double mutant of vMIP-II still showed no significant difference in CCR5 binding compared to the WT vMIP-II. To further confirm the unimportance of the 13th position, we mutated Leu13 to Ala and found that L13A showed no significant difference in CCR5 binding. This is in great contrast to human CC chemokines. For example, mutating Phe13 of MIP-1β to Leu caused a 200-fold decrease in receptor

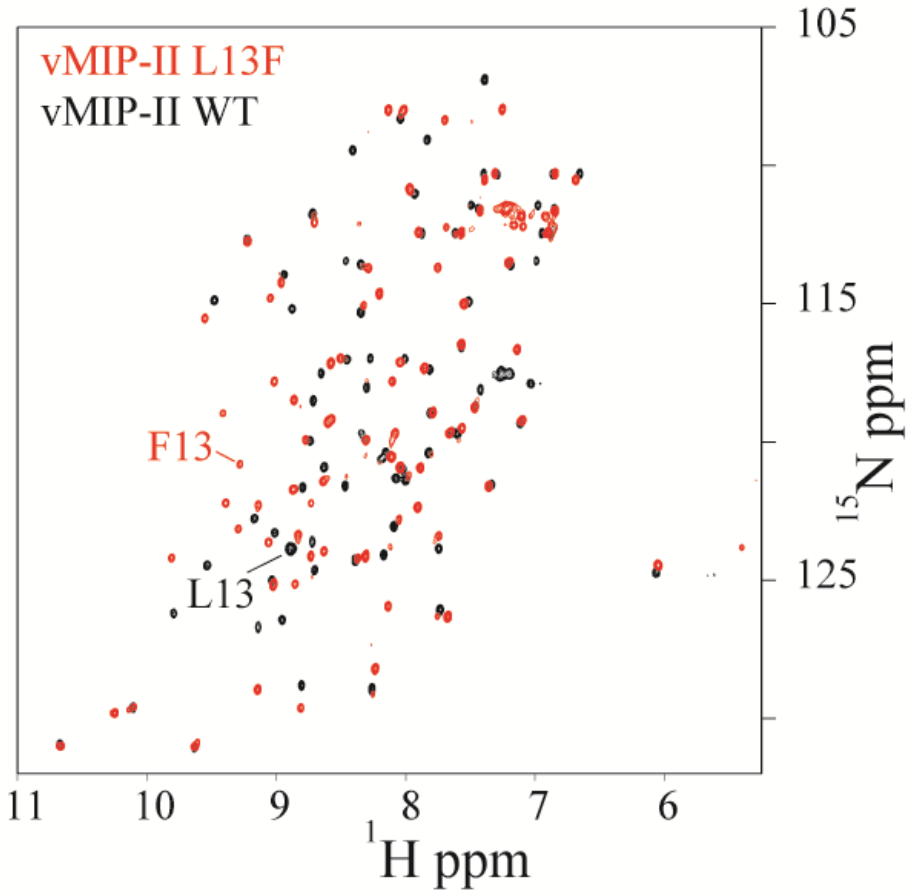

Figure 3.3 Overlay of ^{1}H-^{15}N 2D HSQC spectra of vMIP-II WT (black) and L13F variant (red). Both proteins are nice folded at pH 5.4 and 1 mM concentration. Peak shifts upon mutation were observed at many residues, not only at the mutation site, indicating a quaternary structural shift.

binding, while mutating Phe13 to Ala abolished its ability to bind CCR5. This finding is consistent with previous findings that N-terminal peptide of vMIP-II does not have the ability to bind CCR5 (182-183,185), and further proved that the N-terminus of vMIP-II is not involved in CCR5 binding and that vMIP-II may use a different strategy to bind CC chemokines, especially CCR5. However, putting a charged residue in the 13th position did cause slight disruption of vMIP-II's binding to CCR5. As shown in Table 3.1, L13K and L13E mutation showed 5-7 fold decrease in CCR5 binding, indicating that vMIP-II prefers a non-polar residue at this position for binding CCR5.

Table 3.1 Binding affinities of vMIP-II L13 variants to CCR5 and CXCR4.

vMIP-II mutants	**Binding IC_{50} (nM, CCR5)**	**Binding IC_{50} (nM, CXCR4)**
Wild type	14.8 ± 2.6	33.7 ± 7.8
L13F	18.3	36.8 ± 15.8
P8AL13F	25.6 ± 21.5	15.7 ± 11.3
L13A	24.0 ± 6.9	32.4 ± 4.6
L13E	84.5 ± 10.6	49.6 ± 17.9
L13K	110 ± 17	15.7 ± 11

Results are average IC50 ± the uncertainty of the average (half the difference) or Standard Deviation (nM) from 2 or more independent experiments in triplicate.

Previous studies have shown that the N-terminus of vMIP-II is involved in CXCR4 binding (182-183,185). Luo et al. found that Leu1, Arg7 and Lys9 are the most critical residues for the V1 (1-21) peptide to bind CXCR4 while the N-loop residues are not important (183). To test whether mutations to the N-loop region affects CXCR4 binding for the native vMIP-II protein, variants with mutations at the 13th position were tested for CXCR4 receptor binding. As shown in Table 3.1, all the mutations, even charged mutations, did not affect vMIP-II's binding to CXCR4, confirming that the 13th position, although critical in human CC chemokines, is not involved in vMIP-II's binding to either CCR5 or CXCR4.

The positively charged residues distributed along one surface of vMIP-II are important for vMIP-II's binding to CCR5. Mutation studies at the 13th position of vMIP-II confirmed previous predictions that vMIP-II does not use its N-terminus to bind CCR5. Thus, vMIP-II must have a binding site at its core domain to bind CCR5. Due to the similarity of the distribution pattern of the positively charged residues between vMIP-II and MIP-1β, we hypothesized that these positively charged residues might constitute the binding surface of vMIP-II to interact with the negatively charged N-terminal domain of CCR5.

To verify this hypothesis, we first made a series of single mutations to the positively charged residues on this surface including R18, K45, R46 and R48. All mutants were tested on NMR to verify their structural integrity, and HSQC experiments showed that they were all nicely folded (data not shown). Mutants were then tested for binding to CCR5: all of them showed reduced binding affinity compared to vMIP-II WT.

As shown in Table 3.2, although they all exhibited a moderate decrease in CCR5 binding affinity (6-18 fold worse than WT), none of these residues alone abolished vMI-II's CCR5 binding. This is probably due the large number of positively charged residues on the vMIP-II surface. Because of the cumulative contributions from all these residues, mutation to a single one of them may not yield significant differences. It is also consistent with previous findings in the studies of MIP-1β/CCR5 binding (24) and human growth hormone/receptor interaction (189-190) that a single mutation may not yield significant functional differences.

To further verify the importance of these positively charged residues, multiple mutations were conducted to the conserved BBXB domain at the 40's loop of vMIP-II. Double mutation K45A/R46A and triple mutation K45A/R46A/R48A severely disrupted vMIP-II's CCR5 binding, and no binding could be detected under 2000 nM concentration. Results indicated that just as with human CC chemokines (24,122) the highly conserved, highly basic BBXB domain of vMIP-II is critical for receptor binding.

In addition to the positively charged residues, Pro21 at the N-loop region of MIP-1β also contributes some to its CCR5 binding (Figure 3.2A), P21A mutation caused 4 fold drop in binding affinity (163). Similar mutation on vMIP-II yielded a similar effect on vMIP-II, with a P21A mutation causing a 4 fold drop in vMIP-II's CCR5 binding affinity. It's quite possible that except for the huge differences at the N-terminus and the 13^{th} position, the vMIP-II binds to CCR5 similarly as MIP-1β, using a positively charged binding surface at its core domain.

Table 3.2 Binding affinities of vMIP-II core domain variants to CCR5 and CXCR4.

vMIP-II mutants	Binding IC_{50} (nM, CCR5)	Binding IC_{50} (nM, CXCR4)
Wild type	14.8 ± 2.6	33.7 ± 7.8
R18A	221.5 ± 88	98.2 ± 91.7
K45A	275 ± 46	149.9 ± 84.4
R46A	84.5 ± 9.2	97.3 ± 3.7
R48A	196 ± 28	60.3 ± 0.3
K45A/R46A	> 2000	710.4 ± 674.8
K45A/R46A/R48A	> 2000	> 2000
P21A	60.3 ± 6.7	22.6 ± 22.5
K37A	69	97.2 ± 9.5

Results are average IC50 ± the uncertainty of the average (half the difference) or Standard Deviation (nM) from 2 or more independent experiments in triplicate.

Unlike MIP-1β which has a small number of positively charged residues, vMIP-II has 8 Lys and 5 Arg on its surface, but probably not all of them are involved in receptor binding. Several positively charged residues including R18, K45, R46, and R48 are located on one side of the protein which is analogous to the CCR5 binding surface of MIP-1β as shown in Figure 3.2. On the other side of vMIP-II, there are also several positively charged residues including K37, K54, K60 and K61 (Figure 2.5). We

hypothesized that these positively charged residues, however, may not be involved in receptor binding. The K37A mutation in vMIP-II did not show significant difference in binding compared to vMIP-II WT. More extensive testing including multiple mutations needs to be done to confirm the notion that positively charged residues on this side of the protein do not contribute to CCR5 binding.

Taken together, we conclude that positively charged residues distributed along one surface of the core domain of vMIP-II including R18, K45, R46, and R48 constitute the binding surface for CCR5 receptor binding. vMIP-II binds CCR5 mainly through electrostatic interactions between its positively charged core domain binding surface and the negatively charged N-terminal domain of CCR5. Since vMIP-II may only interact with CCR5 using this site, vMIP-II/CCR5 binding may be a rare exception of the 2-site binding model. This unique 1-site binding is likely a general strategy used by vMIP-II to bind multiple human CC chemokines. As a viral chemokine, vMIP-II is encoded to antagonize as many human chemokine receptors as possible and help the virus to escape from the host immune system. For this purpose, the 1-site binding strategy may be better than the normal 2-site binding strategy, because 1-site binding would make vMIP-II a general binding for many receptors while 2-site binding makes it specific for only a few receptors.

The positively charged residues distributed along one surface of vMIP-II are also important for vMIP-II's binding to CXCR4. Previous studies suggested that the N-terminus of vMIP-II is involved in CXCR4 binding, and that there are other parts of the protein that contribute to the interaction with CXCR4 (182-183,185). However, the

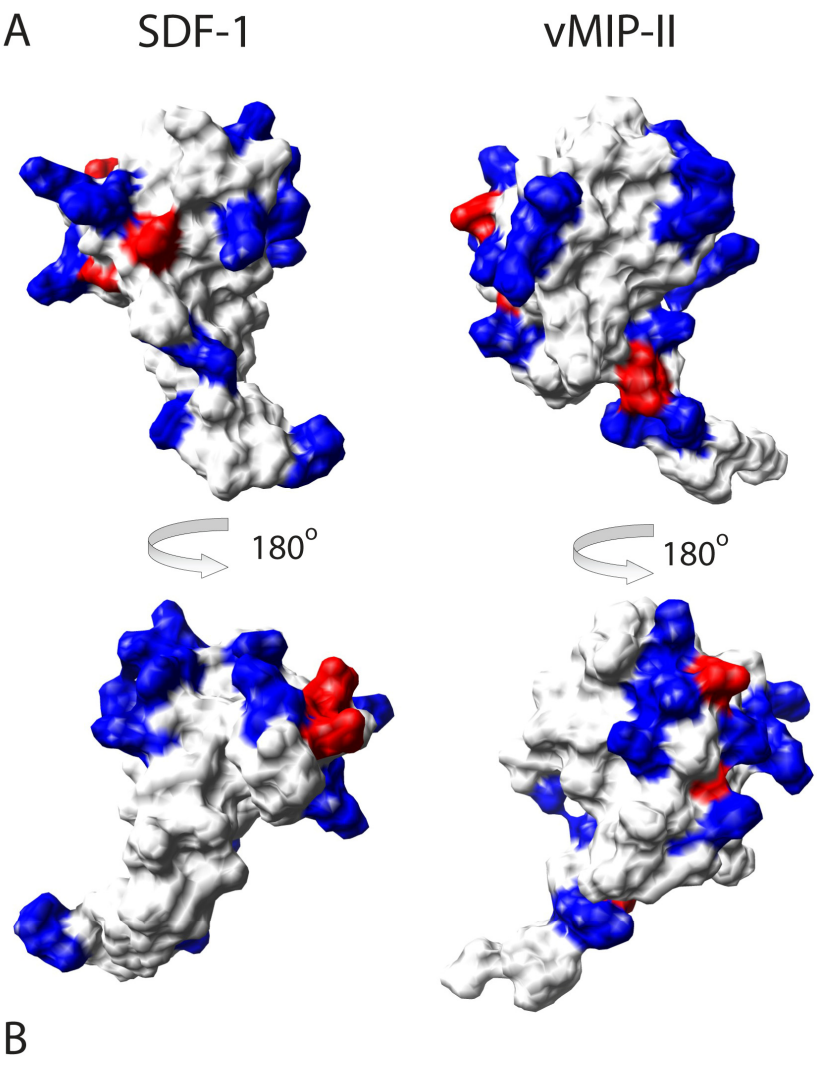

Figure 3.4 Structural comparison and sequence alignment of vMIP-II with SDF-1. **A.** Surfaces of SDF-1 and vMIP-II aligned in the same orientation (front and back). Positively charged residues are labeled in blue, while the negatively charged residues are labeled in red. **B.** Sequence alignment of vMIP-II and SDF-1, important CXCR4 binding residues on SDF-1 are labeled in orange (159).

other CXCR4 binding site of vMIP-II has not yet been characterized. According to the 2-site binding model, the N-terminus of vMIP-II binds to the extracellular loops and the transmembrane domains of CXCR4, while the core domain of vMIP-II should contact the N-terminal domain of CXCR4, just like the interaction between CXCR4 and its only native ligand SDF-1 (158-159). However, as shown in Figure 3.4A, unlike MIP-1β, the residue distribution pattern on the core domain surface of SDF-1 and vMIP-II are very different. Besides, sequence alignment between vMIP-II and SDF-1 showed that vMIP-II lacks the homologous residues that have been shown in SDF-1 to be important in CXCR4 binding (159) (Figure 3.4B). vMIP-II and the CXC chemokine SDF-1 are very different in sequences and surface structures. Further considering the sequence and structural similarities between vMIP-II and CC chemokines and the fact that most receptors vMIP-II bind to are CC chemokine receptors, we hypothesized that vMIP may not use a similar strategy to bind CXCR4 as CXC chemokines do. Because of the negatively charged nature of the N-terminal domain of CXCR4, we further hypothesized that the positively charged surface on the core domain of vMIP-II might also play a role in binding CXCR4.

To verify this hypothesis, we tested the vMIP-II variants with mutations to the positively charged residues for their binding ability to CXCR4. As shown in Table 3.2, just as in CCR5 binding, mutations to the positively charged residues indeed caused a significant drop of binding affinity to CXCR4, and triple mutation at the BBXB domain showed no detectable binding to CXCR4 in our experimental conditions. These results indicated the importance of these positively charged residues in CXCR binding.

Through comparing the CCR5 and CXCR4 binding profile of these variants with mutations at the core domain, we found 2 major differences: 1. the N-loop residues R18 and P21 may not be involved in CXCR4 binding, or at least not as important as other residues. R18A mutation caused 15 fold drop of binding affinity to CCR5, while it only caused a 3 fold difference in CXCR4 binding. P21A mutation decreased vMIP-II binding affinity to CCR5 by 4 fold, but had no effect in CXCR4 binding; 2. The general magnitude of affinity drop caused by mutations are different in CCR5 binding and CXCR4 binding. Mutations caused more significant decrease in CCR5 binding than in CXCR4 binding, probably because these residues are solely responsible for vMIP-II's CCR5 binding, while vMIP-II also bind to CXCR4 using the N-terminus.

Conclusion. As a conclusion of this study, we have found that the highly basic binding surface at the core domain of vMIP-II including residues R18, K45, R46, and R48 is important in receptor binding. This binding surface is solely responsible for vMIP-II's binding to CCR5, and this surface, together with the N-terminus are used by vMIP-II to interact with CXCR4. Considering the fact that the N-termini of most receptors are heavily sulfated and negatively charged, this highly basic core domain binding surface might be the key to vMIP-II's broad-spectrum receptor binding ability.

Future plans. Mutagenesis studies have certain limitations: 1. Single mutations are not sensitive enough. Due to the cumulative contributions made by many residues, mutating one of the residues may not yield detectable functional difference. 2. Only a limited number of mutants were made, so we could not comprehensively map out all the residues involved in vMIP-II's receptor binding.

NMR titration experiments will overcome these limitations and will be a nice complement to the current study. We plan to titrate in different concentrations of tyrosine-sulfated N-terminal peptides of CCR5 and CXCR4 into a fixed concentration of wild type vMIP-II, and map out the peak movements of vMIP-II on 2D-HSQC spectra. Residues of vMIP-II that undergo significant chemical shift changes are probably the residues making direct contact with the receptor N-terminal peptides. Right now, we are actively seeking collaborators who can synthesize the tyrosine sulfated peptides.

CHAPTER IV

DEVELOPING CHEMOKINE-BASED HIGHLY POTENT CHIMERIC HIV-1 ENTRY INHIBITORS

Introduction

Approximately 33 million people are currently infected with HIV, and millions more are infected each year (191). There is currently no vaccine, and treatments usually involve inhibiting viral activity post-infection, by inhibiting the HIV protease or reverse transcriptase. More recently, therapies that target other parts of the viral life cycle have been approved, including an HIV integrase inhibitor (58).

One of the most promising areas in the fight against HIV/AIDS has been the development of entry inhibitors, which generally bind to either the viral surface or the human cell surface to stop HIV before it can enter a cell. Figure 1.3 is a diagram showing the HIV cell entry process: HIV surface protein gp120 first makes contact with human cell surface protein CD4, which causes a conformational rearrangement in gp120, allowing the protein to then bind its co-receptor on the cell surface (either the chemokine receptor CCR5 or CXCR4. During this process, the HIV protein gp41 is exposed and its fusion peptide enters the cell surface. Toward the end of the infection process, the N-terminal helical trimer folds over to contact the C-terminal trimer of gp41, forming a 6-helix bundle that likely pulls the membranes of the two entities in closer proximity to

assist fusion of the virus to the cell (64-65). Recently, it has been reported that some of these events may occur in the endosome (66).

Inhibition of HIV entry can be achieved by blocking one or more of the events that lead to infection. Proteins, particularly lectins that bind to gp120, have been shown to be effective inhibitors (87-89), as are peptides that bind to gp41 to stop 6-helix bundle formation (64). In particular, so-called C-peptides that are derived from the C-terminus of gp41 effectively bind to the N-terminus of gp41 to inhibit infection. One of these peptides, T-20, has been approved for clinical use (90-92). Another strategy to inhibit HIV infection involves binding the co-receptor on the human cell surface, particularly CCR5 (84-86,192-197). Natural ligands for CCR5, namely chemokines MIP-1β, MIP-1α and RANTES, were found to be able to block HIV infection (11). It was later shown that variants of these chemokines, particularly RANTES, could lead to even more highly potent inhibition (85-86,192-194,197). Despite the effectiveness of entry inhibition strategies, many of them have serious drawbacks. While the recent RANTES variants are extremely potent, they work by binding CCR5, so are only effective against R5 tropic virus, not against X4 tropic virus (86). While the C-peptides are effective against most strains of HIV, their potency is limited to nanomolar levels, and the virus can evolve so that the peptides bind less well (64,90-93).

Considering the stepwise nature of the HIV entry process, there are certain time windows in which multiple targets are simultaneously susceptible to inhibition. Binding of co-receptor inhibitors and fusion peptides to their targets can both be achieved after the exposure of gp41 and before gp120 interacts with its co-receptor. Evidence suggests

that co-receptor binding is a key factor in the kinetic properties of fusion, and that lowered co-receptor density or weakened co-receptor-gp120 binding slows down gp41 mediated cell fusion and prolongs the time window of the intermediate states of gp41 for fusion peptides to bind (198-199). We reasoned that a properly engineered chimeric molecule containing one co-receptor inhibitor and one fusion peptide can block HIV cell entry at both steps more potently and could overcome the drawbacks of either individual component.

We chose to use CCR5 ligand RANTES variants 5P12-RANTES and 5P14-RANTES as the co-receptor inhibitor portion of our chimeric protein. These variants were recently developed by Gaertner et al., and are among the most potent R5 entry inhibitors yet developed, with HIV inhibition at mid-picomolar levels in *in vitro* assays (85-86). In addition to their high potency, they are small proteins that are able to be made recombinantly, and are easy to produce at low cost. For the second part of the chimeric inhibitor, C34 and the nearly identical C37, are well characterized C-peptides and are highly effective at nanomolar concentrations *in vitro* (64,92-93,200-201). It has also been shown that covalently-linking C-peptides to a range of un-related proteins did not diminish their anti-HIV activity, and in one case the linked C-peptide showed longer *in vivo* life time (202-203). So C37 was chosen to be part of the chimeric molecule presented here.

We report here the success of this strategy, in which RANTES variants linked to the C-peptide C37 are shown to be even more effective against R5 virus than the parent RANTES variants, leading to low-picomolar HIV inhibition. The chimeric proteins also

exhibited nano-molar anti-X4 activity, which can be further enhanced by co-expression of CCR5 receptor on the target cell surface. A clear mechanism of delivery of C37 by the RANTES variants is observed, even against X4 viral strains.

Experimental Procedures

Protein preparation. The genes for 5P12-RANTES, 5P12-linker-C37, 5P14-RANTES, 5P14-linker-C37 and P2-linker-C37 were made using standard thermocycling method. Oligonuleotides were purchased from Bioneer Corp (Alameda, CA). Mutations to 5P12-linker-C37 were made using the QuikChange Site-Directed Mutagenesis method (Stratagene, La Jolla, CA). These genes were expressed along with an N-terminal SUMO tag in the pET SUMO expression vector from Invitrogen (Carlsbad, CA). The vectors were transformed into BL21(DE3), and grown in 1 liter ^{15}N minimal medium using $^{15}NH_4Cl$ as the only nitrogen source. Protein production was induced with 1 mM IPTG when the absorbance at 600 nM reached 0.7. The cells were incubated with shaking for 20 hours at 22° after induction and then harvested by centrifugation. The cell pellet was resuspended in cracking buffer (500 mM NaCl, 20 mM Tris, pH 8.0) with 10 mM benzamidine, and French pressed twice at 16,000 psi. The solution was centrifuged at 20,000 ×g for 30 minutes. The supernatant was discarded and the pellet was resuspended in 10 ml refolding buffer (5 M Guanidinium/HCl, 3 mM EDTA, 50 mM Tris, 50 mM NaCl, pH 8.0) with 10 mM β-mercaptoethanol. The resuspended solution was incubated at room temperature for 2 hours with stirring followed by a

centrifugation at 20,000 ×g for 60 minutes. The supernatant containing the denatured protein was added drop wise into 90 ml folding buffer (50 mM NaCl, 20 mM Tris, pH 8.0) with 10 mM β-mercaptoethanol. The solution was incubated overnight at 4° and then precipitants were removed by centrifugation at 20,000 ×g for 60 minutes. The supernatant was dialyzed in 4 liter dialysis buffer (50 mM NaCl, 20 mM Tris, pH 8.0) with slow stirring, and the buffer was changed after 6 hours. After dialysis, the solution was centrifuged again, and the supernatant containing the refolded protein was passed through a Ni chelating column (GE Healthcare) and eluted with imidazole in 500 mM NaCl, 50 mM Tris (pH 8.0) buffer. The purified proteins were dialyzed in 4 liter 50 mM NaCl, 20 mM Tris buffer (pH 8.0) to remove imidazole. To cleave the SUMO tag, recombinant yeast ULP1 protease was added and the solution was incubated overnight at 4°. (ULP1 protease was produced and purified in our lab as briefly described: ULP1 was expressed in LB medium using a pET-28b vector and the cells were collected and French pressed. The ULP1 protease from the supernatant was purified using a Ni chelating column). Precipitated matter was removed by centrifugation at 20,000 ×g for 30 minutes and the product was separated from the SUMO tag using an acetonitrile gradient on a C4 reversed phase chromatography column (Vydac, Hesperia, CA) on an Akta purification system (GE Healthcare), and then lyophilized by the Labconco freeze dry system (Labconco Corporation, Kansas City, MO). In our hands, we were able to obtain a yield of 5 mg pure protein from 1 liter *E. coli* prep. For proteins containing a 20-amino-acid linker, the protocol was modified to include an extra step of centrifugation to remove unfolded protein before adding TFA and acetonitrile for the

final C4 column purification step. C37 peptide: The N-acetylated and C-amidated fusion peptide C37 was purchased from Genescript (Piscataway, NJ).

NMR spectroscopy. All NMR data were acquired at 25 °C on a four-channel 600 MHz Bruker Avance III spectrometer equipped with a GRASP II gradient accessory and a TCI cryoprobe, which has an actively-shielded Z-gradient coil. NMR samples were prepared by adding ^{15}N-labeled lyophilized proteins into 20 mM sodium phosphate buffer (pH = 2.5) with 5% D_2O. The chemical shift was referenced relative to internal DSS (2,2-dimethyl-2-silapentane-5-sulfonic acid) (102). The data were processed using NmrPipe (103) and analyzed using PIPP (104). For 2D HSQC spectra, SW=6982.631 Hz (^{1}H) and 1700.030 Hz (^{15}N), with 512* poin^{ts} in ^{1}H and 128* points in ^{15}N.

Cell lines and viruses: HeLa-ADA, and HeLa-P5L cells were kindly provided by Dr. M. Alizon and Dr. Anne Brelot (Cochin Institute, Paris, France) (59). HeLa-TZM-bl, HL2/3 and Magi-CXCR4 cells were obtained through the NIH AIDS Research and Reference Reagent Program, Division of AIDS, NIAID, NIH: Hela-TZM-bl cell line from Dr. John C. Kappes, Dr. Xiaoyun Wu and Tanzyme Inc (204-207); HL2/3 from Dr. Barbara K. Felber and Dr. George N. Pavlakis (208); Magi-CXCR4 was donated by Dr. Michael Emerman (209). 293FT cells were kindly provided by Dr. Jennifer Manilay and were originally obtained from Invitrogen (Carlsbad, CA). Viruses used in replication-competent viral assays and PBMC assays including HIV-1 Ba-L, ADA and IIIB were obtained from the NIH AIDS Research and Reference Reagent Program, Division of AIDS, NIAID, NIH: HIV-1 Ba-L from Dr. Suzanne Gartner, Dr. Mikulas Popovic and

Dr. Robert Gallo (210); HIV-1 ADA-M from Dr. Howard Gendelman (211-214); HIV-1 IIIB from Dr, Robert C. Gallo (215-217).

Cell-cell fusion assay. HIV-1 cell-cell fusion assays were carried out as previously described (59). Briefly, 10^4/well target cells (HeLa-P5L for R5-tropic fusion assay, HeLa-TZM-bl and Magi-CXCR4 for X4-tropic fusion assay) were seeded in a 96 well plate. After 12 hours incubation, the medium was replaced with 50 μL per well fresh RPMI 1640 (DMEM for the X4 assay). Different concentrations of inhibitors were added and mixed well. 10^4/well effector cells (HeLa-ADA for R5 assay, HL2/3 for X4 assay) in 50 μL medium were then added to each well. The cells were incubated at 37 °C for 24 hours to allow fusion. Cells were lysed with 20 μL 0.5% NP-40 (US Biological) in PBS (pH 7.4) for 30 min, then 30 μL PBS with 8 mM substrate CPRG (chlorophenol red-β-D-galactopyranoside, Calbiochem), 20 mM KCl and 10 mM β-mercaptoethanol (Sigma) was added to each well. The absorbance signal at wavelength 570 nm and 630 nm were measured and the 570/630 ratio for each well was calculated. Data was analyzed using KaleidaGraph (Synergy Software, Reading PA).

Single-round viral infection assay. Plasmids used to generate the pseudotyped viral particles were all obtained through the NIH AIDS Research and Reference Reagent Program, Division of AIDS, NIAID, NIH: Plasmid pNL4-3.Luc.R^-E^- (with deletion of the envelope and vpr genes), and envelope plasmids pSV-ADA, pSV-JRFL from Dr. Nathaniel Landau (218); pHEF-VSVG from Lung-Ji Chang (219). pCAGGS-SF162-gp160 from Leonidas Stamatatos and Dr. Cecilia Cheng-Mayer (220-222); HXB2-env from Dr. Kathleen Page and Dr. Dan Littman (223). HIV-1 clone Ba-L.01 from Dr. John

Mascola (224); pSVIII-91US005.11 from Dr. Beatrice Hahn (225); 6535, clone 3 (SVPB5) from Dr. David Montefiori, Dr. Feng Gao and Dr. Ming Li (226). To make the pseudo-typed viral particles, 293FT cells were co-transfected with the pNL4-3.Luc.R^-E^- plasmid and an envelope plasmid using the ProFection Mammalian Transfection System (Promega). 48 hours post-transfection, the supernatant were collected, centrifuged and filtered with a 0.45 μM syringe filter. The viral stocks were stored at -80 °C. For the infection assay, 10^4 per well cells (HeLa-TZM-bl cell for both the R5 and X4 tropic assays, Magi-CXCR4 cells for the control "X4 only" assays) were seeded in a 96 well plate. The next day, after changing the medium, different concentration of inhibitors were added to the wells and mixed, and then the virus particles were added. The final volume was adjusted to 100 μL per well. After incubation for 3 days (the medium was changed once), the cells were lysed and the substrate CPRG was added (as described above). The absorbance signal at wavelength 570 nm and 630 nm were measured and the 570/630 ratio for each well was calculated. The data were plotted using Microsoft Excel, and the IC_{50} was determined using a linear equation fitted between two data points surrounding 50% inhibition. For presentation purposes, data shown in the figures were plotted and fitted as curves using a four-parameter logistic equation in Kaleidagraph (Synergy Software, Reading, PA).

Replication competent viral assay and PBMC assay. The replication competent viral assays were performed as previously described (227). TZM-bl cells were used for both the CCR5 and CXCR4 tropic assays and the HeLa-CXCR4 cells were used for the control X4 only assays. The PBMCs were freshly isolated and used in viral assays as

previously described (227-228). The viruses used to infect the target cells were HIV-1 Ba-L, ADA (CCR5 tropic), and IIIB (CXCR4 tropic) strains. Each assay was conducted in parallel with control compounds AMD3100 (CXCR4 inhibitor; positive control inhibitor for IIIB, and negative control inhibitor for Ba-L and ADA) and TAK779 (CCR5 inhibitor; positive control inhibitor for Ba-L and ADA, and negative control inhibitor for IIIB) (data not shown). Cytotoxicity of the inhibitors was assayed using the CellTiter 96 AQueous One Solution cell proliferation assay (Promega) (227). All tested compounds showed no toxicity at the highest tested concentration (100 nM). Data were plotted and presented as described for the single-round viral assays.

Receptor density comparison using flow cytometry. The CCR5 receptor expression levels on HeLa-TZM-bl cells and HeLa-P5L cells were compared using flow cytometry. The cells were incubated with FITC conjugated anti-CCR5 antibody (clone 2D7, BD Biosciences), and the fluorescence values were determined using a FACSAria cytometer (BD Biosciences). Flow cytometric data was analyzed using FlowJo software (TreeStar).

Results

Design of the chimeric proteins. 5P12-RANTES and 5P14-RANTES are variants of the chemokine RANTES developed by Gaertner et al., each with 10 different amino-acid mutations at the N-terminus (86). Unlike natural RANTES which is an agonist to CCR5, 5P12 triggers neither receptor sequestration nor cell signaling, while 5P14 causes

receptor sequestration but not signaling (86). Lack of receptor-signaling activity is a valuable property in an anti-HIV agent since immunologic activation could lead to more susceptibility to infection. The flexible N-terminus of both 5P12 and 5P14 are critical for their receptor related anti-HIV function (86), but the C-terminal amino acids, which typically form an α-helix in the chemokine structure, are likely not functionally important. So we choose to link the C37 peptide to the C-terminus of 5P12 and 5P14, leaving the N-terminus intact. The C-termini of 5P12-RANTES and 5P14-RANTES were covalently linked to the N-terminus of C37 peptide using 10-amino-acid flexible glycine/serine linkers GGGGSGGGGS. We denoted the engineered chimeric proteins 5P12-linker-C37 and 5P14-linker-C37. All the individual RANTES variants and chimeric inhibitors were expressed in *E. coli*, and purified to no less than 95% purity as determined by SDS-PAGE. Proteins were tested by NMR to determine the structural integrity. ^{1}H-^{15}N correlation spectra revealed that all proteins are nicely folded (Figure 4.1). 5P12-linker-C37 and 5P14-linker-C37 exhibited the same peak placement as free 5P12 and 5P14, respectively, except for the extra peaks in the unstructured region of the spectrum, which are likely caused by the linker and the C37 peptide, which is known to be unstructured in the absence of its binding partner (201). These data indicate that linking C37 to a RANTES variant does not compromise the native structure of the RANTES variant.

Anti-viral potencies of 5P12-linker-C37 and 5P14-linker-C37 against R5-tropic HIV viruses. *In vitro* assays including the cell-cell fusion assay, single-cycle viral infection assay, replication-competent viral assay and PBMC assay were conducted to

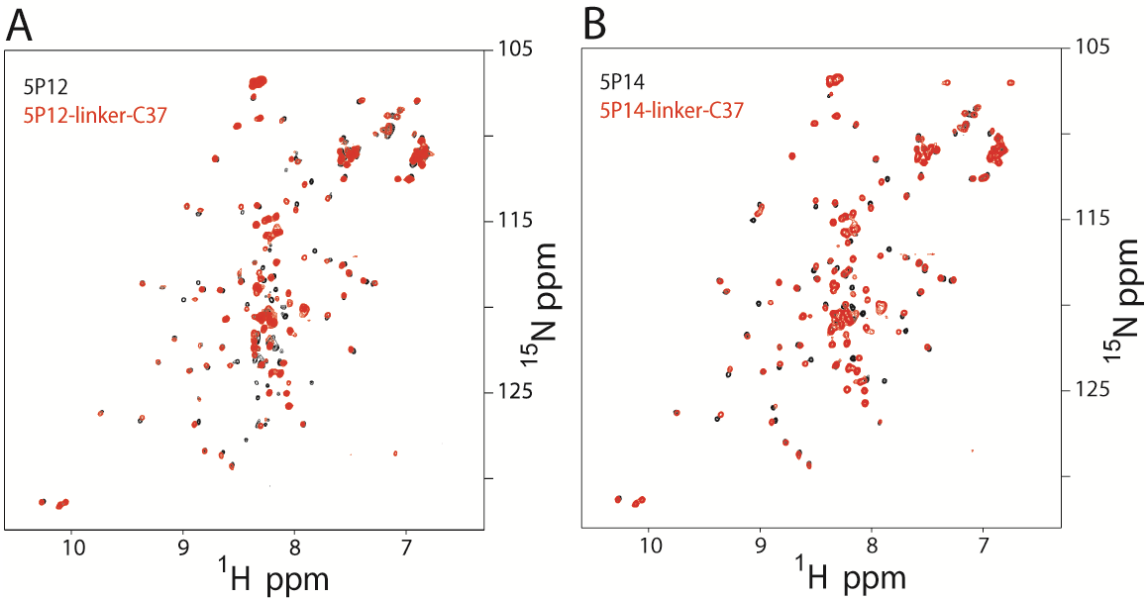

Figure 4.1 ^{1}H-^{15}N 2D HSQC spectra of the chimeric proteins and the parent RANTES variants. **A**. Overlay of 5P12-linker-C37 (red peaks) with 5P12-RANTES (black peaks); **B**. Overlay of 5P14-linker-C37 (red peaks) with 5P14-RANTES (black peaks).

Figure 4.2 Antiviral activities of the chimeric inhibitors against R5 tropic virus. Chimeric inhibitors showed higher anti-HIV potency than the control groups (RANTES variants alone, C37 alone, or 1:1 mixture of the RANTES variants and C37). **A, B**. Cell-cell fusion assay using effector cells expressing ADA viral envelopes. **C, D**. Single-cycle viral infection assay (Ba-L strain pseudoviral particles infecting TZM-bl cells). **E, F**. Replication-competent viral assay (Ba-L strain virus infecting TZM-bl cells). Data shown are typical results of single assays done in triplicate. Error bars represent standard deviations of the data.

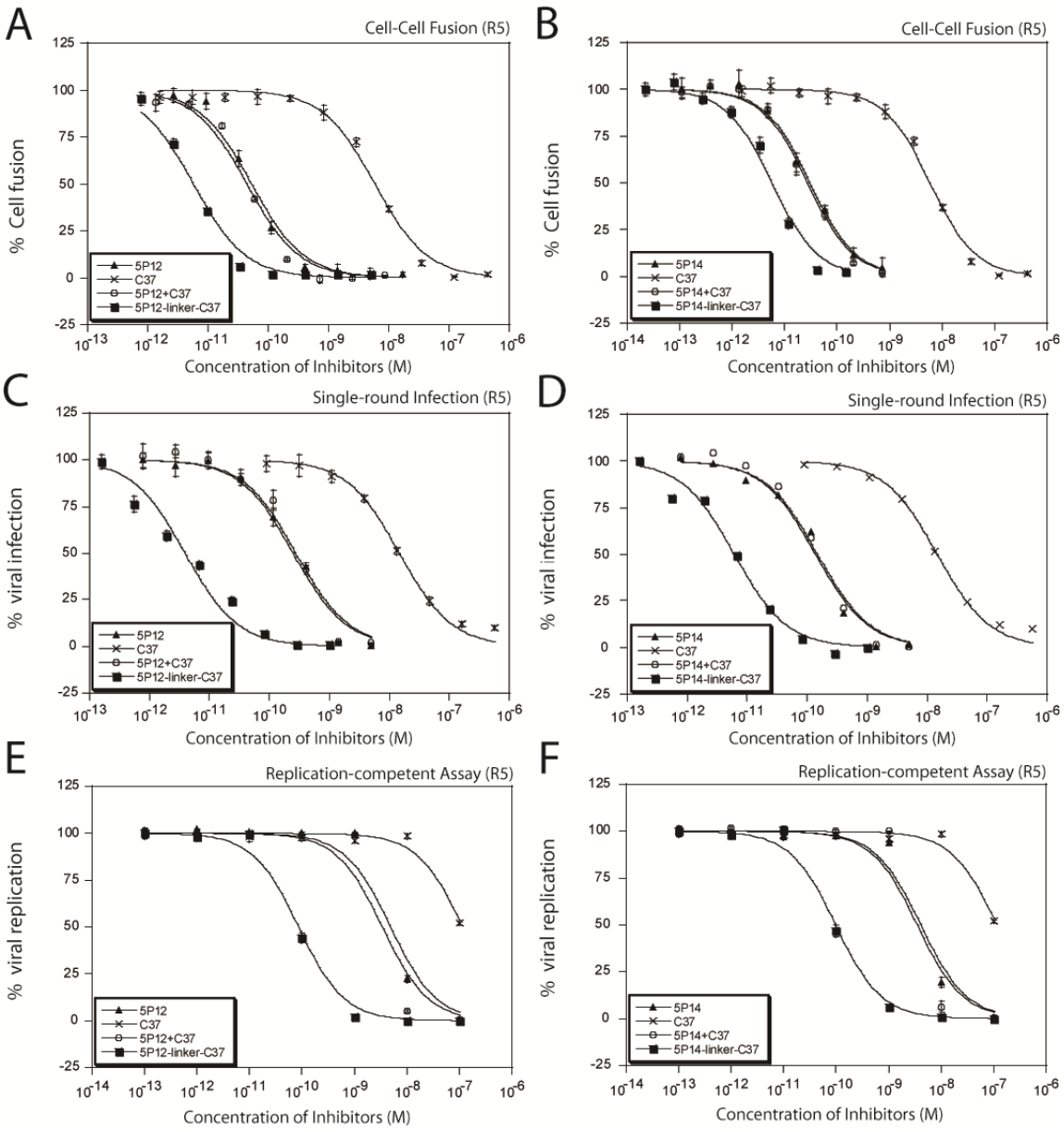
A
Cell-Cell Fusion (R5)
% Cell fusion
Concentration of Inhibitors (M)
5P12
C37
5P12+C37
5P12-linker-C37
B
Cell-Cell Fusion (R5)
% Cell fusion
Concentration of Inhibitors (M)
5P14
C37
5P14+C37
5P14-linker-C37
C
Single-round Infection (R5)
% viral infection
Concentration of Inhibitors (M)
5P12
C37
5P12+C37
5P12-linker-C37
D
Single-round Infection (R5)
% viral infection
Concentration of Inhibitors (M)
5P14
C37
5P14+C37
5P14-linker-C37
E
Replication-competent Assay (R5)
% viral replication
Concentration of Inhibitors (M)
5P12
C37
5P12+C37
5P12-linker-C37
F
Replication-competent Assay (R5)
% viral replication
Concentration of Inhibitors (M)
5P14
C37
5P14+C37
5P14-linker-C37

evaluate the anti-viral potencies of the chimeric inhibitors (Figure 4.2). Control compounds including RANTES variants alone, C37 alone, and a mixture of RANTES variants with C37 (1:1 ratio) were tested in parallel with the chimeric inhibitors.

In R5-tropic cell-cell fusion assays, consistent with previously published data (86), 5P12-RANTES and 5P14-RANTES showed anti-HIV IC_{50} values of 50 pM and 30 pM, respectively, while the IC_{50} of C37 was in the low-nano-molar range, two orders of magnitude higher. As expected, because of the large differences of the RANTES variants and C37 in anti-viral potencies, simply mixing 5P12 or 5P14 with C37 in 1:1 ratio exhibited similar potency as 5P12 or 5P14 alone. But the chimeric inhibitors exhibited anti-viral potencies stronger than either of the components alone, or the unlinked combination of the two (Figure 4.2A, B, Table 4.1). These findings suggest the enhancement is not due to simply adding two inhibitors together, but rather an intra-molecular mechanism of the covalently linked inhibitors.

Further testing with multiple strains of R5 virus in single-cycle viral infection assays in TZM-bl cells revealed similar results (Table 4.2, Figure 4.2C, D). For all 6 strains tested, 5P12-linker-C37 and 5P14-linker-C37 exhibited up to 100 fold greater potency compared to 5P12 and 5P14 alone, or compared to a 1:1 mixtures of them with C37 (Table 4.2 and Table 4.3). It was also found that the potency enhancement is strain dependent: For virus strains that are particularly sensitive to C37, such as Ba-L, 5P12-linker-C37 and 5P14-linker-C37 showed 70 - and 23 - fold potency enhancement over 5P12 and 5P14, respectively. But for virus strains that are less sensitive to C37 such as 6535, 5P12-linker-C37 was only 2.5 fold better than 5P12, while 5P14-linker-C37

Table 4.1 Anti-HIV activities of the chimeric inhibitors in R5 cell-cell fusion assay.

Inhibitor	*5P12*	*5P12+C37*	*5P12-linker-C37*	*C37*	*5P14*	*5P14+C37*	*5P14-linker-C37*
IC_{50} (nM)	0.051 ± 0.01	0.044 ± 0.005	0.009 ± 0.003	9.1 ± 4.1	0.03 ± 0.002	0.03 ± 0.01	0.006 ± 0.001

Results are average IC_{50} ± SD (nM) from 4 or more independent experiments in triplicate. R5 fusion stands for P5L (R5) cells fusion with Hela-ADA cells.

Table 4.2 Anti-HIV activities of the chimeric inhibitors in single-cycle viral assay.

HIV virus	*Tropism*	*5P12-linker-C37*	*5P12*	*C37*	*5P14-linker-C37*	*5P14*
Ba-L	R5	0.004 ± 0.001	0.29 ± 0.09	15 ± 0.6	0.007 ± 0.001	0.16 ± 0.01
SF162	R5	0.006 ± 0.001	0.59 ± 0.09	38 ± 13	0.017 ± 0.005	0.22 ± 0.06
ADA	R5	0.025 ± 0.004	0.47 ± 0.09	44 ± 14	0.037 ± 0.002	0.18 ± 0.03
JRFL	R5	0.015 ± 0.001	0.51 ± 0.01	49 ± 7.4	0.02 ± 0.006	0.14 ± 0.03
US005	R5	0.03 ± 0.006	0.20 ± 0.02	59 ± 16	0.025 ± 0.006	0.09 ± 0.03
6535	R5	0.22 ± 0.05	0.55 ± 0.07	261 ± 57	0.08 ± 0.02	0.10 ± 0.03
HXB2 (Magi-X4)	X4	18 ± 7.4	> 500	9.6 ± 1.3	14 ± 5.0	> 500
HXB2 (TZM)	X4	0.001 ± 0.0003	> 500	6.1 ± 0.3	0.001 ± 0.0001	> 500
VSV-G	Ctrl	> 500	> 500	> 500	> 500	> 500

Results are average IC_{50} ± Standard deviation (nM) from 4 or more independent experiments in triplicate. 5P12+C37 and 5P14+C37 groups showed similar R5 anti-viral activity to 5P12 and 5P14 alone, and similar X4 anti-viral activity to C37 (Table S3)

Table 4.3 Anti-HIV activities of 5P12+C37 and 5P14+C37 in single-cycle viral assay.

HIV virus	*Tropism*	*5P12+C37*	*5P14+C37*
BaL	R5	0.30 ± 0.05	0.16 ± 0.03
SF162	R5	0.61 ± 0.11	0.13 ± 0.08
ADA	R5	0.54 ± 0.06	0.13 ± 0.009
JRFL	R5	0.56 ± 0.05	0.19 ± 0.09
US005	R5	0.28 ± 0.08	0.10 ± 0.01
6535	R5	0.7 ± 0.2	0.08 ± 0.008
HXB2 (Magi-X4)	X4	9.6 ± 1.3	8.5 ± 1.5
HXB2 (TZM)	X4	3.6 ± 0.1	4.6 ± 0.3
VSV-G	> 500	> 500	> 500

Results are average IC_{50} ± SD (nM) from 4 or more independent experiments in triplicate.

showed no enhancement over 5P14. These data indicate that the linked C-peptide is critical for the enhancement of the inhibition of the RANTES variant in the chimera, and suggest that the effect of the fusion peptide on the specific viral strain determines the magnitude of the relative potency of the enhancement over the RANTES variant alone against Ba-L strain (Figure 4.3).

A series of assays with replication-competent virus was also carried out. CCR5 tropic HIV-1 ADA and HIV-1 Ba-L strains were used to infect TZM-bl cells at different concentrations of inhibitors. Compared to the results of the single-round viral infection assay, all inhibitors were less effective in inhibiting viral replication. For example, 5P12-RANTES and 5P14-RANTES had nanomolar rather than mid-picomolar inhibition against tested strains. But the chimeric inhibitors consistently showed stronger inhibition, with 5P12-linker-C37 showing up to 157 fold enhancement over 5P12 alone,

and with 5P14-linker-C37 showing up to 56 fold better inhibition than 5P14 alone (Table 4.4, Figure 4.2E, F).

As describe above, the chimeric inhibitors consistently showed better inhibition than the parent compounds against HIV in engineered cell lines, which may be different than natural human cells in properties such as receptor expression level. To determine the success of these chimeric inhibitors on primary human cells and to get an estimation of their real potency against HIV on its natural targets, the inhibitors were tested on human peripheral blood mononuclear cells (PBMCs). The PBMC results confirmed the previous findings, with 5P12-linker-C37 being 45 fold better than 5P12 alone, and 5P14-linker-C37 being 26 fold better than 5P14 alone against the Ba-L strain (Table 4.5).

Anti-viral potencies of 5P12-linker-C37 and 5P14-linker-C37 against X4-tropic HIV viruses. Since 5P12 and 5P14 work by binding CCR5 and are therefore only effective against R5-tropic virus, they showed no inhibition against X4 envelopes, either in cell-cell fusion assays or in viral assays using X4-tropic virus against Magi-X4 cells, as expected (Tables 4.2 and 4.6, Figure 4.4A, B). In contrast, the peptide C37 is active against both R5 and X4 tropic virus due to its ability to bind gp41, and this peptide exhibits nanomolar-level inhibition potency in X4 fusion and viral assays. The designed chimeric inhibitors 5P12-linker-C37 and 5P14-linker-C37 also show anti-X4 activity due to the action of the C37 portion of the molecule, as shown in Figure 4.4A and B. These chimeric inhibitors exhibit IC_{50} values nearly identical to C37, demonstrating the effectiveness even when one portion (the RANTES variant) is not utilized for the inhibition.

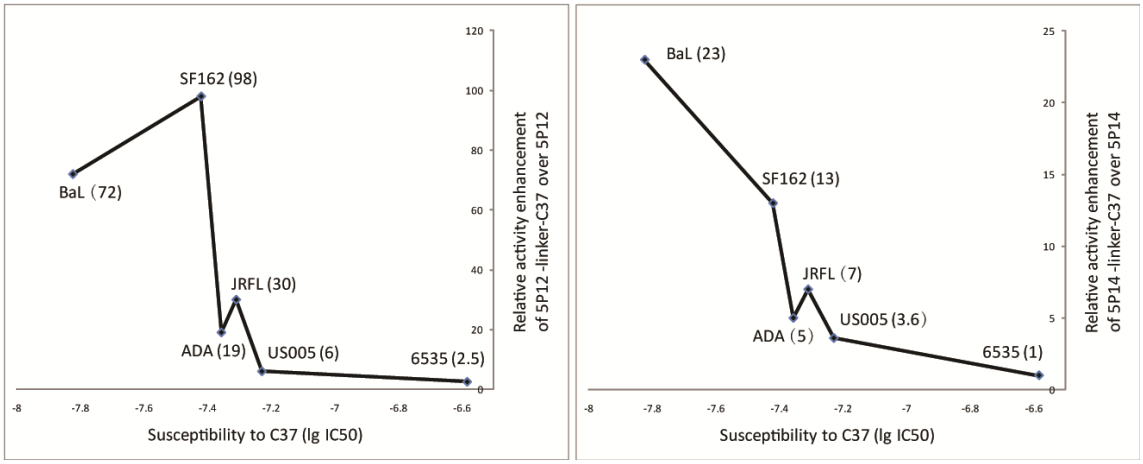

Figure 4.3 The correlation between the viral sensitivity to C37 and the magnitude of the relative potency enhancement of the chimeric inhibitors over RANTES variants alone. Numbers in parentheses are fold of relative potency enhancement

Table 4.4 Anti-HIV activities of the chimeric inhibitors in replication-competent viral assay.

HIV virus	*Tropism*	*5P12-linker-C37*	*5P12*	*C37*	*5P14-linker-C37*	*5P14*
Ba-L	R5	0.08 ± 0	12.61 ± 8.19	>100	0.08 ± 0.01	4.52 ± 0.64
ADA	R5	0.65 ± 0.08	28.5 ± 5.9	>100	0.63 ± 0.06	21.8 ± 0.1
IIIB (HeLa-X4)	X4	10.1 ± 0.1	> 500	10.4 ± 0.2	9.23 ± 1.77	> 500
IIIB (TZM)	X4	0.05 ± 0	> 500	77.1 ± 21.1	0.04 ± 0	> 500

Results are average IC_{50} ± the uncertainty of the average (half the difference) (nM) from 2 independent experiments in triplicate. ± 0 indicates the two experiments yielded identical IC_{50} values.

Table 4.5 Anti-HIV activities of the chimeric inhibitors in PBMC assay.

HIV virus	*Ba-L (R5)*	*IIIB (X4)*
5P12-linker-C37	0.015 ± 0.005	0.44 ± 0.02
5P12	0.675 ± 0.5	> 100
C37	13.85 ± 8.3	7.0 ± 2.5
5P14-linker-C37	0.015 ± 0.005	3.1 ± 2.3
5P14	0.395 ± 0.26	> 100

Results are average IC50 ± the uncertainty of the average (half the difference) (nM) from 2 independent experiments in triplicate.

Table 4.6 Anti-HIV activities of the chimeric inhibitors in X4 cell-cell fusion assay.

IC_{50} (nM)	*C37*	*5P12-linker-C37*	*5P12 + C37*	*5P14-linker-C37*	*5P14 + C37*
Magi-X4 (X4)	1.5 ± 0.3	4.7 ± 0.9	2.2 ± 0.2	4.3 ± 0.5	2.4 ± 0.7
TZM-bl (R5/X4)	2.1 ± 0.8	0.006 ± 0.003	2.1 ± 0.2	0.005 ± 0.002	2.6 ± 1.0

Results are average IC50 ± SD from 4 or more independent experiments in triplicate.

X4 fusion stands for Magi-X4 cells fusion with HL2/3 cells.

R5/X4 fusion stands for TZM (R5/X4) cells fusion with HL2/3 cells.

Figure 4.4 Antiviral activities of the chimeric inhibitors against X4 tropic virus. The chimeric inhibitors retain the anti-viral activity of C37 in X4 assays: **A.** Magi-X4 cell (expresses only CXCR4, but not CCR5, on the surface) based cell-cell fusion assays; **B**. Magi-X4 cell based single-cycle viral infection assays. The anti-viral activity of chimeric inhibitors against X4 virus is greatly enhanced if the cells co-express CCR5 receptors: **C.** TZM-bl cell (expresses both CCR5 and CXCR4 on the surface) based fusion assays; **D**. TZM-bl based single-cycle viral infection assays. This enhancement of the chimeric protein requires binding to CCR5: When the CCR5 receptors on the cell surface are occupied by pre-incubation with CCR5-binding protein, the chimeric inhibitors showed no enhancement over C37: **E.** TZM-bl cell based fusion assays; **F**. TZM-bl cell based single-cycle viral infection assays. The cells were pre-incubated with 100 nM 5P12 or 5P14. Data shown are typical results of single assays done in triplicate. Error bars represent standard deviations of the data.

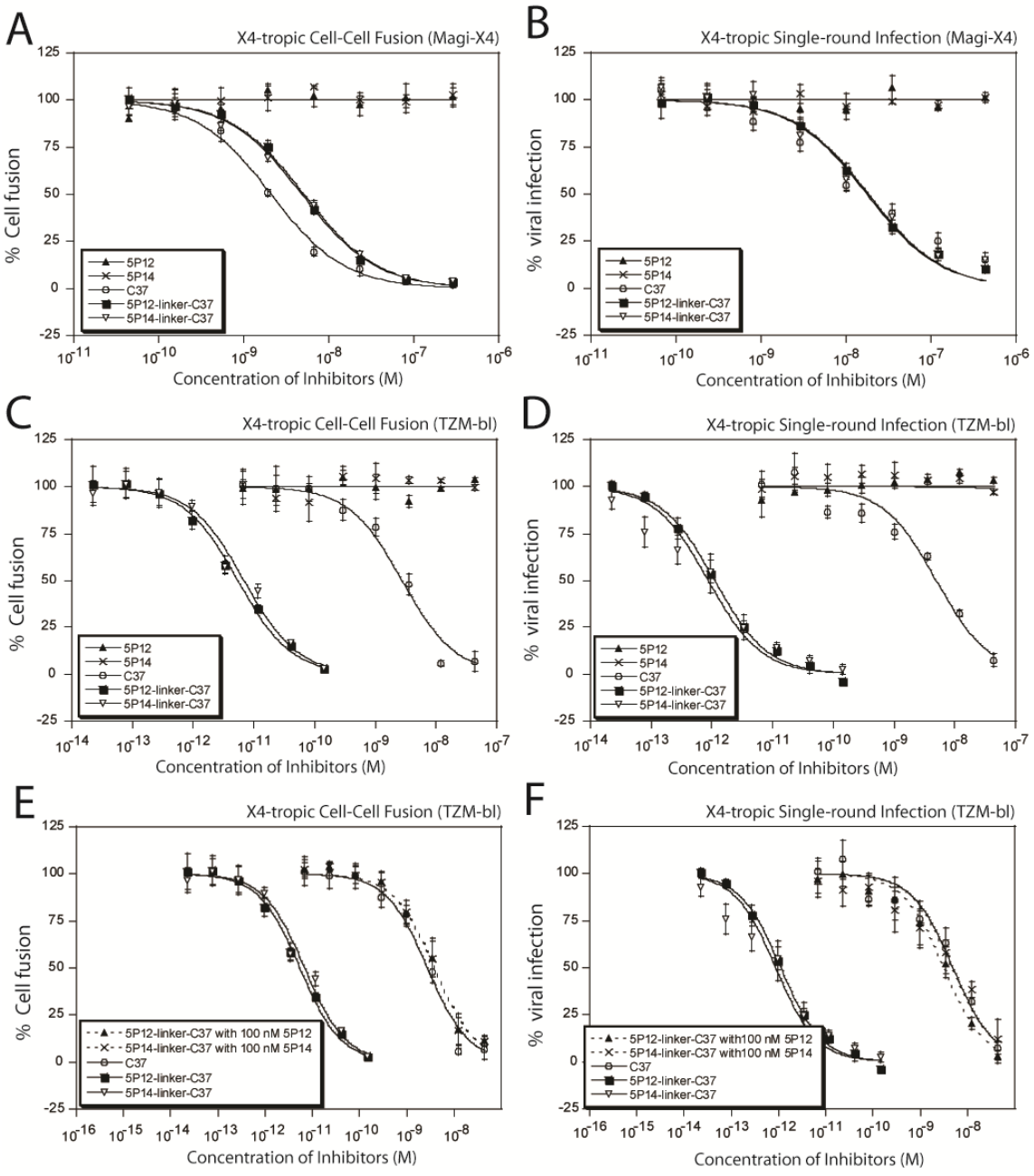
A
X4-tropic Cell-Cell Fusion (Magi-X4)
% Cell fusion
Concentration of Inhibitors (M)
5P12
5P14
C37
5P12-linker-C37
5P14-linker-C37
B
X4-tropic Single-round Infection (Magi-X4)
% viral infection
Concentration of Inhibitors (M)
C
X4-tropic Cell-Cell Fusion (TZM-bl)
D
X4-tropic Single-round Infection (TZM-bl)
E
X4-tropic Cell-Cell Fusion (TZM-bl)
5P12-linker-C37 with 100 nM 5P12
5P14-linker-C37 with 100 nM 5P14
F
X4-tropic Single-round Infection (TZM-bl)
5P12-linker-C37 with100 nM 5P12
5P14-linker-C37 with100 nM 5P14

More striking results are observed when performing assays with X4-tropic virus on the TZM-bl cell line, which expresses both CXCR4 and CCR5 receptors. While the IC_{50} of C37 alone remains the same as on the Magi-X4 cell line, the anti-viral potency of the chimeric inhibitors increased 400 - and 6,000 - fold compared to C37 in cell fusion assays and in single-cycle viral assays against the HXB2 strain, respectively (Tables 4.2 and 4.6, Figure 4.4C, D). Parent protein controls 5P12-RANTES and 5P14-RANTES showed no inhibition, indicating that CCR5 binding by the RANTES variants does not inhibit X4-tropic viral entry, as expected. Furthermore, potency enhancement was not seen when 5P12 or 5P14 were mixed with C37, which led to the same activity as C37 alone. The high potency of the chimeric proteins against X4 virus under these conditions suggests a strong enhancement by the intra-molecular action of both components of the chimeric protein. This enhancement likely involves the RANTES variants being bound to CCR5 receptors, placing the C37 part of the chimera in the proper position to bind its target gp41.

Given the fact that CCR5 and CXCR4 receptors form hetero-oligomers on the cell surface (229-230), it is very likely that by binding to the CCR5 receptors, the RANTES variants in the chimeric protein could specifically deliver C37 to its virus target, which is presumably using the nearby CXCR4 as a co-receptor, to achieve the strong enhancement of X4 inhibition potency. To provide evidence for this, we carried out experiments in which the CCR5 receptors were blocked prior to adding X4 tropic virus and the chimeric inhibitors. In both fusion and single-cycle viral assays, target cells were pre-incubated with 100 nM 5P12 or 5P14 before 5P12-linker-C37 or 5P14-linker-

C37 were added. Since the CCR5 receptors were blocked by excessive amount of RANTES variants and the chimeric inhibitors could not bind to CCR5 receptors, their X4 inhibition potency reverted to that of C37 alone (Figure 4.4E, F)

Replication-competent viral assays were also conducted to confirm the anti-viral activities of chimeric inhibitors against X4-tropic virus replication. Similar results were observed as from the single cycle assays: while the chimeric inhibitors 5P12-linker-C37 and 5P14-linker-C37 showed the same IC_{50} values as C37 on HeLa-X4 cells (which express only CXCR4 receptors on the surface), they exhibited 1500-1900 fold increased potency over C37 against the X4 tropic HIV-1 IIIB strain on TZM-bl cells which co-expressed CCR5 and CXCR4 receptors (Table 4.4). Altogether, the data show that chimeric inhibitors fully retain the anti-X4 activity of C37, and that this anti-X4 potency can be further enhanced when the target cells co-express CCR5 on the surface.

Viral assays against PBMC, some of which also express both CCR5 and CXCR4 receptors on the surface, were then carried out to evaluate the X4 tropic anti-viral potencies of these chimeric inhibitors on natural human cells. As expected, 5P12 and 5P14 alone did not show any inhibition against the X4-tropic HIV-1 IIIB strain since these proteins are only able to bind the CCR5 coreceptor and not CXCR4. The peptide C37 alone showed an IC_{50} of 7 nM. The chimeric inhibitors, however, showed inhibition that was up to 16 fold better than C37 alone as judged by IC_{50}, most likely due to the coexpression of CCR5 receptors on some of the cells (Table 4.5). This result showed that the chimeric inhibitors were extremely potent against X4-tropic viruses even on natural human cells.

Mechanism of the chimeric inhibitors. Several assays, including R5 and X4 tropic cell fusion assays, single-cycle viral infection assays, replication-competent viral assays, and PBMC assays indicate the success of the strategy to covalently link RANTES variants with a C-peptide. These experiments also provide evidence suggesting the high potency is probably due to the excellent inhibition of the RANTES variants, along with its ability to specifically deliver C37 to its gp41 target. Therefore, experiments were designed to further characterize the mechanism of action of the chimeric inhibitors, first focusing on the relative importance of the C37 portion.

A series of mutations were made to 5P12-linker-C37 (Figure 4.5, Tables 4.7 and 4.8), and the corresponding effects were evaluated with cell fusion and single-cycle viral assays. It has previously been shown that that the mutation of Ile to Asp in position 642 in the C-peptide causes a 10,000 fold drop of anti-HIV activity, almost completely abolishing its function, while the Ile mutation to Asp at position 656 causes a moderate, 80 fold decrease of activity (198). Therefore, mutations to Asp were made in the 642th and 656th positions of C37 in 5P12-linker-C37. To test whether these mutations reduce the activity of the C37 segment of the chimeric protein, we tested the mutants with Magi-X4 cell based fusion and viral assays. 5P12-linker-C37I642D completely lost its ability to inhibit X4-tropic virus at lower than 500 nM concentration, while 5P12-linker-C37I656D showed 10 - and 3 - fold decrease in activity in fusion and viral assays, respectively compared to the wild type chimera (Figure 4.5A, Table 4.7, 4.8). These mutants that weaken the potency of the C-peptide also reduced the overall effectiveness of the chimeric protein against R5-tropic viruses. The anti-viral potency of both the

Figure 4.5 Mechanism of action of the chimeric inhibitors. **A.** Mutations on the C37 segment of 5P12-linker-C37 cause reduced or loss of activity against X4-tropic virus, while substitution of 5P12 with a different N-terminus (that of P2-RANTES) has no effect against X4-tropic virus. The X4-tropic antiviral potency was determined on Magi-X4 cells (which express only CXCR4, but not CCR5, on the surface) against HXB2 strain pseudotyped virus particles. **C.** Mutations on either the RANTES variant segment or the C37 segment of 5P12-linker-C37 cause reduced activity against R5-tropic virus. The R5-tropic antiviral potency was determined using TZM-bl cells (which express both CCR5 and CXCR4 on the surface) against Ba-L strain pseudotyped virus particles. **E**. When the cells co-express CCR5, mutations on either the RANTES variant segment or the C37 segment of 5P12-linker-C37 cause reduced activity against X4-tropic virus. The X4-tropic antiviral potency was determined on TZM cells (which express both CCR5 and CXCR4 on the surface) against HXB2 strain pseudotyped virus particles. **B**. Changing the original 10-amino-acid linker to a shorter 3-amino-acid linker or a longer 20-amino-acid linker does not affect the native activity of C37 against X4 tropic virus. The X4-tropic antiviral potency was determined on Magi-X4 cells (which express only CXCR4, but not CCR5, on the surface) against HXB2 strain pseudotyped virus particles. **D, F.** 5P12-3AA-C37 shows reduced anti-viral activity in both R5-tropic single-cycle viral assays and TZM-bl cell based X4-tropic single-cycle viral assays, while 5P12-20AA-C37 shows very similar activity to 5P12-linker-C37. The R5-tropic antiviral potency was determined using TZM-bl cells (which express both CCR5 and CXCR4 on the surface) against Ba-L strain pseudotyped virus particles **(**D**)**. The TZM-bl cell based

X4-tropic antiviral potency was determined on TZM cells against HXB2 strain pseudotyped virus particles **(**F**)**. Data shown are typical results of single assays done in triplicate. Error bars represent standard deviations of the data.

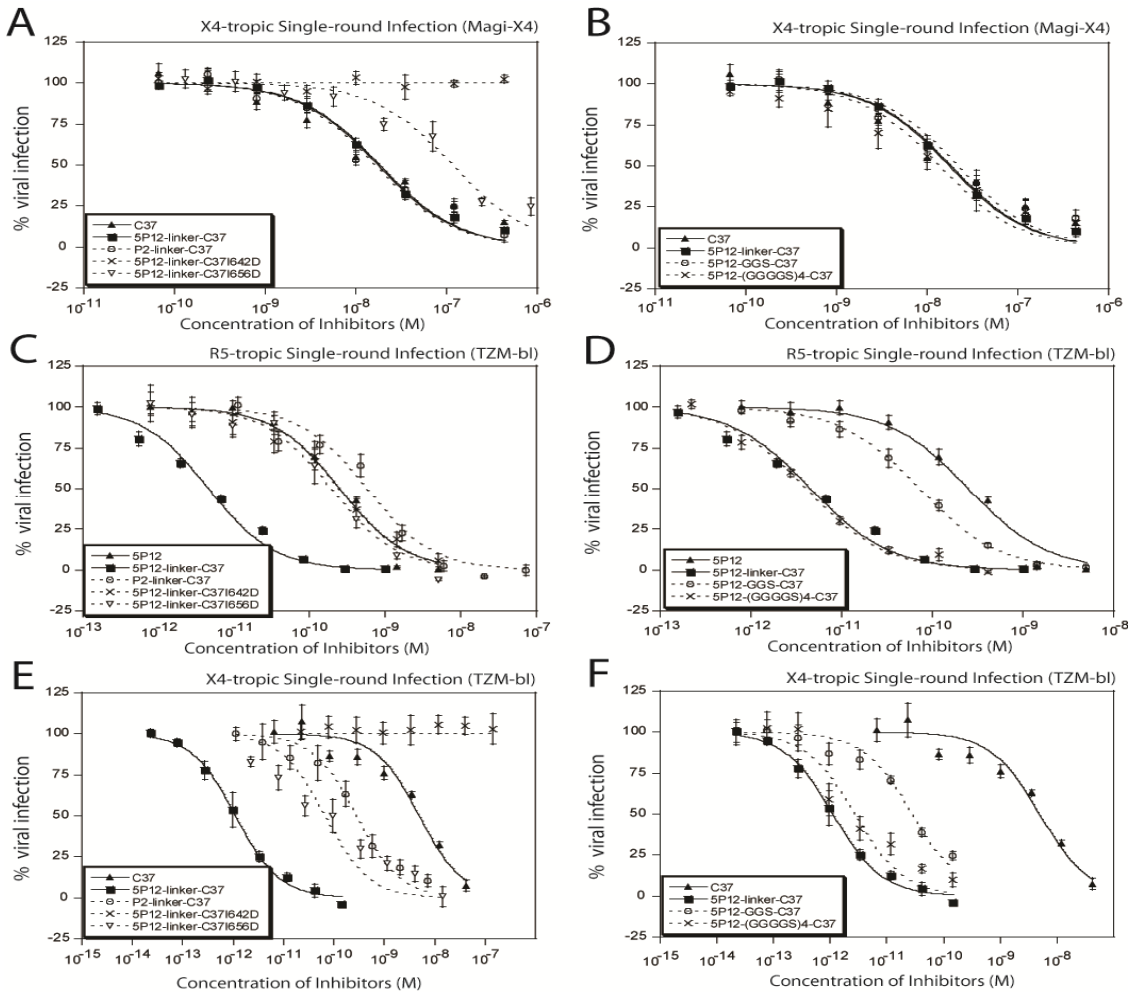

Table 4.7 Anti-HIV activities of 5P12-linker-C37 mutations in single-cycle viral assay.

HIV virus	*Tropism*	*5P12-linker-C37*	*Mutation in RANTES*	*Mutation in C37*		*Change of linker length*	
			P2-RANTES-linker-C37	5P12-linker-C37I642D	5P12-linker-C37I656D	5P12-GGS-C37	5P12-$(GGGGS)_4$-C37
Ba-L	R5	0.004 ± 0.001	0.82 ± 0.09	0.24 ± 0.04	0.20 ± 0.02	0.06 ± 0.001	0.002 ± 0.001
SF162	R5	0.006 ± 0.001	0.80 ± 0.02	0.75 ± 0.36	0.27 ± 0.07	0.1 ± 0.02	0.004 ± 0.0005
ADA	R5	0.025 ± 0.004	0.61 ± 0.05	0.29 ± 0.02	0.15 ± 0.02	0.1 ± 0.003	0.016 ± 0.004
HXB2 (Magi-X4)	X4	18 ± 7.4	17 ± 2.4	> 500	60 ± 20	27 ± 3.1	11 ± 6.4
HXB2 (TZM)	X4	0.001 ± 0.0003	0.28 ± 0.07	> 500	0.10 ± 0.02	0.28 ± 0.05	0.002 ± 0.001
VSV-G	Ctrl	> 500	> 500	> 500	> 500	> 500	> 500

Results are average IC_{50} ± Standard deviation (nM) from 4 or more independent experiments in triplicate.

Table 4.8 Anti-HIV activities of 5P12-linker-C37 mutations in cell-cell fusion assay.

Tropism	*5P12-linker-C37*	*Mutation in RANTES*	*Mutation in C37*		*Change of linker length*	
		P2-RANTES-linker-C37	5P12-linker-C37I642D	5P12-linker-C37I656D	5P12-GGS-C37	5P12-$(GGGGS)_4$-C37
R5	0.009 ± 0.003	1.2 ± 0.09	0.06 ± 0.005	0.07 ± 0.003	0.03 ± 0.01	0.01 ± 0.002
X4 (Magi-X4)	4.7 ± 0.9	3.9 ± 0.5	> 500	59.4 ± 15.4	4.1 ± 0.9	6.1 ± 1.7
X4 (TZM)	0.006 ± 0.003	0.2 ± 0.09	> 500	0.05 ± 0.01	0.008 ± 0.003	0.003 ± 0.001

Results are average IC50 ± SD (nM) from 4 or more independent experiments in triplicate.

5P12-linker-C37I642D and 5P12-linker-C37I656D were much lower compared to 5P12-linker-C37, inhibiting similarly to free 5P12 (Figure 4.5C, Tables 4.7 and 4.8). Similar results were observed in X4 assays with TZM-bl cells that contain both CCR5 and CXCR4 on the surface (Figure 4.5E, Tables 4.7 and 4.8).

The RANTES portion of 5P12-linker-C37 was also mutated to determine the effect of the RANTES portion on the overall chimeric protein. In particular, the potent 5P12 N-terminus was changed into that of another RANTES variant, P2-RANTES, which differs from 5P12 by the first 10 amino-acids. P2-RANTES is also an R5 ligand, but with lower anti-viral potency against R5 virus (nanomolar-level inhibition in cell fusion and pseudotyped viral infection) (85). Substitution of the RANTES part of the linker protein did not affect the C-peptide portion of the chimera, as evidenced by the similar activity as 5P12-linker-C37 and C37 in X4-tropic assays under conditions where only the C37 portion would be expected to be active (Tables 4.7 and 4.8, Figure 4.5A). But this variant did show decreased activity in R5 and TZM-bl X4 assays (Tables 4.7 and 4.8, Figure 4.5C, E). Therefore the RANTES portion of the chimeric protein is also critical for the enhanced activity.

These data indicate that both parts of the linker protein are necessary and that they have to be functioning on the same molecule to show an enhancement of potency.

Having demonstrated the necessity of both portions of the chimera, we hypothesized that the observed enhancement of the chimeric inhibitors was likely due to the specific delivery of C37 to the nearby gp41 target by the RANTES variant as it binds to the CCR5 co-receptor. To probe this possibility, we tested the effects of different

linker length on the overall activity of the linker protein. Mutant chimeric inhibitors with 3-amino-acid linker "GGS" and 20-amino-acid linker "$(GGGGS)_4$" were made to compare with our 5P12-linker-C37 which has a flexible 10-amino-acid linker $(GGGGS)_2$. NMR experiments were done to confirm the structural integrity of the mutants (data not shown). The spectra showed that the 20-amino-acid long linker led to a significant portion of unfolded protein using our regular purification method, so we modified the protocol to obtain pure and fully folded chimeric protein with the 20-amino-acid long linker. Finally, 2D HSQC spectra verified the structural integrity of all mutant chimeric proteins and showed that the change of linker length did not affect the structure of 5P12 (data not shown). As a control, X4-tropic single round virus assays using MAGI-X4 cells (containing no CCR5) confirmed that different linker length did not affect the anti-viral function of the C37 portion of these chimera (Table 4.7, Figure 4.5B). This was expected, since we have already shown that under these conditions the C-peptide is the only component involved in inhibition while the RANTES variant is not active against X4 tropic strains. In contrast, R5 tropic viral assays with 3 different strains showed that the shorter linker 5P12-GGS-C37 has the lowest anti-viral potency, 15-fold lower compared to that 5P12-linker-C37. The moiety with the longer linker 5P12-$(GGGGS)_4$-C37 showed almost the same activity as 5P12-linker-C37 (Table 4.7, Figure 4.5D). Similar results were observed in X4-tropic assays using TZM-bl (containing both surface R5 and X4) as target cells, where 5P12-GGS-C37 showed the lowest ability to inhibit and where 5P12-linker-C37 has similar activity to 5P12-$(GGGGS)_4$-C37 (Table 4.7, Figure 4.5F).

Since the individual activities of 5P12 and C37 were not affected, the change of anti-viral activity in these altered chimeras was likely caused by the change in linker length. The data suggests that the linker has to be long enough to allow both parts of the linker protein to both be functional and supports the hypothesis that the enhancement of potency in the chimeric inhibitor is due to the specific delivery of C37 to the nearby gp41 target by the RANTES variant as it binds to CCR5.

Discussion

In this paper, a potent strategy to inhibit HIV by targeting multiple steps of HIV cell entry is described. It was reasoned that during the HIV entry process, there are time windows when co-receptor inhibition and gp41 fusion inhibition can be achieved simultaneously. Based on this hypothesis, we designed chimeric inhibitors that contain both a co-receptor inhibitor and a fusion peptide, and the two components were linked together using a flexible glycine/serine linker. The chimeric inhibitors 5P12-linker-C37 and 5P14-linker-C37 exhibited anti-viral potency higher than either of the individual components alone or in combination. They were able to inhibit R5 tropic HIV at low picomolar level in all the *in vitro* assays, and therefore are among the most potent entry inhibitors yet reported. The chimeric inhibitors also fully retained the anti-X4 activity of C37, and this anti-X4 potency can be further enhanced when the cells co-express CCR5 on the surface. The chimeric inhibitors therefore overcome the major drawbacks of the parent co-receptor inhibitors 5P12 and 5P14 which lack activity against X4 tropic virus.

Another advantage is that by blocking HIV entry at two steps, the chimeric inhibitors are less likely to be evaded by virus through mutations.

A few potent protein-based chimeric HIV entry inhibitors have been previously reported (94-96). Most relevant to the present work is a similar strategy recently reported using an antibody to CCR5 covalently linked to two T-2635 fusion peptides (94). This molecule, called BFFI, also blocks HIV at both the co-receptor binding step and the 6-helix bundle formation step, and showed very strong anti-viral activities. However, this BFFI only exhibited 2 fold potency enhancement over the parent CCR5mAb in PBMC assays against R5 tropic viruses, despite the large enhancement showed in the TZM-bl cell based *in vitro* assays. BFFI also failed to inhibit X4-tropic viruses on cell lines expressing only CXCR4 receptors or on PBMCs. Against X4-tropic virus, BFFI was only active when the cells co-expressed large amounts of CCR5 along with CXCR4. This is probably because the large mAb sterically blocked the effective binding of the fusion peptide to its target, so the fusion peptide could not act alone due to the hindrance of its chimeric partner (203). Also BFFI was produced in mammalian cells, making large-scale production of this inhibitor less feasible due to expense. Our chimeric inhibitors, on the other hand, are straightforward and inexpensive to produce in *E. coli*, highly active against R5 viruses, active against X4-tropic viruses regardless of the presence of CCR5 receptors on the surface of the target cell, and are extremely potent on PBMCs.

The overall effectiveness of our chimeric inhibitors relies heavily on two major factors aside from the components' innate effectiveness: viral susceptibility to the C37

peptide, and CCR5 receptor density on the target cell. As shown in Table 1, we tested the effectiveness of the chimeric inhibitors on 6 different single-cycle R5 viruses. The viruses showed variable sensitivity to C37, with C37 inhibition IC_{50} ranging from 15 nM to 261 nM, while showing quite similar sensitivity to 5P12 or 5P14 alone. The relative potency enhancement of the chimeric inhibitors over the parent RANTES variants similarly varied from 1 to 100 fold, and was largely in proportion to the virus' susceptibility to C37: generally, the more sensitive the virus to C37, the more potency enhancement of the chimeric inhibitor over the RANTES variants alone against that virus (Figure 4.3).

The effectiveness of the chimeras also depend on receptor density on the target cells, which is also true for other inhibitors (231): Lower receptor density leads to more sensitivity to inhibition. In the present work, R5-tropic fusion assays were carried out on two cell lines with differing amounts of CCR5 on the surface, and the results showed that the lower the CCR5 density, the more potent the chimeric inhibitor (Figure 4.6, Table 4.9).

Extensive *in vitro* viral assays and mutagenesis studies were carried out to investigate the mechanism of the chimeric inhibitors. In R5 tropic viral assays, the chimeric inhibitors showed up to 100 fold potency enhancement over the parent RANTES variants while a simple mixture of the RANTES variants and C37 showed no enhancement, indicating that C37 enhanced the R5 anti-viral potency of the RANTES variants, and the mechanism involves both components being covalently linked. Similar conclusions can be drawn from the results of an X4 tropic viral assay on TZM-bl cells,

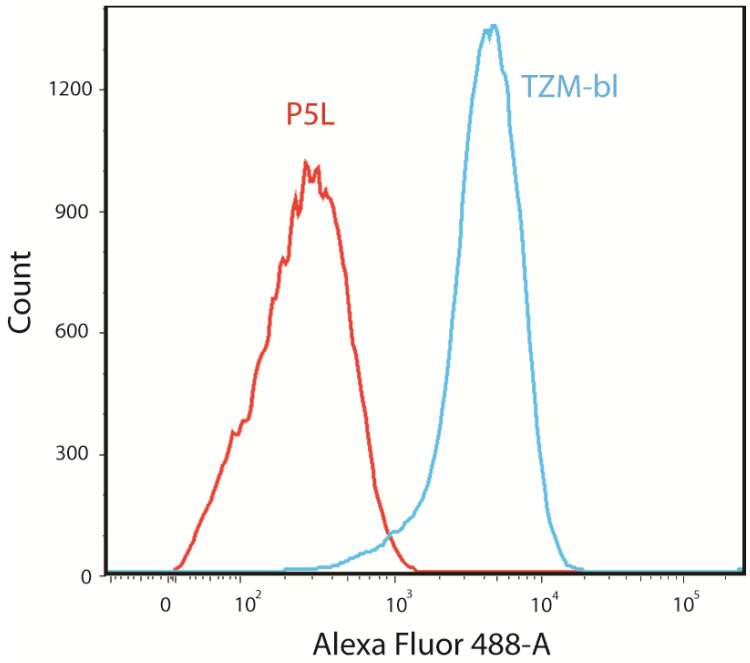

Figure 4.6 CCR5 receptor density comparison by flow cytometry. The CCR5 receptor expression levels on HeLa-TZM-bl cells and HeLa-P5L cells were compared using flow cytometry.

Table 4.9 Anti-HIV activities of the chimeric inhibitors in R5 tropic fusion assays with P5L and TZM-bl as target cells.

Cell lines	*Hela-P5L*	*TZM-bl*
CCR5 density	Low	High
5P12	0.051 ± 0.01	14 ± 1.4
5P12+C37	0.044 ± 0.005	7.0 ± 1.3
5P12-linker-C37	0.009 ± 0.003	0.8 ± 0.2
C37	9.1 ± 4.1	340 ± 80
5P14	0.03 ± 0.002	11 ± 2.4
5P14+C37	0.03 ± 0.01	4.8 ± 0.2
5P14-linker-C37	0.006 ± 0.001	0.6 ± 0.02

Results are average IC_{50} ± SD (nM) from 4 or more independent experiments in triplicate.

which contain both CCR5 and CXCR4 on their surface. While the only active part of the chimeric inhibitor against X4 tropic virus is C37, as much as 6000 fold enhancement of potency was observed. This effect disappeared when the CCR5 receptors were blocked, suggesting that the RANTES variant is binding CCR5 and specifically delivering the C37 portion of the chimera to gp41. Mutagenesis on either part of the chimeric protein showed that both parts are essential and they are functioning at the same time. Change of linker length also provided valuable information about the space requirements of this intra-molecular mechanism.

Based on these findings we propose the following model to explain the mechanism of our chimeric inhibitors on both R5 and X4 tropic viruses. The inhibitors likely inhibit R5 tropic virus by binding to both the CCR5 co-receptor and the gp41 N-terminal trimer of hairpin simultaneously or near-simultaneously. By binding to the co-receptor, the chimeric inhibitors could specifically deliver C37 near to its target on gp41, and potentially increase the local concentration of C37 on the cell surface (Figure 4.7A). When inhibiting X4 virus on cells containing only CXCR4 receptors, the chimeric inhibitors behave essentially as C37 alone by binding only to gp41 (Figure 4.7B). When the cells express both CCR5 and CXCR4, the chimeric inhibitors can deliver C37 to its target by binding to a CCR5 receptor that is presumably in proximity to a CXCR4 that is being used as a co-receptor for infection due to the known hetero-oligomerization of CCR5 with CXCR4 (229-230). By specific delivery of C37 to its target and possibly increasing the local concentration of C37 on the cell surface, the chimeric inhibitors block HIV more efficiently than C37 alone (Figure 4.7C).

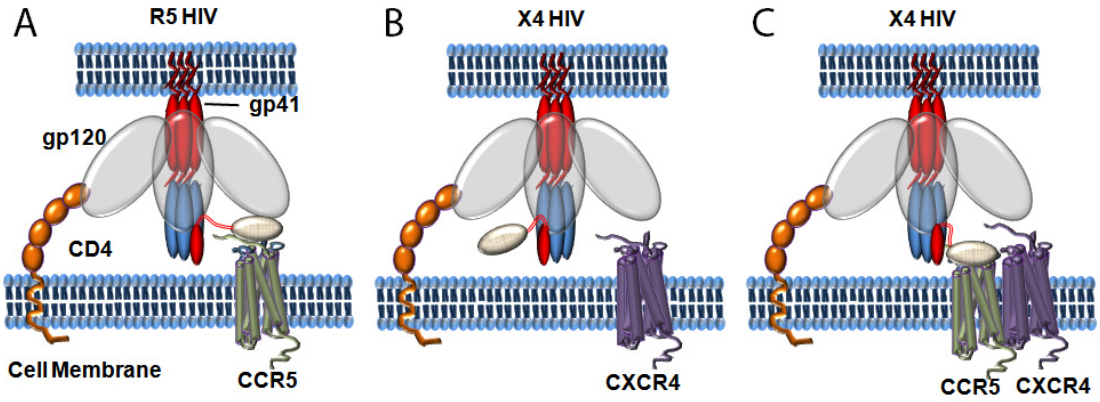

Figure 4.7 Model of action of the chimeric inhibitors: **A**. during the process of R5 tropic viral entry, the chimeric inhibitor can bind to the CCR5 receptor and block the co-receptor-gp120 interaction, and at the same time delivers the C37 fusion peptide to the nearby gp41 targets. In this way, the chimeric inhibitor blocks R5-tropic HIV entry at both steps more effectively. **B**. during the process of X4-tropic viral entry, only the C37 part of the chimeric inhibitor is active, and the chimeric inhibitor functions exactly as a fusion peptide by binding to the N-terminal trimer-of-hairpins of gp41. **C**. When the target cells of the X4-tropic virus co-express both CCR5 and CXCR4 receptors, the chimeric inhibitors can inhibit viral entry more efficiently. Since CCR5 and CXCR4 form hetero-oligomers on the cell surface, the chimeric inhibitors can bind to CCR5 and deliver the C37 peptide to the nearby X4 infection site. By specific delivery of C37 to its target and possibly increasing the local concentration of C37 on the cell surface, the chimeric inhibitors block HIV more efficiently than C37 alone.

We report here the success of a strategy to covalently link potent CCR5 binding proteins with a gp41-binding C-peptide. The chimeric inhibitors exhibited extremely high anti-viral potency, and were able to inhibit both R5 and X4 tropic viruses. Since the inhibitors block HIV at two steps, they are likely more resistant to viral mutations. Also, as fully recombinant inhibitors, they are inexpensive and relatively easy to produce. Overall, these inhibitors are excellent candidates for HIV microbicides. This work could also provide insight for a general approach for optimizing existing HIV entry inhibitors or designing new inhibitors.

CHAPTER V

SUMMARY AND CONCLUSIONS

Chemokines are important immune proteins, carrying out their function by binding to glycosaminoglycans (GAGs) on the endothelial surface, and to cell surface chemokine receptors. A unique viral chemokine analog, viral macrophage inflammatory protein-II (vMIP-II), encoded by human herpesvirus-8, has garnered interest because of its ability to bind to multiple chemokine receptors including both HIV coreceptors. In addition, vMIP-II binds to cell surface GAGs much more tightly than most human chemokines, which may be the key to its anti-inflammatory function *in vivo*. The first part of the present work was to determine the mechanism of action of vMIP-II by characterizing its GAG-binding and receptor-binding mechanisms.

To determine vMIP-II's GAG-binding mechanism, the interaction of vMIP-II with heparin-derived disaccharide was characterized using NMR. Important binding sites were further analyzed by mutagenesis studies, in which corresponding vMIP-II mutants were tested for GAG binding ability using heparin chromatography and NMR. It was found that despite having many more basic residues than some chemokines, vMIP-II shares a characteristic binding site similar to its human analogs, utilizing basic residues R18, R46 and R48. Interestingly, a particular mutation (Leu13Phe) caused vMIP-II to forms a pH dependent CC-chemokine-type dimer as determined by analytical ultracentrifugation and NMR. To our knowledge, this is the first example of engineering a naturally predominantly monomeric chemokine into a dissociable dimer by a single

mutation. This dimeric vMIP-II mutant binds to heparin much more tightly than wild type vMIP-II, and provides a new model to study the relationship between chemokine quaternary structure and various aspects of function. Structural differences between monomeric and dimeric vMIP-II upon GAG binding were characterized by NMR and molecular docking. We found that there is a shift in the GAG-binding sites between the dimer and monomer forms of vMIP-II, where the N-terminus was involved in GAG binding for the dimer. The N-terminus of one dimer subunit reaches over to the positively charged binding pocket of the other subunit, and forms a new binding pocket which has been shown to be more favorable for GAG binding. This study, for the first time, provides a model that explains the mechanism of how quaternary structure affects chemokine-GAG binding.

Mutagenesis and competitive binding assays were conducted to study the receptor-binding mechanism of vMIP-II. We focused our study on vMIP-II's binding to CCR5 and CXCR4 which are two major receptors from two different subfamilies. We have found that the highly basic binding surface at the core domain of vMIP-II, including residues R18, K45, R46, and R48, plays a pivotal role in vMIP-II's receptor binding. This binding surface is solely responsible for vMIP-II's binding to CCR5, and this surface, together with the N-terminus, are used by vMIP-II to interact with CXCR4. Considering the fact that the N-termini of most receptors are heavily sulfated and negatively charged, this highly basic core domain binding surface might be the key to vMIP-II's broad-spectrum receptor binding ability. NMR titration experiment are ongoing to provide more detailed information on how this positively charged binding

surface interact with the tyrosine-sulfated N-termini of CCR5 and CXCR4 which will be a nice complement to the current study.

The second part of this work was to rationally design HIV-1 entry inhibitors based on our knowledge of the mechanisms of chemokine-receptor binding and HIV-1 cell entry. We successful designed two highly potent chimeric HIV entry inhibitors composed of CCR5 targeting RANTES variants (5P12-RANTES and 5P14-RANTES; (86)) linked to a gp41 targeting C-peptide, C37. Chimeric inhibitors 5P12-linker-C37 and 5P14-linker-C37 showed extremely high anti-viral potency in single-cycle and replication competent viral assays against R5 tropic viruses with IC_{50} values as low as 0.004 nM. This inhibition was somewhat strain dependent and was up to 100 fold better than the RANTES variant alone or in combination unlinked with C37. The chimeric inhibitors also fully retained the antiviral activity of C37 against X4 tropic viruses, and this inhibition can be further enhanced significantly if the target cell co-expresses CCR5 receptor. On human peripheral blood mononuclear cells, the inhibitors showed very strong inhibition against R5 tropic Ba-L strain and X4-tropic IIIB strain, with IC_{50} values as low as 0.015 nM and 0.44 nM, which are 45 and 16 better than the parent inhibitors, respectively. A clear delivery mechanism requiring a covalent linkage between the two segments of the chimera was observed and characterized. Furthermore, the two chimeric inhibitors are fully recombinant and are easily produced at low cost. These attributes make them excellent candidates for anti-HIV microbicides. The results also suggest a potent approach for optimizing existing HIV entry inhibitors or designing new inhibitors.

REFERENCES

1. Baggiolini, M., Dewald, B., and Moser, B. (1997) *Annu. Rev. Immunol.* **15**, 675-705
2. Baggiolini, M. (1998) *Nature* **329**, 565-568
3. Mackay, C. R. (2001) *Nature Immunology* **2**, 95-101
4. Lazennec, G., and Richmond, A. (2010) *Trends Mol. Med.* **16**, 133-144
5. Esche, C., Stellato, C., and Beck, L. A. (2005) *Journal of Investigative Dermatology* **125**, 615-628
6. Hannan, N. J., and Salamonsen, L. A. (2007) *Curr. Opin. Obstet. Gynecol.* **19**, 266-272
7. Zaja-Milatovic, S., and Richmond, A. (2008) *Histol. Histopathol.* **23**, 1399-1407
8. Belperio, J. A., Keane, M. P., Arenberg, D. A., Addison, C. L., Ehlert, J. E., Burdick, M. D., and Strieter, R. M. (2000) *J. Leukoc. Biol.* **68**, 1-8
9. Strieter, R. M., Burdick, M. D., Gomperts, B. N., Belperio, J. A., and Keane, M. P. (2005) *Cytokine Growth Factor Rev.* **16**, 593-609
10. Berger EA, M. P., Farber JM. (1999) *Annu. Rev. Immunol.* **17**, 657-700
11. Cocchi, F., Devico, A., Garzinodemo, A., Lusso, P., and Gallo, R. C. (1995) *Science* **270**, 1811
12. Alkhatib, G., Combadiere, C., Broder, C. C., Feng, Y., Kennedy, P. E., Murphy, P. M., and Berger, E. A. (1996) *Science* **272**, 1955-1958

13. Murphy, P. M., Baggiolini, M., Charo, I. F., Hebert, C. A., Horuk, R., Matsushima, K., Miller, L. H., Oppenheim, J. J., and Power, C. A. (2000) *Pharmacol. Rev.* **52**, 145-176

14. Bazan, J. F., Bacon, K. B., Hardiman, G., Wang, W., Soo, K., Rossi, D., Greaves, D. R., Zlotnik, A., and Schall, T. J. (1997) *Nature* **385**, 640-644

15. Kelner, G. S., Kennedy, J., Bacon, K. B., Kleyensteuber, S., Largaespada, D. A., Jenkins, N. A., Copeland, N. G., Bazan, J. F., Moore, K. W., Schall, T. J. (1994) *Science* **266**, 1395-1399

16. Fernandez, E. J., and Lolis, E. (2002) *Annual Review of Pharmacology & Toxicology* **42**, 469-499

17. Holst, P. J., Luttichau, H. R., Schwartz, T. W., and Rosenkilde, M. M. (2003) *Contrib. Microbiol.* **10**, 232-252

18. Moore, P. S., Boshoff, C., Weiss, R.A., and Chang, Y. (1996) *Science* **274**, 1739-1744

19. Bonecchi, R., Savino, B., Borroni, E. M., Mantovani, A., and Locati, M. (2010) *Curr Top Microbiol. Immunol.* **341**, 15-36

20. Alcami, A. (2003) *Nature Reviews Immunology* **3**, 36-50

21. Patel, A. H., Gaffney, D. F., Subak-Sharpe, J. H., and Stow, N. D. (1990) *J. Gen. Virol.* **71 (Pt 9)**, 2013-2021

22. Smith, C. A., Smith, T. D., Smolak, P. J., Friend, D., Hagen, H., Gerhart, M., Parik, L., Pickup, D. J., Torrance, D., Mohler, K., Schooley, K., and Goodwin, R. G. (1997) *Virology* **236**, 316-327

23. Ali, S., Palmer, A. C. V., Banerjee, B., Fritchley, S. J., and Kirby, J. A. (2000) *J. Biol. Chem.* **275**, 11721-11727

24. Laurence, J. S., Blanpain, C., De Leener, A., Parmentier, M., and LiWang, P. J. (2001) *Biochemistry* **40**, 4990-4999

25. Valenzuela-Fernandez, A., Palanche, T., Amara, A., Magerus, A., Altmeyer, R., Delaunay, T., Virelizier, J. L., Baleux, F., Galzi, J. L., and Arenzana-Seisdedos, F. (2001) *J. Biol. Chem.* **276**, 26550-26558

26. Amara A, L. O., Valenzuela A, Magerus A, Thelen M, Montes M, Virelizier JL, Delepierre M, Baleux F, Lortat-Jacob H, and Arenzana-Seisdedos F. (2001) *J. Biol. Chem.* **274**, 23916-23925

27. Proudfoot, A. E., Handel, T. M., Johnson, Z., Lau, E. K., LiWang, P., Clark-Lewis, I., Borlat, F., Wells, T. N., and Kosco-Vilbois, M. H. (2003) *Proc. Natl. Acad. Sci. USA* **100**, 1885-1890

28. Tuinstra, R. L., Peterson, F. C., Kutlesa, S., Elgin, E. S., Kron, M. A., and Volkman, B. F. (2008) *Proc. Natl. Acad. Sci. USA* **105**, 5057-5062

29. Bernfield, M., Gotte, M., Park, P. W., Reizes, O., Fitzgerald, M. L., Lincecum, J., and Zako, M. (1999) *Annu. Rev. Biochem.* **68**, 729-777

30. Ley, K. (2003) *Microcirculation* **10**, 289-295

31. Wang, L., Fuster, M., Sriramarao, P., and Esko, J. D. (2005) *Nat. Immunol.* **6**, 902-910

32. Lau, E. K., Allen, S., Hsu, A. R., and Handel, T. M. (2004) *Advances in Protein Chemistry* **68**, 351-391

33. Yoshie, O., Imai, T., and Nomiyama, H. (2001) *Adv. Immunol.* **78**, 57-110

34. Rot, A. (1993) *Eur. J. Immunol.* **23**, 303-306

35. Wiedermann, C. J., Kowald, E., Reinisch, N., Kaehler, C. M., von Luettichau, I., Pattison, J. M., Huie, P., Sibley, R. K., Nelson, P. J., and Krensky, A. M. (1993) *Curr. Biol.* **3**, 735-739

36. Middleton, J., Patterson, A. M., Gardner, L., Schmutz, C., and Ashton, B. A. (2002) *Blood* **100**, 3853-3860

37. Parish, C. R. (2006) *Nat. Rev. Immunol.* **6**, 633-643

38. Vives, R. R., Imberty, A., Sattentau, Q. J., and Lortat-Jacob, H. (2005) *J. Biol. Chem.* **280**, 21353-21357

39. Webb, L. M., Ehrengruber, M. U., Clark-Lewis, I., Baggiolini, M., and Rot, A. (1993) *Proc. Natl. Acad. Sci. USA* **90**, 7158-7162

40. Hoogewerf, A. J., Kuschert, G. S., Proudfoot, A. E., Bortat, F., Clark-Lewis, I., Power, C. A., and Wells, T. N. (1997) *Biochemistry* **36**, 13570-13578

41. Park, P. W., Reizes, O., and Bernfield, M. (2000) *J. Biol. Chem.* **275**, 29923-29926

42. Chen, S., Bacon, K. B., Li, L., Garcia, G. E., Xia, Y., Lo, D., Thompson, D. A., Siani, M. A., Yamamoto, T., Harrison, J. K., and Feng, L. (1998) *J. Exp. Med.* **188**, 193-198

43. Kledal, T. N., Rosenkilde, M. M., Coulin, F., Simmons, G., Johnsen, A. H., Alouani, S., Power, C. A., Luttichau, H. R., Gerstoft, J., Clapham, P. R., Clark-Lewis, I., Wells, T. N., and Schwartz, T. W. (1997) *Science* **277**, 1656-1659

44. Sozzani, S., Luini, W., Bianchi, G., Allavena, P., Wells, T. N. C., Napolitano, M., Bernardini, G., Vecchi, A., D'Ambrosio, D., Mazzeo, D., Sinigaglia, F., Santoni, A., Maggi, E., Romagnani, S., and Mantovani, A. (1998) *Blood* **92**, 4035-4039

45. Weber, K. S., Grone, H. J., Rocken, M., Klier, C., Gu, S., Wank, R., Proudfoot, A. E., Nelson, P. J., and Weber, C. (2001) *Eur. J. Immunol.* **31**, 2458-2466

46. Luttichau, H. R., Lewis, I. C., Gerstoft, J., and Schwartz, T. W. (2001) *Eur. J. Immunol.* **31**, 1217-1220

47. Davis, C. N., Zujovic, V., and Harrison, J. K. (2004) *Mol. Pharmacol.* **66**, 1431-1439

48. Takami, S., Minami, M., Nagata, I., Namura, S., and Satoh, M. (2001) *Journal of Cerebral Blood Flow & Metabolism* **21**, 1430-1435

49. Ghirnikar, R. S., Lee, Y. L., and Eng, L. F. (2001) *Journal of Neuroscience Research* **64**, 582-589

50. DeBruyne, L. A., Li, K., Bishop, D. K., and Bromberg, J. S. (2000) *Gene Therapy* **7**, 575-582

51. Pillai, R. G., Beutelspacher, S. C., Larkin, D. F. P., and George, A. J. T. (2008) *Tranplantation* **85**, 1640-1647

52. Cherqui, S. K., Kenneth, M., Thorpe, C., Kurian, S. M., and Salomon, D. R. (2007) *Molecular Therapy* **15**, 1264-1272

53. LiWang, A. C., Wang, Z. X., Sun, Y., Peiper, S. C., and LiWang, P. J. (1999) *Protein Science* **8**, 2270-2279

54. Shao, W., Fernandez, E., Wilken, J., Thompson, D. A., Siani, M. A., West, J., Lolis, E., and Schweitzer, B. I. (1998) *FEBS Letters* **441**, 77-82

55. Shao, W., Fernandez, E., Sachpatzidis, A., Wilken, J., Thompson, D. A., Schweitzer, B. I., and and Lolis, E. (2001) *European Journal of Biochemistry* **268**, 2948-2959

56. Fernandez, E. J., Wilken, J., Thompson, D. A., Peiper, S. C., and Lolis, E. (2000) *Biochemistry* **39**, 12837-12844

57. Li, Y., Liu, D., Cao, R., Kumar, S., Dong, C., An, J., Wilson, S. R., Gao, Y. G., and Huang, Z. (2007) *Proteins* **67**, 243-246

58. Pace, P., and Rowley, M. (2008) *Curr. Opin. Drug. Discov. Devel.* **11**, 471-479

59. Pleskoff, O., Treboute, C., Brelot, A., Heveker, N., Seman, M., and Alizon, M. (1997) *Science* **276**, 1874-1878

60. Alkhatib, G., Locati, M., Kennedy, P. E., Murphy, P. M., and Berger, E. A. (1997) *Virology* **234**, 340-348

61. Amara, A., Gall, S. L., Schwartz, O., Salamero, J., Montes, M., Loetscher, P., Baggiolini, M., Virelizier, J. L., and Arenzana-Seisdedos, F. (1997) *Journal of Experimental Medicine* **186**, 139-146

62. Bjorndal, A., Deng, H., Jansson, M., Fiore, J. R., Colognesi, C., Karlsson, A., Albert, J., Scarlatti, G., Littman, D. R., and Fenyo, E. M. (1997) *J. Virol.* **71**, 7478-7487

63. Samson, M., Labbe, O., Mollereau, C., Vassart, G., and Parmentier, M. (1996) *J. Biol. Chem.* **35**, 3362-3367

64. Root, M. J., and Steger, H. K. (2004) *Current Pharmaceutical Design* **10**, 1805-1825

65. Eckert, D. M., and Kim, P. S. (2001) *Annu. Rev. Biochem.* **70**, 777-810

66. Miyauchi, K., Kim, Y., Latinovic, O., Morozov, V., and Melikyan, G. B. (2009) *Cell* **137**, 433-444

67. Connor, R. I., Sheridan, K. E., Ceradini, D., Choe, S., and Landau, N. R. (1997) *J. Exp. Med.* **185**, 621-628

68. Scarlatti, G., Tresoldi, E., Bjorndal, A., Fredriksson, R., Colognesi, C., Deng, H. K., Malnati, M. S., Plebani, A., Siccardi, A. G., Littman, D. R., Fenyo, E. M., and Lusso, P. (1997) *Nat. Med.* **3**, 1259-1265

69. Penn, M. L., Grivel, J. C., Schramm, B., Goldsmith, M. A., and Margolis, L. (1999) *Proc. Natl. Acad. Sci. U S A* **96**, 663-668

70. Schramm, B., Penn, M. L., Speck, R. F., Chan, S. Y., De Clercq, E., Schols, D., Connor, R. I., and Goldsmith, M. A. (2000) *J. Virol.* **74**, 184-192

71. Fouchier, R. A., Groenink, M., Kootstra, N. A., Tersmette, M., Huisman, H. G., Miedema, F., and Schuitemaker, H. (1992) *J. Virol.* **66**, 3183-3187

72. Cocchi, F., DeVico, A. L., Garzino-Demo, A., Cara, A., Gallo, R. C., and Lusso, P. (1996) *Nat. Med.* **2**, 1244-1247

73. Oberlin, E., Amara, A., Bachelerie, F., Bessia, C., Virelizier, J. L., Arenzana-Seisdedos, Schwartz, O., Heard, J. M., Clark-Lewis, I., Legler, D.F., Loetscher, M., Baggiolini, M., Moser, B. (1996) *Nature* **382**, 833-835

74. Kelly, M. D., Naif, H. M., Adams, S. L., Cunningham, A. L., and Lloyd, A. R. (1998) *J. Immunol.* **160**, 3091-3095

75. Marozsan, A. J., Torre, V. S., Johnson, M., Ball, S. C., Cross, J. V., Templeton, D. J., Quinones-Mateu, M. E., Offord, R. E., and Arts, E. J. (2001) *J. Virol.* **75**, 8624-8638

76. Gordon, C. J., Muesing, M. A., Proudfoot, A. E., Power, C. A., Moore, J. P., and Trkola, A. (1999) *J. Virol.* **73**, 684-694

77. Mosier, D. E., Picchio, G. R., Gulizia, R. J., Sabbe, R., Poignard, P., Picard, L., Offord, R. E., Thompson, D. A., and Wilken, J. (1999) *J. Virol.* **73**, 3544-3550

78. Trkola, A., Gordon, C., Matthews, J., Maxwell, E., Ketas, T., Czaplewski, L., Proudfoot, A. E., and Moore, J. P. (1999) *J. Virol.* **73**, 6370-6379

79. Schols, D., Proost, P., Struyf, S., Wuyts, A., De Meester, I., Scharpe, S., Van Damme, J., and De Clercq, E. (1998) *Antiviral Res.* **39**, 175-187

80. Proost, P., De Meester, I., Schols, D., Struyf, S., Lambeir, A. M., Wuyts, A., Opdenakker, G., De Clercq, E., Scharpe, S., and Van Damme, J. (1998) *J. Biol. Chem.* **273**, 7222-7227

81. Proudfoot, A. E., Power, C. A., Hoogewerf, A. J., Montjovent, M. O., Borlat, F., Offord, R. E., and Wells, T. N. (1996) *J. Biol. Chem.* **271**, 2599-2603

82. Daopin, S., Li, M., and Davies, D. R. (1993) *Proteins* **17**, 176-192

83. Simmons, G., Clapham, P. R., Picard, L., Offord, R. E., Rosenkilde, M. M., Schwartz, T. W., Buser, R., Wells, T. N. C., and Proudfoot, A. E. (1997) *Science* **276**, 276-279

84. Lederman, M. M., Veazey, R. S., Offord, R., Mosier, D. E., Dufour, J., Mefford, M., Piatak, M., Jr., Lifson, J. D., Salkowitz, J. R., Rodriguez, B., Blauvelt, A., and Hartley, O. (2004) *Science* **306**, 485-487

85. Hartley, O., Dorgham, K., Perez-Bercoff, D., Cerini, F., Heimann, A., Gaertner, H., Offord, R. E., Pancino, G., Debre, P., and Gorochov, G. (2003) *J. Virol.* **77**, 6637-6644

86. Gaertner, H., Cerini, F., Escola, J. M., Kuenzi, G., Melotti, A., Offord, R., Rossitto-Borlat, I., Nedellec, R., Salkowitz, J., Gorochov, G., Mosier, D., and Hartley, O. (2008) *Proc. Natl. Acad. Sci. USA* **105**, 17706-17711

87. Mori, T., O'Keefe, B. R., Sowder, R. C., 2nd, Bringans, S., Gardella, R., Berg, S., Cochran, P., Turpin, J. A., Buckheit, R. W., Jr., McMahon, J. B., and Boyd, M. R. (2005) *J. Biol. Chem.* **280**, 9345-9353

88. Wang, H. G., Williams, R. E., and Lin, P. F. (2004) *Curr. Pharm. Des.* **2004**, 1785-1793

89. Emau, P., Tian, B., O'Keefe B, R., Mori, T., McMahon, J. B., Palmer, K. E., Jiang, Y., Bekele, G., and Tsai, C. C. (2007) *J. Med. Primatol.* **36**, 244-253

90. Champagne, K., Shishido, A., and Root, M. J. (2009) *J. Biol. Chem.* **284**, 3619-3627

91. Liu, S., Lu, H., Niu, J., Xu, Y., Wu, S., and Jiang, S. (2005) *J. Biol. Chem.* **280**, 11259-11273

92. Poveda, E., Briz, V., and Soriano, V. (2005) *AIDS Reviews* **7**, 139-147

93. Root, M. J., Kay, M. S., and Kim, P. S. (2001) *Science* **291**, 884-888

94. Kopetzki, E., Jekle, A., Ji, C., Rao, E., Zhang, J., Fischer, S., Cammack, N., Sankuratri, S., and Heilek, G. (2008) *Virol. J.* **5**, 56

95. Ji, C., Kopetzki, E., Jekle, A., Stubenrauch, K. G., Liu, X., Zhang, J., Rao, E., Schlothauer, T., Fischer, S., Cammack, N., Heilek, G., Ries, S., and Sankuratri, S. (2009) *J. Biol. Chem.* **284**, 5175-5185

96. Kagiampakis, I., Gharibi, A., Mankowski, M. K., Snyder, B. A., Ptak, R. G., Alatas, K., and LiWang, P. J. (2011) *Antimicrob. Agents Chemother.* **55**, 264-275

97. McCornack, M. A., Cassidy, C. K., and LiWang, P. J. (2003) *J. Biol. Chem.* **278**, 1946-1956

98. Shaw, J. P., Johnson, Z., Borlat, F., Zwahlen, C., Kungl, A., Roulin, K., Harrenga, A., Wells, T. N., and Proudfoot, A. E. (2004) *Structure* **12**, 2081-2093

99. Lau, E. K., Paavola, C. D., Johnson, Z., Gaudry, J. P., Geretti, E., Borlat, F., Kungl, A. J., Proudfoot, A. E., and Handel, T. M. (2004) *J. Biol. Chem.* **279**, 22294-22305

100. Jin, H., Shen, X., Baggett, B., Kong, X., and LiWang, P. (2007) *J. Biol. Chem.* **282**, 27976-27983

101. McCornack, M. A., Boren, D. M., and LiWang, P. J. (2004) *Biochemistry* **43**, 10090-10101

102. Wishart, D. S., Bigam, C. G., Yao, J., Abildgaard, F., Dyson, H. J., Oldfield, E., Markley, J. L., and Sykes, B. D. (1995) *J. Biomol. NMR* **6**, 135-140

103. Delaglio, F., Grzesiek, S., Vuister, G. W., Hu, G., Pfeifer, J., and Bax, A. (1995) *J. Biomol. NMR* **6**, 277-293

104. Garrett, D. S., Powers, R., Gronenborn, A. M., and Clore, G. M. (1991) *J. Magn. Reson.* **95**, 214-220

105. Garret, D. S., Seok, Y., Peterkofsky, A., Clore, G. M., and Gronenborn, A. M. (1997) *Biochemistry* **36**, 4393-4398

106. Mayer, K. L., and Stone, M. J. (2000) *Biochemistry* **39**, 8382-8395

107. Gayle, R. B., 3rd, Sleath, P. R., Srinivason, S., Birks, C. W., Weerawarna, K. S., Cerretti, D. P., Kozlosky, C. J., Nelson, N., Vanden Bos, T., and Beckmann, M. P. (1993) *J. Biol. Chem.* **268**, 7283-7289

108. Kouchakdjian, E., M., Johnson, F., Grollman, A. P., Patel, D. J. (1991) *Biochemistry* **30**, 3262-3270

109. Johnson, M. L., Correia, J. J., Yphantis, D. A., and Halvorson, H. R. (1981) *Biophysical Journal* **36**, 575-588

110. Correia, J. J., Chacko, B. M., Lam, S. S., and Lin, K. (2001) *Biochemistry* **40**, 1473-1482

111. Nilges, M., and O'Donoghue, S. I. (1998) *Progress in Nuclear Magnetic Resonance Spectroscopy* **32**, 107-139

112. Schüttelkopf, A. W., and van Aalten, D. M. (2004) *Acta crystallographica. Section D, Biological crystallography* **60**, 1355-1363

113. Daura, X., Gademann, K., Jaun, B., Seebach, D., Van Gunsteren, W. F., and Mark, A. E. (1999) *Angewandte Chemie International Edition* **38**, 236-240

114. Veldkamp, C. T., Peterson, F. C., Pelzek, A. J., and Volkman, B. F. (2005) *Protein Science* **14**, 1071-1081

115. Laurence, J. S., Blanpain, C., Parmentier, M., Burgner, J. W., and LiWang, P. J. (2000) *Biochemistry* **39**, 3401-3409

116. Hoover, D. M., Boulegue, C., Yang, D., Oppenheim, J. J., Tucker K., Lu, W., and Lubkowski, J. (2002) *J. Biol. Chem.* **277**, 37647-37654

117. Lortat-Jacob, H., Grosdidier, A., and Imberty, A. (2002) *Proc. Natl. Acad. Sci. U S A.* **99**, 1229-1234

118. Crump, M. P., Gong, J.-H., Loetscher, P., Rajarathnam, K., Amara, A., Arenzana-Seisdedos, F., Virelizier, J.-L., Baggiolini, M., Sykes, B., and Clark-Lewis, I. (1997) *EMBO J.* **16**, 6996-7007

119. Shao, W., Jerva, L. F., West, J., Lolis, E., and Schweitzer, B. I. (1998) *Biochemistry* **37**, 8303-8313

120. Handel, T. M., Johnson, Z., Crown, S. E., Lau, E. K., and Proudfoot, A. E. (2005) *Annual Review of Biochemistry* **74**, 385-410

121. Kuschert, G. S., Coulin, F., Power, C. A., Proudfoot, A. E., Hubbard, R. E., Hoogewerf, A. J., and Wells, T. N. (1999) *Biochemistry* **38**, 12959-12968

122. Proudfoot, A. E. I., Fritchley, S., Borlat, F., Shaw, J. P., Vilbois, F., Zwahlen, C., Trkola, A., Marchant, D., Clapham, P. R., and Wells, T. N. C. (2001) *J. Biol. Chem.* **276**, 10620-10626

123. Paavola, C. D., Hemmerich, S., Grunberger, D., Polsky, I., Bloom, A., Freedman, R., Mulkins, M., Bhakta, S., McCarley, D., Wiesent, L., Wong, B., Jarnagin, K., and Handel, T. M. (1998) *J. Biol. Chem.* **273**, 33157-33165

124. Dominiguez, C., Boelens, R., and Bonvin, A. M. (2003) *Journal of American Chemistry Society* **125**, 1731-1737

125. Schieborr, U., Vogtherr, M., Elshorst, B., Betz, M., Grimme, S., Pescatore, B., Langer, T., Saxena, K., and Schwalbe, H. (2005) *Chembiochem* **6**, 1891-1898

126. Crump, M. P., Rajarathnam, K., Kim, K.-S., Clark-Lewis, I., and Sykes, B. D. (1998) *J. Biol. Chem.* **273**, 22471-22479

127. Lowman, H. B., Fairbrother, W. J., Slagle, P. H., Kabakoff, R., Liu, J., Shire, S., and Hebert, C. A. (1997) *Protein Sci.* **6**, 598-608

128. Kim, S., Jao, S. C., Laurence, J. S., and LiWang, P. J. (2001) *Biochemistry* **40**, 10782-10791

129. Kim, K.-S., Rajarathnam, K., Clark-Lewis, I., and Sykes, B. D. (1996) *FEBS Lett.* **395**, 277-282

130. Lodi, P. J., Garrett, D. S., Kuszewski, J., Tsang, M. L.-S., Weatherbee, J. A., Leonard, W. J., Gronenborn, A. M., and Clore, G. M. (1994) *Science* **263**, 1762-1767

131. Handel, T. M., and Domaille, P. J. (1996) *Biochemistry* **35**, 6569-6584

132. Skelton, N. J., Aspiras, F., Ogez, J., and Schall, T.J. (1995) *Biochemistry* **34**, 5329-5342

133. Clore, G. M., Appella, E., Yamada, M., Matsushima, K., and Gronenborn, A.M. (1990) *Biochemistry* **29**, 1689-1696

134. Wu, B., Chien, E. Y., Mol, C. D., Fenalti, G., Liu, W., Katritch, V., Abagyan, R., Brooun, A., Wells, P., Bi, F. C., Hamel, D. J., Kuhn, P., Handel, T. M., Cherezov, V., and Stevens, R. C. (2010) *Science* **330**, 1066-1071

135. Palczewski, K., Kumasaka, T., Hori, T., Behnke, C. A., Motoshima, H., Fox, B. A., Le Trong, I., Teller, D. C., Okada, T., Stenkamp, R. E., Yamamoto, M., and Miyano, M. (2000) *Science* **289**, 739-745

136. Cherezov, V., Rosenbaum, D. M., Hanson, M. A., Rasmussen, S. G., Thian, F. S., Kobilka, T. S., Choi, H. J., Kuhn, P., Weis, W. I., Kobilka, B. K., and Stevens, R. C. (2007) *Science* **318**, 1258-1265

137. Rasmussen, S. G., Choi, H. J., Rosenbaum, D. M., Kobilka, T. S., Thian, F. S., Edwards, P. C., Burghammer, M., Ratnala, V. R., Sanishvili, R., Fischetti, R. F., Schertler, G. F., Weis, W. I., and Kobilka, B. K. (2007) *Nature* **450**, 383-387

138. Serrano-Vega, M. J., Magnani, F., Shibata, Y., and Tate, C. G. (2008) *Proc. Natl. Acad. Sci. USA* **105**, 877-882

139. Jaakola, V. P., Griffith, M. T., Hanson, M. A., Cherezov, V., Chien, E. Y., Lane, J. R., Ijzerman, A. P., and Stevens, R. C. (2008) *Science* **322**, 1211-1217

140. Clark-Lewis, I., Schumacher, C., Baggiolini, M., and Moser, B. (1991) *J. Biol. Chem.* **266**, 23128-23134

141. Moser, B., Dewald, B., Barella, L., Schumacher, C., Baggiolini, M., and Clark-Lewis, I. (1993) *J. Biol. Chem.* **268**, 7125-7128

142. Clark-Lewis, I., Dewald, B., Geiser, T., Moser, B., and Baggiolini, M. (1993) *Proc. Natl. Acad. Sci. USA* **90**, 3574-3577

143. Clark-Lewis, I., Dewald, B., Loetscher, M., Moser, B., and Baggiolini, M. (1994) *J. Biol. Chem.* **269**, 16075-16081

144. Schraufstatter, I. U., Ma, M., Oades, Z. G., Barritt, D. S., and Cochrane, C. G. (1995) *J. Biol. Chem.* **270**, 10428-10431

145. Hammond, M. E., Shyamala, V., Siani, M. A., Gallegos, C. A., Feucht, P. H., Abbott, J., Lapointe, G. R., Moghadam, M., Khoja, H., Zakel, J., and Tekamp-Olson, P. (1996) *J. Biol. Chem.* **271**, 8228-8235

146. Williams, G., Borkakoti, N., Bottomley, G. A., Cowan, I., Fallowfield, A. G., Jones, P. S., Kirtland, S. J., Price, G. J., and Price, L. (1996) *J. Biol. Chem.* **271**, 9579-9586

147. Skelton, N. J., Quan, C., Reilly, D., and Lowman, H. (1999) *Structure* **7**, 157-168

148. LaRosa, G. J., Thomas, K. M., Kaufmann, M. E., Mark, R., White, M., Taylor, L., Gray, G., Witt, D., and Navarro, J. (1992) *J. Biol. Chem.* **267**, 25402-25406

149. Wu, L., Ruffing, N., Shi, X., Newman, W., Soler, D., Mackay, C. R., and Qin, S. (1996) *J. Biol. Chem.* **271**, 31202-31209

150. Hebert, C. A., Chuntharapai, A., Smith, M., Colby, T., Kim, J., and Horuk, R. (1993) *J. Biol. Chem.* **268**, 18549-18553

151. Katancik, J. A., Sharma, A., and de Nardin, E. (2000) *Cytokine* **12**, 1480-1488

152. Booth, V., Keizer, D. W., Kamphuis, M. B., Clark-Lewis, I., and Sykes, B. D. (2002) *Biochemistry* **41**, 10418-10425

153. Campanella, G. S., Lee, E. M., Sun, J., and Luster, A. D. (2003) *J. Biol. Chem.* **278**, 17066-17074

154. Crump, M. P., Gong, J. H., Loetscher, P., Rajarathnam, K., Amara, A., Arenzana-Seisdedos, F., Virelizier, J. L., Baggiolini, M., Sykes, B. D., and Clark-Lewis, I. (1997) *EMBO J.* **16**, 6996-7007

155. Loetscher, P., Gong, J. H., Dewald, B., Baggiolini, M., and Clark-Lewis, I. (1998) *J. Biol. Chem.* **273**, 22279-22283

156. Brelot, A., Heveker, N., Montes, M., and Alizon, M. (2000) *J. Biol. Chem.* **275**, 23736-23744

157. Zhou, N., Luo, Z., Luo, J., Liu, D., Hall, J. W., Pomerantz, R. J., and Huang, Z. (2001) *J. Biol. Chem.* **276**, 42826-42833

158. Veldkamp, C. T., Seibert, C., Peterson, F. C., De la Cruz, N. B., Haugner, J. C., 3rd, Basnet, H., Sakmar, T. P., and Volkman, B. F. (2008) *Sci. Signal* **1**, ra4

159. Kofuku, Y., Yoshiura, C., Ueda, T., Terasawa, H., Hirai, T., Tominaga, S., Hirose, M., Maeda, Y., Takahashi, H., Terashima, Y., Matsushima, K., and Shimada, I. (2009) *J. Biol. Chem.* **284**, 35240-35250

160. Blanpain, C., Doranz, B. J., Bondue, A., Govaerts, C., De Leener, A., Vassart, G., Doms, R. W., Proudfoot, A., and Parmentier, M. (2003) *J. Biol. Chem.* **278**, 5179-5187

161. Blanpain, C., Lee, B., Vakili, J., Doranz, B.J., Govaerts, C., Migeotte, I., Sharron, M., Dupriez, V., Vassart, G., Doms, R.W., and Parmentier, M. (1999) *J. Biol. Chem.* **274**, 18902-18908

162. Blanpain, C., Doranz, B. J., Vakili, J., Rucker, J., Govaerts, C., Baik, S. S. W., Lorthioir, O., Migeotte, I., Libert, F., Baleux, F., Vassart, G., Doms, R. W., and Parmentier, M. (1999) *J. Biol. Chem.* **274**, 34719-34727

163. Bondue, A., Jao, S. C., Blanpain, C., Parmentier, M., and LiWang, P. J. (2002) *Biochemistry* **41**, 13548-13555

164. Chung, I. Y., Kim, Y. H., Choi, M. K., Noh, Y. J., Park, C. S., Kwon, D. Y., Lee, D. Y., Lee, Y. S., Chang, H. S., and Kim, K. S. (2004) *Biochem. Biophys. Res. Commun.* **314**, 646-653

165. Gong, J. H., Uguccioni, M., Dewald, B., Baggiolini, M., and Clark-Lewis, I. (1996) *J. Biol. Chem.* **271**, 10521-10527

166. Han, K. H., Green, S. R., Tangirala, R. K., Tanaka, S., and Quehenberger, O. (1999) *J. Biol. Chem.* **274**, 32055-32062

167. Shinkai, A., Komuta-Kunitomo, M., Sato-Nakamura, N., and Anazawa, H. (2002) *Protein Eng.* **15**, 923-929

168. Pakianathan, D. R., Kuta, E. G., Artis, D. R., Skelton, N. J., and Hebert, C. A. (1997) *Biochemistry* **36**, 9642-9648

169. Monteclaro, F. S., and Charo, I. F. (1996) *J. Biol. Chem.* **271**, 19084-19092

170. Ye, J., Kohli, L. L., and Stone, M. J. (2000) *J. Biol. Chem.* **275**, 27250-27257

171. Duma, L., Haussinger, D., Rogowski, M., Lusso, P., and Grzesiek, S. (2007) *J. Mol. Biol.* **365**, 1063-1075

172. Mueller, A., Mahmoud, N. G., and Strange, P. G. (2006) *Biochem. Pharmacol.* **72**, 739-748

173. Jerva, L. F., Sullivan, G., and Lolis, E. (1997) *Protein Sci.* **6**, 1643-1652

174. Mizoue, L. S., Bazan, J. F., Johnson, E. C., and Handel, T. M. (1999) *Biochemistry* **38**, 1402-1414

175. Rajagopalan, L., and Rajarathnam, K. (2006) *Biosci. Rep.* **26**, 325-339

176. Rajagopalan, L., and Rajarathnam, K. (2004) *J. Biol. Chem.* **279**, 30000-30008

177. Chung, C., Cooke, R. M., Proudfoot, A .E., and Wells, T.N. (1995) *Biochemistry* **34**, 3907-9314

178. Dairaghi, D. J., Oldham, E. R., Bacon, K. B., and Schall, T. J. (1997) *J. Biol. Chem.* **272**, 28206-28209

179. Ponath, P. D., Qin, S., Ringler, D. J., Clark-Lewis, I., Wang, J., Kassam, N., Smith, H., Shi, X., Gonzalo, J. A., Newman, W., Gutierrez-Ramos, J. C., and Mackay, C. R. (1996) *J. Clin. Invest.* **97**, 604-612

180. Czaplewski, L. G., McKeating, J., Craven, C. J., Higgins, L. D., Appay, V., Brown, A., Dudgeon, T., Howard, L. A., Meyers, T., Owen, J., Palan, S. R., Tan, P., Wilson, G., Woods, N. R., Heyworth, C. M., Lord, B. I., Brotherton, D., Christison, R., Craig, S., Cribbes, S., Edwards, R. M., Evans, S. J., Gilbert, R., Morgan, P., Randle, E., Schofield, N., Varley, P. G., Fisher, J., Waltho, J. P., and Hunter, M. G. (1999) *J. Biol. Chem.* **274**, 16077-16084

181. Sticht, H., Escher, S. E., Schweimer, K., Forssmann, W.-G., Rosch, R., and Adermann, K. (1999) *Biochemistry* **38**, 5995-6002

182. Zhou, N., Luo, Z., Luo, J., Hall, J. W., and Huang, Z. (2000) *Biochemistry* **39**, 3782-3787

183. Luo, Z., Fan, X., Zhou, N., Hiraoka, M., Luo, J., Kaji, H., and Huang, Z. (2000) *Biochemistry* **39**, 13545-13550

184. Crump, M. P., Elisseeva, E., Gong, J., Clark-Lewis, I., and Sykes, B. D. (2001) *FEBS Letters* **489**, 171-175

185. Dong, C. Z., Kumar, S., Choi, W. T., Madani, N., Tian, S., An, J., Sodroski, J. G., and Huang, Z. (2005) *J. Med. Chem.* **48**, 7923-7924

186. Liu, D., Madani, N., Li, Y., Cao, R., Choi, W., Kawatkar, S. P., Lim, M. Y., Kumar, S., Dong, C., Wang, J., Russell, J. D., Lefebure, C. R., An, J., Wilson, S., Gao, Y., Pallansch, L. A., Sodroski, J. G., and Huang, Z. (2007) *J. Virol.* **81**, 11489-11498

187. Navenot, J. M., Wang, Z. X., Trent, J. O., Murray, J. L., Hu, Q. X., DeLeeuw, L., Moore, P. S., Chang, Y., and Peiper, S. C. (2001) *J. Mol. Biol.* **313**, 1181-1193

188. Zhao, B., and Liwang, P. J. (2010) *Biochemistry* **49**, 7012-7022

189. Clackson, T., and Wells, J. A. (1995) *Science* **267**, 383-386

190. Cunningham, B. C., and Wells, J. A. (1993) *J. Mol. Biol.* **234**, 554-563

191. 2010 Global Report on HIV/AIDS, UNAIDS. (2010). Access date: Feb 13th, 2011. *Website: http://www.unaids.org/globalreport/Global_report.htm*

192. Hartley, O., and Offord, R. E. (2005) *Current Protein & Peptide Science* **6**, 207-219

193. Hartley, O., Gaertner, H., Wilken, J., Thompson, D., Fish, R., Ramos, A., Pastore, C., Dufour, B., Cerini, F., Melotti, A., Heveker, N., Picard, L., Alizon, M.,

Mosier, D., Kent, S., and Offord, R. (2004) *Proc. Natl. Acad. Sci. USA* **101**, 16460-16465

194. Kawamura, T., Bruse, S. E., Abraha, A., Sugaya, M., Hartley, O., Offord, R. E., Arts, E. J., Zimmerman, P. A., and Blauvelt, A. (2004) *J. Virol.* **78**, 7602-7609

195. Pastore, C., Picchio, G. R., Galimi, F., Fish, R., Hartley, O., Offord, R. E., and Mosier, D. E. (2003) *Antimicrob. Agents. Chemother.* **47**, 509-517

196. Kuhmann, S. E., and Hartley, O. (2008) *Annu. Rev. Pharmacol. Toxicol.* **48**, 425-461

197. Gaertner, H., Lebeau, O., Borlat, I., Cerini, F., Dufour, B., Kuenzi, G., Melotti, A., Fish, R. J., Offord, R., Springael, J. Y., Parmentier, M., and Hartley, O. (2008) *Protein Eng. Des. Sel.* **21**, 65-72

198. Kahle, K. M., Steger, H. K., and Root, M. J. (2009) *PLoS Pathog.* **5**, e1000674

199. Furuta, R. A., Wild, C. T., Weng, Y., and Weiss, C. D. (1998) *Nature Structural Biology* **5**, 276-279

200. Chan, D. C., Chutkowski, C. T., and Kim, P. S. (1998) *Proc. Natl. Acad. Sci. USA* **95**, 15613-15617

201. Lu, M., and Kim, P. S. (1997) *J. Biomol. Struct. Dyn.* **15**, 465-471

202. Stoddart, C. A., Nault, G., Galkina, S. A., Thibaudeau, K., Bakis, P., Bousquet-Gagnon, N., Robitaille, M., Bellomo, M., Paradis, V., Liscourt, P., Lobach, A., Rivard, M. E., Ptak, R. G., Mankowski, M. K., Bridon, D., and Quraishi, O. (2008) *J. Biol. Chem.* **283**, 34045-34052

203. Hamburger, A. E., Kim, S., Welch, B. D., and Kay, M. S. (2005) *J. Biol. Chem.* **280**, 12567-12572

204. Takeuchi, Y., McClure, M. O., and Pizzato, M. (2008) *J. Virol.* **82**, 12585-12588

205. Wei, X., Decker, J. M., Liu, H., Zhang, Z., Arani, R. B., Kilby, J. M., Saag, M. S., Wu, X., Shaw, G. M., and Kappes, J. C. (2002) *Antimicrob. Agents. Chemother.* **46**, 1896-1905

206. Derdeyn, C. A., Decker, J. M., Sfakianos, J. N., Wu, X., O'Brien, W. A., Ratner, L., Kappes, J. C., Shaw, G. M., and Hunter, E. (2000) *J. Virol.* **74**, 8358-8367

207. Platt, E. J., Wehrly, K., Kuhmann, S. E., Chesebro, B., and Kabat, D. (1998) *J. Virol.* **72**, 2855-2864

208. Ciminale, V., Felber, B. K., Campbell, M., and Pavlakis, G. N. (1990) *AIDS Res. Hum. Retroviruses* **6**, 1281-1287

209. Vodicka, M. A., Goh, W. C., Wu, L. I., Rogel, M. E., Bartz, S. R., Schweickart, V. L., Raport, C. J., and Emerman, M. (1997) *Virology* **233**, 193-198

210. Gartner, S., Markovits, P., Markovitz, D. M., Kaplan, M. H., Gallo, R. C., and Popovic, M. (1986) *Science* **233**, 215-219

211. Gendelman, H. E., Baca, L. M., Kubrak, C. A., Genis, P., Burrous, S., Friedman, R. M., Jacobs, D., and Meltzer, M. S. (1992) *J. Immunol.* **148**, 422-429

212. Westervelt, P., Gendelman, H. E., and Ratner, L. (1991) *Proc. Natl. Acad. Sci. USA* **88**, 3097-3101

213. Gendelman, H. E., Orenstein, J. M., Baca, L. M., Weiser, B., Burger, H., Kalter, D. C., and Meltzer, M. S. (1989) *AIDS* **3**, 475-495

214. Gendelman, H. E., Orenstein, J. M., Martin, M. A., Ferrua, C., Mitra, R., Phipps, T., Wahl, L. A., Lane, H. C., Fauci, A. S., Burke, D. S., and et al. (1988) *J. Exp. Med.* **167**, 1428-1441

215. Popovic, M., Read-Connole, E., and Gallo, R. C. (1984) *Lancet.* **2**, 1472-1473

216. Popovic, M., Sarngadharan, M. G., Read, E., and Gallo, R. C. (1984) *Science* **224**, 497-500

217. Ratner, L., Haseltine, W., Patarca, R., Livak, K. J., Starcich, B., Josephs, S. F., Doran, E. R., Rafalski, J. A., Whitehorn, E. A., Baumeister, K., and et al. (1985) *Nature* **313**, 277-284

218. Connor, R. I., Chen, B. K., Choe, S., and Landau, N. R. (1995) *Virology* **206**, 935-944

219. Chang, L. J., Urlacher, V., Iwakuma, T., Cui, Y., and Zucali, J. (1999) *Gene Ther.* **6**, 715-728

220. Cheng-Mayer, C., Liu, R., Landau, N. R., and Stamatatos, L. (1997) *J. Virol.* **71**, 1657-1661

221. Stamatatos, L., Wiskerchen, M., and Cheng-Mayer, C. (1998) *AIDS Res. Hum. Retroviruses* **14**, 1129-1139

222. Stamatatos, L., Lim, M., and Cheng-Mayer, C. (2000) *AIDS Res. Hum. Retroviruses* **16**, 981-994

223. Page, K. A., Landau, N. R., and Littman, D. R. (1990) *J. Virol.* **64**, 5270-5276

224. Li, Y., Svehla, K., Mathy, N. L., Voss, G., Mascola, J. R., and Wyatt, R. (2006) *J. Virol.* **80**, 1414-1426

225. Gao, F., Morrison, S. G., Robertson, D. L., Thornton, C. L., Craig, S., Karlsson, G., Sodroski, J., Morgado, M., Galvao-Castro, B., von Briesen, H., Beddows, S., Weber, J., Sharp, P. M., Shaw, G. M., and Hahn, B. H. (1996) *J. Virol.* **70**, 1651-1667

226. Li, M., Gao, F., Mascola, J. R., Stamatatos, L., Polonis, V. R., Koutsoukos, M., Voss, G., Goepfert, P., Gilbert, P., Greene, K. M., Bilska, M., Kothe, D. L., Salazar-Gonzalez, J. F., Wei, X., Decker, J. M., Hahn, B. H., and Montefiori, D. C. (2005) *J. Virol.* **79**, 10108-10125

227. Lackman-Smith, C., Osterling, C., Luckenbaugh, K., Mankowski, M., Snyder, B., Lewis, G., Paull, J., Profy, A., Ptak, R. G., Buckheit, R. W., Jr., Watson, K. M., Cummins, J. E., Jr., and Sanders-Beer, B. E. (2008) *Antimicrob. Agents Chemother.* **52**, 1768-1781

228. Ptak, R. G., Gallay, P. A., Jochmans, D., Halestrap, A. P., Ruegg, U. T., Pallansch, L. A., Bobardt, M. D., de Bethune, M. P., Neyts, J., De Clercq, E., Dumont, J. M., Scalfaro, P., Besseghir, K., Wenger, R. M., and Rosenwirth, B. (2008) *Antimicrob. Agents Chemother.* **52**, 1302-1317

229. Babcock, G. J., Farzan, M., and Sodroski, J. (2003) *J. Biol. Chem.* **278**, 3378-3385

230. Percherancier, Y., Berchiche, Y. A., Slight, I., Volkmer-Engert, R., Tamamura, H., Fujii, N., Bouvier, M., and Heveker, N. (2005) *J. Biol. Chem.* **280**, 9895-9903

231. Heredia, A., Gilliam, B., DeVico, A., Le, N., Bamba, D., Flinko, R., Lewis, G., Gallo, R. C., and Redfield, R. R. (2007) *AIDS* **21**, 1317-1322

VITA

Name: Bo Zhao

Address: Texas A&M University
Department of Biochemistry/Biophysics
103 Biochemistry Building
2I28TAMU
College Station, TX 77843-2128
c/o Patricia LiWang or Vladislav Panin

Email Address: BoZhao@tamu.edu

Education: B.S., Biotechnology, Peking University, Beijing, China, 2004
Ph.D., Biochemistry, Texas A&M University, 2011